NOTE TO USERS

This reproduction is the best copy available.

UMI®

A PERCOLATION BIOFILM-GROWTH MODEL FOR

BIOMASS CLOGGING IN BIOFILTERS

by

Fethiye Ozis

_____

A Dissertation Presented to the
FACULTY OF THE GRADUATE SCHOOL
UNIVERSITY OF SOUTHERN CALIFORNIA
In Partial Fulfillment of the
Requirements for the Degree
DOCTOR OF PHILOSOPHY
ENGINEERING
(ENVIRONMENTAL ENGINEERING)

August 2005

UMI Number: 3196869

INFORMATION TO USERS

The quality of this reproduction is dependent upon the quality of the copy
submitted. Broken or indistinct print, colored or poor quality illustrations and
photographs, print bleed-through, substandard margins, and improper
alignment can adversely affect reproduction.

In the unlikely event that the author did not send a complete manuscript
and there are missing pages, these will be noted. Also, if unauthorized
copyright material had to be removed, a note will indicate the deletion.

UMI®

UMI Microform 3196869
Copyright 2006 by ProQuest Information and Learning Company.
All rights reserved. This microform edition is protected against
unauthorized copying under Title 17, United States Code.

ProQuest Information and Learning Company
300 North Zeeb Road
P.O. Box 1346
Ann Arbor, MI 48106-1346

ACKNOWLEDGEMENTS

For the past several years a number of people have been directly involved with the development of my work. First, I would like to express my deepest gratitude to my advisor, Dr. Joseph Devinny, for his guidance and encouragement throughout my academic life. I have learned a great deal from him about how to be an ideal researcher and a teacher. I would also like to express my appreciation to Dr. Constantinos Siuotas and Dr. Yannis Yortsos, who provided me with their constructive suggestions and valuable assistance on my dissertation whenever I needed despite their overloaded agenda. Special thanks go to my colleagues and friends at USC; Manisha Singh, Arash Bina, Jamie Sayre, Joshua Steele, Atosa Vahdati, Mike Geller, Satya Sardar, Bhabesh Chakrabarti and Eric Hernandez for their immeasurable assistance.

Last but certainly not least, I am deeply grateful to my husband, Ismail Ozis for his endless understanding and generous patience during my graduate study. I will never forget the walks that we took to the lab in middle of the night. Without his unconditional optimism, it would have been impossible for me to accomplish my Ph.D. degree.

ii

TABLE OF CONTENTS

iv

LIST OF FIGURES

vi

viii

ix

LIST OF TABLES

x

ABSTRACT

Biomass accumulation has been recognized as a limiting factor in the operation of biofilters. As the biofilm thickens, portions at the base may no longer be exposed to contaminants and oxygen. Smaller pores are filled with biomass so that air no longer flows into them. As pores are blocked, air may be prevented from reaching some pores even when they are not filled. Eventually blockage becomes sufficiently widespread so that increasing head loss and decreasing removal efficiency require that the system be shut down. Optimization necessitates a better understanding of the mechanisms by which biofilter clogs. Percolation theory was developed for application to similar problems in other fields such as oil recovery and catalyst bed design. In this work, a numerical percolation model of the blockage process was developed for application to biofilters. It allows comparison of pore blockage histories for various pore size distributions, and predicts biomass accumulation, head loss, and treatment efficiency as a function of time, as well as total time until blockage prevents further operation.

A model was developed and applied to two theoretical biofilters having log-normal pore size distribution with $\mu = 4$ and 7. It was also used to simulate two bench-scale biofilters with experimentally determined pore size distributions.

This model accounts for biomass growth and its impact on head loss, contaminant removal and channeling in the biofilter. It will be useful in biofilter design, particularly in the choice of appropriate packing. A complete understanding

of the clogging process, and ultimately its control, would increase biofilter efficiency and broaden the range of applications.

Finally, the removal efficiency of granular filters packed with lava rock and sand was studied for collection of airborne particles 0.05 to 2.5μm in diameter in anticipation of the possibility that either inert granular filters or biofilters could be used for treatment of fine particles. The effects of filter depth, packing wetness, grain size and flow rate on collection efficiency were investigated. Packed-bed granular filters were proved effective for removal of fine and ultrafine particles from air.

xii

1 INTRODUCTION

1.1 Background

1.1.1 History

Biological treatment has been proved successful for treating wastewater and solid waste throughout the twentieth century. However, biological treatment for waste air is relatively new. The earliest known biofilter systems were using soil as media and constructed as open pits in 1950s (Pomeroy, 1957). Biofiltration was initially employed to control mainly sewer odor emissions generated by wastewater treatment plants (Kennes and Veiga, 2001).

In the 1970s, significant and stricter air quality regulations accelerated the interest in biofilters, because of their advantages of low operating costs. Germany and the Netherlands led the way in terms of biofilter technology advancement. The development of biofiltration for control of Volatile Organic Carbons (VOCs) [1] and air toxics took place in the 1980s (Leson and Winer, 1991). Since then, computer-operated enclosed biofilter systems have been designed with the help of extensive

---

[1] Volatile organic compounds constitute substances such as alkanes (e.g. methane), alkenes (e.g. ethylene), alkynes (e.g. acetylene), aromatics (e.g. benzene), alcohols (e.g. ethanol), aldehydes (e.g. formaldehyde), ethers (e.g. ethyl ether), ketones (e.g. acetone), and chlorinated substances (e.g. trichloroethane). Volatile organic compounds are often found in mixtures, and can evaporate into the atmosphere under ambient temperature and pressure conditions.

1

research on different biofilter media, bed configurations, waste gas mixtures, microflora, and mathematical modeling of the process.

As biofilter technology is accepted by regulators as a cost-effective, reliable means of controlling low-concentration biodegradable waste gases, more research will be required to move the technology forward.

1.1.2 Biofilter Mechanism

Biofiltration uses microorganisms fixed to a porous medium to break down pollutants present in an air stream. The microorganisms grow in a biofilm on the surface of a medium or are suspended in the water phase surrounding the medium particles.

The filter-bed media are mainly of two types. The first type includes natural organic media such as compost, peat, wood bark and/or soil, the second type is an inert synthetic medium like polypropylene rings, ceramics, extruded diatomaceous earth and polyurethane foam. Granular activated carbon has also been used successfully as biofilter medium (Webster et al. 1996). Sometimes, a combination of two types has been employed (Ortíz et al. 1998). Ideal media should ensure large surface attachment area, minimal backpressure and additional nutrient supply (Devinny et al. 1999).

Generally, waste gases are de-dusted, heated, cooled or humidified as necessary, then pulled into to the filter bed (Madl, 1998). In the filter bed, the moist

2

filter medium provides physical and chemical conditions appropriate for transferring the contaminant(s) from the air phase to the water phase; biodegradation of the contaminant(s) in the water phase; and mass transfer of the biodegradation products from the water phase to the air phase. The mechanism of the biofiltration process includes a combination of adsorption, absorption and microbial degradation. A portion of the contaminants from the waste air is adsorbed on the surface of the media while the rest is absorbed by the thin film of liquid surrounding individual grains. Aerobic microorganisms, generally bacteria and fungi, oxidize VOCs, biodegradable gases, and vapors in processes identical to those naturally occurring in soil. The digested pollutants become primarily water, carbon dioxide, mineral salts, and microbial biomass. Ideally, the resultant air stream is clean, colorless, and odorless (Madl, 1998; Janni et al. 2000).

The first biofilters were excavated pits filled with soil, with air distributed at the bottom and treated as it rose through the media (Pomeroy, 1957). Since then, biofilters have been built as conventional open single-bed systems, open multiple story systems, or totally enclosed systems. Multiple- story systems save space as having each layer as separate reactor and increasing detention time. Enclosed systems operate slightly above or below atmospheric pressure and have been designed in many shapes, including cylindrical and rectangular.

3

1.1.3 Biofilter Applications

Biofiltration can be applied to those compounds that are biologically treatable including alcohols, aldehydes, aromatic hydrocarbons, ketones, and inorganic compounds like ammonia and hydrogen sulfide (Devinny et al. 1999). Experience gained as a result of many years of work with the biofiltration in different industries suggests that biofiltration is a viable option for the following industries (Table 1- 1).

Table 1-1: Commercial applications of biofilters

VOC Control	Odor Abatement	Both Odor& VOC
Chemical and petrochemical industry	Agricultural and meat processing	Composting
Rubber Productions	Rendering	Soil Vapor Extraction
Automotive industry	Slaughter houses	Waste treatment
Oil and gas industry	Sewage treatment	Waste water treatment
Synthetic resins	Tobacco, cocoa and sugar industry	Soil remediation
Paints and coatings	Gelatin and glue plants	Groundwater remediation
Pharmaceutical industry	Flavor and fragrance	Pulp & Paper Mills

Due to continuing expansion of urban areas into the surrounding countryside where they encroach on land dedicated to waste treatment, industry, and agriculture, the control of VOCs and odor is becoming a more pressing air quality problem (Ozis et al. 2005). Biofilters can combat VOCs and odor in a safe, natural and sustainable way. Biofilter systems work at room temperature without toxic chemicals. They are safer than incineration or chemical scrubbing; they use less energy, do not produce

4

hazardous end products, and can be characterized as a "natural" process (Ozis et al. 2005). The growing desire for sustainability is expected to give a further edge to biofilter systems as an alternative for air pollution control in the existing regulatory climate.

1.1.4 Ethanol Emissions

Ethanol is produced by fermenting and distilling starch and sugar crops such as maize, sorghum, potatoes, wheat, and sugar-cane. Because ethanol is miscible in all proportions with water and with most organic solvents, it has many industrial uses as either solvent, antiseptic, or cleaner in making perfumes, paints, lacquers, inks, household cleaning products, external pharmaceuticals like rubbing alcohol and explosives.

Ethanol is the primary volatile organic compound (VOC) emitted during the leavening process of bread baking. The yeast fermentation of 100 lbs of sugar produces 49 lbs ethanol, which is vaporized and emitted from the oven when the temperature reaches the boiling point of ethanol (EPA 453/R-82-017).

Ethanol is also emitted in significant amounts from the manufacture of beverages, breweries, candy, and confections, and from foundries (Arulneyam and Swaminathan, 2000). Emission sources from chemical processes include heaters and boilers; valves, flanges, pumps and compressors; storage and transfer of products and intermediates; waste water handling; and emergency vents (EPA, Paper #42952).

5

In addition, ethanol has been proposed as green burning fuel additive. In fact, it is the only alternative currently available in large, economically priced quantities, to meet oxygen standards for reformulated gasoline, if MTBE (Methyl Tertiary Butyl Ether) is eliminated from gasoline. Potential consequences for this usage are expected to add more emissions of ethanol to the atmosphere either when it is produced or used.

Goldstein et al. (2002) observed ethanol to be ubiquitously present in the continental boundary layer (Trinidad Head, California) at concentrations typically in the range of 0-10 ppb. In this range, ethanol can be important for PAN formation and ozone photochemistry.

Ethanol is probably one of the earliest toxicants to receive serious toxicological evaluation and metabolic study (James, 1996). Lester and Greenberg (1951) studied human inhalation of ethanol, and showed 62% of the ethanol from inspired air (at concentrations ranging from 11-19 mg/L) is absorbed by the respiratory system. Short term exposures to ethanol are known to induce irritation of mucosal surfaces, central-nervous-system depression, headache, dizziness and nausea (James, 1996). Although it is rare, accumulated experience in workers exposed to ethanol have shown that ethanol inhalation can cause liver injury (James, 1996).

In 1991, National Institute for Occupational Safety and Health (NIOSH), and in 1995, the American Conference of Governmental Industrial Hygienists, Inc.

(ACGIH) and Occupational Safety & Health Administration (OSHA) have set the permissible exposure limit for ethanol as 1000 ppm.

1.2 Biofilter Operating Parameters

The most important operating parameters that influence medium life time and biofilter elimination capacity at the maximum extent include water content, pH, and temperature (Devinny et al. 1999). Other factors having a smaller effect are nutrient concentrations, surface load, contaminant load, oxygen concentration, and air flow direction. In the scope of this research, the effects of water content, pH, temperature and nutrients will be discussed.

1.2.1   Water Content

Water availability is a major determinant of pollution degradation rates (Bohn and Bohn, 1999), and neglecting the water content is identified as the most common cause of poor biofilter operation (Devinny et al. 1999; Bohn and Bohn, 1999; Reyes et al. 1999; Striebig et al. 2001). Water content affects both the physics and biology of the system (Gostomski et al. 1997). Water is essential for the microorganisms' survival and activity. The presence of water also affects the partitioning of contaminants. Therefore, maintaining the proper water content is crucial for successful biofilter operation. Excessive water content can cause a variety

7

of problems. First of all, the air pressure drop increases as water displaces air in the pore space, thereby restricting the air flow. Wet organic biofilter media tend to consolidate, which further restricts air flow. Too much water slows the diffusion and transfer of air contaminants, oxygen, and CO_2 across the water film surrounding the microorganisms. The decrease in oxygen transfer may promote anaerobic zones in the biofilter. In addition, if excessive water leads to free flowing conditions, nutrients can be washed away from the biofilter media, becoming a high strength, low pH leachate that requires further treatment (Striebig et al. 2001). On the other hand, low water content may reduce the sorption of gaseous pollutants or the survival of biological activity (Auria et al. 1998).

Three factors largely control the water content in a biofilter: the humidity of the air stream, evaporation due to the heat generated by microbial oxidation; and the redistribution of liquid water in the biofilter media due to water potential gradient. Moist incoming air, warmer than the biofilter media, can add water as it cools and condenses within the biofilter. The microbial oxidation of organic matter is an exothermic reaction; the heat generated in the biofilter this way can promote water evaporation. Temperature increases from biooxidation have been reported to range from 2° C to 10 ° C (Morales et al. 1998). The third mechanism will not cause a change in the overall water content, but will drive the water through the unsaturated biofilter media and influence the effect of other water loss mechanisms. Gostomski et al. (1997) concluded that among three mechanisms, microbial heat generation and

8

the humidity of incoming air were the dominant mechanisms for water content changes in biofilter.

The optimum moisture content for biofilters depends on the media composition as well as the physical characteristics of the target pollutant(s). For most organic media, optimal water content ranges from 40 to 60% on a weight basis (Auria et al. 1998). For hydrophobic VOCs, moisture in the lower range is more appropriate because of greater mass transfer resistance in the biofilm; however, biofilters for hydrophilic VOCs have higher optimum moisture content (Reyes et al. 1999).

Moisture is best maintained by assuring proper humidification of incoming air, continuous monitoring of water content throughout the media and periodic water addition. Proper humidification, the most important step in the water maintenance, can be done by employing spray chambers, steam injection systems, Venturi scrubbers, or packed-bed towers. The placement of the blower is also important. If the blower is located after the humidifier; compression of the air by the blower increases temperature and consequently decreases the relative humidity in the air (Striebig et al. 2001).

Monitoring of water content can be accomplished by determining overall weight loss, spot checks, or electronically by using time domain reflectometry (TDR). Changes in water content have traditionally been determined by overall weight loss; however, Gostomski et al. (1997) have demonstrated that this method is

9

unacceptable for biofiltration because the moisture content changes are time and position dependent and are associated with many mechanisms that can happen simultaneously; therefore, overall weight change has limited use for identifying localized water content changes. The average moisture content in the bed can be adequate while some sections of the bed are extremely dry. More thorough monitoring of water content in the packed bed can be accomplished by removing cores from the bed, which are weighed before and after drying at 105° C. Water contents, calculated as the mass of the water divided by the total mass, can be expressed on wet or dry weight basis. Wet weight is more common for organic media, and dry weight basis is more used for inorganic media. Confusion about wet and dry weight bases and the difference between inorganic and organic media moisture contents could be resolved if moisture content is expressed by volumetric units. Another way of water content monitoring is TDR, which determines the volumetric water content of the biofilter media by measuring changes in the propagation speed of an electromagnetic pulse in bed material. TDR probes can be placed in biofilter media to provide on-line data without disturbing the process (Striebig et al. 2001). TDR is the most promising method for measuring moisture contents in biofilters, because it is well suited for in-situ measurements and automated data collection, and has been used successfully in biofilter media (Gostomski et al. 1997).

10

Periodic water addition can be performed by an internal irrigation system. Multiple layers of drip irrigation piping, or spray irrigation systems that add water in the direction of the air stream improve the distribution of water.

Auria et al. (1998) described the influence of water content on ethanol degradation in peat biofilter. The average elimination capacity for water contents ranging from 49% to 70% was much higher than that for 35%. When the packing media dried from 70% water content to 59%, they observed the effects of drying were not readily reversible. Bohn and Bohn (1999) have stated that the success of periodic water addition or rewetting is more dependent on water- media interactions than the microbial community. Rewetting is different for hydrophilic (inorganic) and hydrophobic (organic) media, because they have different air-water-solid contact angles. Surfaces like soil or other inorganic media have low to zero contact angles and wet easily. In biofilters that are inadvertently allowed to dry the drying front advances until it reaches the outlet zone and the system fails. Restarting the system may require replacement of the support medium, rather than simple rewetting (Gostomski et al. 1997, Reyes et al. 1999).

1.2.2   pH

The pH of the medium, another crucial factor in biofilter success, is important for both microorganisms' survival and enzyme activity, in particular if the enzymes are extracellular or membrane bound (Wu et al. 1999). Each species of

11

microorganisms has a certain range of pH, in which they are the most active (Devinny et al. 1999). For the majority of microorganisms, the optimum pH for growth is between 6 and 8. Only a few species can grow at pH values of less than 2 or greater than 10 (Son and Striebig, 2000). Fungi as a group are more acid-tolerant; they can predominate in the filter bed at pH 5 or even as low as 2 (Madigan et al. 1997; Marek et al. 2001). However, generally microorganisms do not tolerate pH fluctuations of more than 2 or 3 pH units (Kennes and Veiga, 2001).

Wani et al. (1998), Cox et al. (1997), Webster et al. (1997) and Ergas et al. (1994) reported pH reduction during biofilter operation. The biodegradation of VOCs and other pollutants results in the formation of acidic metabolites such as sulfuric acid or organic acids, all of which in turn may reduce the pH of the biofilter during the process. Devinny and Hodge (1995) reported that accumulation of acidic metabolic intermediates including acetaldehyde, acetic acid, and ethyl acetate during degradation of ethanol in an overloaded biofilter. This reduced the medium pH, inhibiting some of the organisms present and interfering with degradation of intermediates. The ultimate result was an acidified system (pH $\leq$ 4) with poor elimination capacity.

In contrast, biofiltration of styrene (Cox et al. 1997) and alkylbenzenes (Kennes et al. 1996; Veiga and Kennes, 2001) have proven to be possible at low pH values with 95% and above removal efficiency. Webster et al. (1997) reported that compost-biofilter treating acetone, aklybenzenes and hydrogen sulphide could adopt

12

very low pH values without having an adverse effect on performance. Marek et al. (2001) concluded that the lower pH values of peat biofilter bed resulted in higher removal of toluene from the mixture of pollutants.

Some biotransformation processes, on the other hand, may cause pH increase. Chou and Shiu (1997) reported a gradual pH increase in a methylamine-degrading biofilter due to accumulation of ammonia. When the pH was over 8.8, system upset in the biofilter was observed.

Because biofilter performance is often pH sensitive, the majority of researchers have tried to maintain a neutral pH in biofilters. Son and Striebig (2000) have tabulated the pH values from the literature; the range is between 6.8 and 8.5. The best approach for dealing with acids may depend on whether these are final products or intermediates that will soon be converted to non-acidic end products (Devinny et al. 1999). The pH is generally controlled by adding inorganic reagents provided via humidifying or nutrient solution (KH_2PO_4, K_2HPO_4, NaOH, $NaHCO_3$), with or without a buffer additive like crushed oyster shells, $CaCO_3$ present in the packing media.

Wu et al. (1999) concluded that urea might be an attractive alternative as an aqueous nutrient to control both the pH and the biomass accumulation in the filter bed. Urea controls the pH through its buffering capacity and biomass accumulation because ureases are genetically expressed when nitrogen is limiting. Once urea is metabolized, NH_4^+ becomes available for those strains that are unable to decompose

13

the added urea. Control of both the pH and the biomass accumulation in the filter bed make the process more stable and dependable.

Several researchers have concluded that acidification is accelerated by low moisture content in the biofilters (Cardenas-Gonzalez et al. 1999; Son and Striebig, 2000).

1.2.3 Temperature

Microbial activity, and therefore, biofilter removal efficiency are greatly affected by temperature; the optimum biofilter temperature should be determined according to the species present. If the temperature is too low, the metabolism will be slow; some species may become inactive while others die. Most chemical reaction rates approximately double when temperature increases by 10° C (Devinny et al. 1999); however, as temperature increases, each microbial species reaches a point where necessary functions cease because of the heat. Klasson and Davison (2001) studied temperature effects on a nitric oxide biofilter; when temperature was increased to 50° C, the reactor stopped converting NO, leaving the effluent and the influent gas compositions the same.

Sorial et al. (1997) studied the impact of temperature on removal of toluene in a peat biofilter. The EBRT was 2 minutes and toluene loading was 50 ppm$_v$, and the performance was sensitive to temperature changes. With the increase of temperature from 11.1 to 15.6° C, the original biofilter removal efficiency of 58%

14

was increased to 77% first, and stabilized at 63%. Then, as the temperature gradually increased to 21.1° C to 26.7° C, the performance of biofilter increased to 83%-87%, and 96% respectively. Conversely, some authors have observed a less significant influence of temperature on biofilter performance. Prado et al. (2002) performed experiments on toluene removal in a perlite biofilter; biofilter performance basically remained unchanged between 25 -33° C. Similarly, Darlington et al. (2001) observed that between 23 and 26° C, the temperature did not affect the performance of biofilter degrading toluene, ethylbenzene and xylene, although the biological activity started decreasing at 20° C. Cox et al. (2001) reported that two biofilters working under a wide temperature range; one operating at 22° C and the other at 53° C had similar ethanol removal efficiencies.

Unfortunately, control of temperature in biofilters is often limited to control of the temperature of the incoming waste air, and in many cases this is not economically feasible. The radial temperature gradients in biofiltration systems have been observed previously by Deshusses et al. (1997) and Gostomski et al. (1997); with the outside of the media is cooler and moister than the inside due to heat exchange with the surroundings. Under these circumstances insulation of ducting, and/or biofilter itself may ensure more stability.

1.2.4 Nutrients

The nutrient content in the biofilter medium is necessary for growth, enzyme activity, membrane transport and above all, for biodegradation of pollutants. Inadequate amounts of nutrients inhibit the microbial activity and ultimately reduce the elimination rates in biofilter. Carbon, oxygen, nitrogen, phosphorus and hydrogen are among the basic elements required. Carbon and oxygen can be obtained from the waste air. Organic media typically serve as nutrient reservoirs and may supply adequate nutrients in available form. In contrast, inorganic and synthetic media require addition of appropriate nutrients either in the form of an aqueous solution or as slow release fertilizers.

Prado et al. (2002) tested several methodologies to supply nutrients to a down-flow perlite biofilter treating toluene, and concluded that not only the water content but also the nutrient content will remain high enough for at least one month without any addition of aqueous nutrient solution. However, after start-up, the periodic supply of a nutrient solution remains a prerequisite to maintain high efficiency during the life of biofilters (Prado et al. 2002).

Togna and Singh (1994) observed a decrease in performance from 70% to 10%, after 200 days of operation of a peat moss biofilter treating isopentane. They suggested nutrient limitation as one of the possible reasons for a decrease in performance of their biofilter.

16

Similarly, Morgenroth et al. (1996) studied removal of hexane in a compost biofilter. After 33 days of operation, the hexane removal efficiency reached 85%, but then decreased to 50% as operation continued. Two different nutrient solutions were used. SOL #1 included 13.1 g/L KNO_3 and 13.8 g/L KH_2PO_4, and SOL #2 included 131.1 g/L of KNO_3, which was ten times the amount in SOL #1. One liter of SOL #1 was added on 82nd day of operation. Removal efficiency increased to 60%, and decreased again. After highly concentrated nutrient solution (SOL #2) is added, the removal efficiency increased to > 99% and stayed steady for the following two months for inlet concentrations of 200 ppm_v.

Nitrogen makes up about 15% of the dry cell weight and is a major constituent of proteins and nucleic acids (Morgenroth et al.1996). Wu et al. (1999) correlated lower nitrogen concentrations in the nutrient solution with the lower filter bed elimination capacities. They also concluded that nutrient supplies have greater effect on the bed performance than has microbial inoculation.

Gribbins and Loehr (1995) reported that toluene elimination rates increased with increasing soluble nitrogen concentration in the compost-perlite biofilter media.

Pérez et al. (2002) studied the influence of sequential mineral nutrients addition to a sugar cane bagasse biofilter degrading ethanol. They have first used ammonium sulfate as the N-source, and then ammonium hydroxide. The results clearly showed that both N-sources were able to restore biomass growth, and thus the elimination capacity.

17

The literature shows addition of nutrients during biofilter operation may be necessary to maintain optimum removal over a long period of time regardless of the media type. However, the supply of nutrients should be optimized somehow either at low concentrations or at relatively low frequency in order to slow down biomass accumulation that might otherwise generate high pressure drops.

Prado et al. (2002) combined nutrient supply with a biomass control strategy, using air sparging, without causing any adverse affect on biofilter performance when compared to supplying nutrients alone.

18

2 RESEARCH OBJECTIVES

2.1 Numerical Model for Clogging in Biofilters

Biofilters succeed because microorganisms present in the filter use the contaminant as food, or substrate. The compound may serve as energy source or building material, or both (Devinny et al. 1999). In a well-designed biofilter, a large active biomass must be available to carry out rapid biodegradation (Barton et al. 1997). Although microorganisms strive to grow and reproduce, under many circumstances almost half of the carbon from the compound end up being converted into biomass (Devinny et al. 1999).

Previous experience has shown that the conditions most favorable for successful biodegradation are equally contribute to excess biomass formation and clogging (Hodge 1993; Van Lith et al. 1994; Weber and Hartmans 1994; Torkian et al. 2002).

Biofilters operate as plug flow reactors; concentrations of compound decline as the air passes through the biofilter leaving higher concentrations at the inlet section (Devinny et al.1999). Therefore, characteristics of microbial flora change accordingly. Microbial populations were found to be distributed such that higher biomass densities existed nearer the inlet of the column, where growth continued till clogging occurs or till nutrients become limiting (Devinny et al. 1999; Ergas et al. 1994; Medina et al. 1995)

19

Biomass accumulation leads to change in bed characteristics in terms of spatial distribution of microbial populations, reduction of interparticle void space and compaction of natural packing materials, which further cause channeling and increased pressure drops (Spencer and Alix, 2003; Morgan-Sagastume et al. 2001). Channeling let the contaminated air pass through the medium untreated at a higher rate than biofilter design, therefore cause removal deficiency, and in some cases fouling. Van Lith et al. (1994) and Weber and Hartmans (1994) reported waste gas treatment using biotrickling filters is seriously hampered due to excessive biomass formation. Torkian et al (2002) observed high microbial growth and consequent excessive pressure drops because of high loading rates of Toluene and Xylene.

Consequently, the prevention or remediation of clogging in a biofilter application is essential for its success. Investigations into this field have been numerous in the literature. It is possible to imagine biofilters in which excess biomass is removed by washing, chemical dissolution, or implementing short periods of starvation by controlling limiting nutrient. Sorial et al. (1994) operated trickle bed biofilters with different backwashing flow rates to control biofilm thickness. Backwashing was first utilized at 100 liters at 6gpm for ½ hour period once a week. As of day 45, backwashing was performed with 200 liters of water twice a week 6 gpm. The contaminant removal rate stayed constant at 99%. Alonso et al. (1997) also removed the excess biomass via full media fluidization and backwashing of the biofilter. Van Lith et al. (1994) have demonstrated the effect of salt introduction to

20

control excessive biomass. It has been shown that increasing salt concentration leads to growth rates of biomass being reduced more than decomposition rates of the compounds of interest. Weber and Hartmans (1994) have employed nutrient limitation with the ionic strength to prevent clogging. Cox and Deshusses (1997) utilized protozoan predation to decrease biomass yield in toluene degrading biotrickling filters. Protozoa have a tendency to grow in suspension and were easily flushed out of the system via continuous purge of the scrubbing solution.

Each of the above described biofilm growth control processes, however, requires expensive operating techniques and equipment or decreases the rate of pollution degradation - a packed bed is a simple and inexpensive system. In the long run, biomass clogging remains an important limiting factor in biofilter applications. Perhaps the most significant disadvantage biofilters face in competition with other air pollution control technologies is their large size. For a given discharge, reduction in size implies increase in the pollutant load per unit volume, but biofilters treating large amounts of contaminant experience correspondingly rapid growth of biofilm that results in clogging. A complete understanding of the clogging process, and ultimately its control, would increase biofilter efficiency and broaden the range of applications.

This work concentrated on creating a numerical model, which applies Percolation Theory to the clogging phenomenon in biofilters. Percolation theory has

been well developed to understand similar problems in fields such as oil recovery and catalyst bed design.

Whether the additional expense of more elaborate systems with specific biofilm growth control will be justified depends on the attendant improvement in efficiency and the associated reduction in biofilter size. This developed model may be able to predict those improvements, and help guide development of new biofilter designs.

The strategy of this research was to device experiments that included two biofilters with different media and pore size characteristics, but degrading easily biodegradable ethanol till clogging happens.

22

3 PERCOLATION THEORY CONCEPTS

3.1 Literature Review on Percolation Theory

Percolation theory is a very powerful tool that has emerged to account for the important role of connectivity in both macro and microstructures. Over the past two decades the theory with its extensions (including Invasion, Gradient, Directed and Correlated Percolation) served as a key to understanding and modeling a wide variety of phenomena in disordered systems. Examples include earthquakes, and fracture-fault patterns, single-or two phase flow in porous media, properties of branched polymers and gels, hopping conductivity in semiconductors, percolation aspects of antigen-antibody reactions in immunological systems (Sahimi, 1994) or habitat fragmentation in ecosystems (Boswell et al. 1998).

Broadbent and Hammersley (1957) were the first to initiate the mathematical study of a fluid spreading randomly through a medium, where "medium" and "fluid" terms were abstract and could be interpreted according to context. In contrast to the well-known diffusion process, in percolation process the underlying randomness was ascribed to the multidimensional medium itself. To make the problem mathematically tractable, the medium was generally taken to have a regular lattice structure.

In the original formulation by Broadbent and Hammersley (1957), which is also called Ordinary Percolation (OP), two different random mechanisms, site

23

percolation and bond percolation, were considered. In the site percolation, each site independently has a probability p of being open and probability (1-p) of being closed, or blocked. The fluid flows along the bonds (subject to orientation) to open sites only. On the other hand, in bond percolation, fluid flows along the open bonds only (having a probability of p of being open, and again subject to orientation). In both cases, the idea is to make probability statements about the set of sites reached by the fluid. In many cases these two conformations can be converted to an equivalent problem in the other formalism (Yortsos, 1997). However, not every site problem can be converted to bond problem; in this sense the site problem is more general. It was selected for use here.

OP theory states the existence of a finite percolation threshold (p_c), where a phase acquires (or losses) macroscopic connectivity for the first time (Yortsos, 1997). To be definite, take an example of 2-dimensional square lattice of size (L×L). Assume that at random a fraction of sites is blocked (removed), so that remaining fraction of open pores is p (0< p <1). As long as $p<<p_c$; although the occupied fraction varies smoothly, the largest connected cluster of occupied sites stays as very small-finite size, and there exists no connected path of occupied sites that traverses the network from one end to the other. However, when open pore fraction reaches or exceeds the percolation threshold (p_c), a sample spanning ("infinite") connected cluster first develops in sharp transition, and macroscopic flow takes place (Yortsos, 1997).

24

The existence of a threshold is assured regardless of the particular lattice used; however, the numerical values of the percolation thresholds are sensitive to the lattice type (Yortsos, 1997). Higher coordination numbers (Z, number of bonds that emanate from a site), lead to better connectivity, and lower percolation threshold when defining first macroscopic flow to take place. The second fundamental characteristic of the OP model is the dependence of the various quantities on the distance from the critical point (p_c), where scaling laws should be observed.

Advances of the original work by Broadbent and Hammersley (1957) came with understanding its importance; studies by Morrow (1970), Melrose and Bradner (1974), Chatzis (1977), and Dullien et al. (1979) have developed essential features of percolation. Later, Lenormand and Bories (1980), Chandler et al. (1982), and Wilkinson and Barsony (1984) captured the additional features of the invasion process. In the Invasion Percolation (IP) model, the network is initially filled with the fluid to be displaced. In contrast to OP, where growth of the new phase occurs internally, IP describes constant rate invasion of the displacing fluid that is injected into the medium from a side and displaces the defender at each time step by choosing the site on the interface that has the smallest random number. Therefore it is an inherently dynamic process (Sahimi, 1994; Yortsos, 1997). At the moment a cluster reaches the exit face, a sample spanning cluster has formed. Wilkinson and Barsony (1984) have shown that IP clusters and OP clusters are the same for both two and three dimensional cases. Therefore, they belong to the same universality class,

25

having many quantities and scaling ratios in common. However, from a fundamental point of view, invasion percolation was viewed as more appropriate model to describe immiscible displacements than the ordinary percolation model (Sahimi, 1994).

Both in OP and IP, percolation processes were viewed in random and statistically homogenous media, where randomness determines the spatial correlations; however in almost all practical applications there is a gradient component, which changes the fraction of the accessible pores along the media. Percolation in gradients can be treated either as Ordinary Percolation in a Gradient (or simply Gradient Percolation, GP), or Invasion Percolation in a Gradient (IPG).

There exist other extensions of percolation theory including correlated and directed percolation; however, here I would like to account for the ones that are closer in spirit to what is going on in biofilters.

Percolation theory examines two- or three-dimensional arrays of elements that may or may not be connected with adjacent elements. Investigators consider how many clusters of connected elements are present as a function of the total number of connections, and how large the clusters are likely to be. In particular, the number of connections necessary to make it likely that a cluster will span the entire array is determined. It has been used successfully for determining fluid flow properties in natural porous media like oil reservoirs because a pore network is the most representative model of a porous medium (Yortsos, 1997).

26

The quantities that are significant for transport in porous media include percolation probability and conductance. The percolation probability is the fraction of sites occupied by the infinite cluster. When fraction of open pores, p is below the threshold; probability is identically zero; however, when p_c is exceeded probability rises sharply to nonzero values (Yortsos, 1997). The conductance of the medium is the ratio of total flow across the lattice to the applied potential difference. However, the conductivity (flow permeability), which will be explained later on, is of more fundamental interest to our context.

3.1.1 Effective Medium Approximation (EMA)

A powerful approach to transport properties in disordered systems is the effective medium approximation (EMA), which tries to eliminate the difficulty of incomplete knowledge and uncertainty in properties, by averaging the quantities (Yortsos, 1997). It has been applied with considerable success to conduction in mixtures, various alloy problems, and various other transport and optical properties (Toledo et al. 1992).

Gupte and Tsamopoulos (1990) have used the effective medium approach to determine transport coefficients in a model describing densification of porous ceramic cylinders by chemical vapor infiltration of a gaseous precursor. Their predicted values were close to the experimental observations.

27

A version of the effective medium theory appropriate to isotropic random networks was introduced by Kirkpatrick (1973). As long as very low values of conductance do not dominate the system, most elements have a similar conductance; the effective conductance (g_m) of the network can be identified by solving the following integral equation. The total derivation can be seen in Kirkpatrick (1973).

$$\int_0^\infty G(g)\left[\frac{g_m - g}{g + (z/2 - 1)g_m}\right]dg = 0 \qquad (3.1)$$

where G (g) is the conductance distribution, Z is the coordination number. The potential across any conducting bond can be expressed as the superposition of a uniform external field and a local fluctuating field, the space average of which over a sufficiently large volume is zero. Therefore, all bonds in the network can be replaced by bonds of the same conductance, g_m, the value of which is calculated by requiring that the average of the local fluctuations be zero. Potential difference corresponds to pressure difference, and higher the pressures produce higher flows. Therefore, conductance distribution is a function of open pores, and trivially related to the size distribution. In this work, conductance was presumed proportional to the cube of the pore radius.

3.2 Applications to Porous Media and Biofilters

Percolation theory can define and work with both open and closed pore clusters to model macroscopic flow existence or disappearance. For the transport in porous media three major needs are served by Percolation Theory:

i. The determination of the distribution of phases in processes, where local equilibrium criteria dictate the pore space occupancy

ii. The determination of transport coefficients such as conductivity

iii. The understanding of deep-bed filtration processes (Yortsos, 1997).

Application of percolation theory to two-phase immiscible flow requires accounting for additional forces, the surface forces at fluid-fluid and fluid-solid interfaces, or capillarity. Many processes pertinent to engineering operations involve the physicochemical interactions of fluids with solid surfaces, where operation is usually characterized by continuous reduction of the available surface area. Yortsos and Sharma (1986) have used percolation theory to explain non-catalytic gas-solid reactions, which result in reduced surface area as well as pore closure. They have applied a special type of lattice, the Bethe lattice, which does not admit reconnections between two points. Closed from expressions for plugging times were developed for Poisson, Gaussian, and Rayleigh pore size distributions for different coordination numbers.

29

In this work we followed the approach based on a network representation of the porous medium. The population balances and elements developed by Yortsos and Sharma (1986), which accounts for the effect of geometrical (e.g., pore size distribution) and topological (e.g., connectivity, accessibility) aspects of the porous media on the evolution in time of the above quantities, were combined with the biological growth models, which simulate the clogging of pores.

Although clogging in porous media could result from non-biological sources such as chemical reactions leading to the formation of a solid phase (Yortsos and Shankar, 1984), noncatalytic gas-solid reactions (Yortsos and Sharma, 1986), or mechanical clogging of pores due to particles in fluid flow (Kaiser, 1997; Datta and Redner, 1998); some considered biological clogging (Cunningham et al. 1991; Dupin and McCarty, 2000; Kim and Fogler, 2000; Thullner et al. 2002). These studies focused on the interrelationship between porous media hydrodynamic properties including porosity, permeability, and the accumulation rate as well as spatial distribution of biofilm, and they observed significant reduction of hydraulic conductivity of porous media due to biomass clogging.

The effect of biomass accumulation on the pressure drop studied by Morgan-Sagastume et al. (2001, 2003) and modeled by using Ergun equation. It was observed that the pressure drop decreased as flow channels developed in the medium.

Several models have been introduced to simulate the observed relationship between biomass growth and the hydraulic properties of the porous media. The

30

general assumption, though, was the homogeneous biofilm covered surfaces of the bundles of parallel plate pores (Taylor et al. 1990; Vandevivere et al.1995; Clement et al. 1996). It is worth noting that the limiting model of parallel bundles, corresponding to coordination number (Z $=\infty$), has a zero percolation threshold (Yortsos, 1997). The discrepancy between model predictions and experimental results of these studies concluded that using pore networks instead of pore bundles would account for inter-pore connections better (Loehle and Johnson, 1994; Vandevivere et al. 1995). Suchomel et al. (1998) introduced a pore network model that was assuming the growth of biofilm on the walls of cylindrical pores successful to reproduce experimental results. Kim and Fogler (2000) were mostly studying the effect of shear forces and starvation. The study successfully reproduced experiments with pore network simulations. Dupin and McCarty (2000) were able to show that the morphology of microbial growth depends on the pH-value, and concluded that their results could be explained by pore network model having biofilm growth in aggregates.

Recent study by Thullner et al. (2002) also used pore network model, namely a bond percolation model, as a tool to simulate hydraulic changes in porous media resulting from biomass growth. The model was accounting for two dimensional inter-pore connections, and different morphologies for biofilm growth. The growth of the microorganisms was not only coupled to the concentration of a nutrient in the pores but to the radius of the pores in order to be able to define growth in aggregates.

The net change of biomass was including shear force detachment; however, it was shown that that was not a dominant process under their case of constant head that creates decreasing flow velocity in the pores. No diffusive processes were included in the equations of the model to describe the transport of a solute within pore grid because of its small influence on the results of the simulation. Their significant finding was that the decrease in hydraulic conductivity was strongly under-predicted by a biofilm scenario (whole coverage) for grain sizes below 1 mm. Whereas, the reduction in hydraulic conductivity for a grain size 1mm was only slightly over-predicted by biofilm scenario. Therefore, they have concluded that for porous media with grain sizes below 1 mm, a better assumption is that the biomass is growing in colonies and not in a biofilm (Thullner et al. 2002).

To the best of our knowledge, application of network models to biofilter media started with Schwarz et al. (2000), who introduced a pore network model to understand the effects of biomass growth at the pore network level, and hence, account for large scale heterogeneities in the biofilter media. The model has shown that both biofilter removal efficiency and the pressure drop strongly dependant on the beds' evolving pore network structure (Schwarz et al. 2001). Additionally, the model was used to describe biofilter operation parameters like biomass axial gradient, surface area, and residence time distribution (Schwarz et al. 2001).

Nukunya et al. (2002) applied a version of the model developed by Schwarz et al. (2000, 2001) to explain behavior of a bench-scale biofilter treating ethanol. In

32

the model, the biofilter pore structure was described by a cubic lattice of cylindrical pores of uniform length and varying diameters. One of the input parameters of the model was the matrix dimensions representing the porous media; the computation time needed for the model restricted the application of the model. While only a small portion of the biofilter could be modeled, it was believed to be representative. Although the first couple of days of operation, where the sharp increase in removal efficiency is usually seen, were modeled quite closely, the model predictions deviated from the experiments later on when the effect of clogging was more significant. An important factor not included in the model was the death or deactivation of biomass (Nukunya et al. 2002). Model predictions for pressure drop were both later and smaller than actual values, which reflected inaccuracy of pore size distribution used in the model (Nukunya et al. 2002). Later on, Nukunya et al. (2005) has employed the same pore network structure but following an experimentally determined pore size distribution. The model also assumed that at the pore level biomass growth depends on the oxygen diffusion in the biofilm and on oxygen-limited Monod type kinetics. The model seemed to better account for biomass growth in the biofilter and its interaction with airflow distribution. The simulation results were in reasonable agreement with the experimental data from a bench-scale biofilter (Nukunya et al. 2005).

Percolation theory was first applied to define and characterize the biofilter medium by Shariati (2000). Particular features of percolation theory for biofilters

33

were common to previously investigated processes in which reduction of the surface area available for two phase interaction led to decrease of the capacity for flow, diffusion, and reaction, progressively lower rates of conversion efficiency, and ultimately to pore clogging (Yortsos and Sharma,1986). Shariati et al. (2000) have described initial efforts to determine conditions under which percolation theory is applicable to biofiltration. The porous medium was represented with a connectivity of 6, combining pore throats and pore bodies. Rate at which individual pores close determined by the geometry of the pore (flat plates and cylinders) and the growth kinetics, which were presumed proportional to existing biomass volume or surface area (Shariati et al. 2000). As the process evolves, the pores will fall into three classes: those that are filled, those that are open and accessible to flow, and those that are open but inaccessible to flow. Shariati et al. (2000) determined these population balances, and the plugging time of the pores. A Poisson distribution was used to represent pore size distribution in porous media; the theoretical results for evolution of accessible surface area, biomass volume, and permeability relative to their initial values were shown. The decline of all these quantities as the plugging time is approached was evident (Shariati et al. 2000).

3.2.1 Other Models for Biofilters

Although predictive mathematical models have been available for a wide variety of biological systems, development and verification studies of models for

34

biofilters remain sparse in the literature. Hence, they are not currently used to predict biofilter behavior or to design biofilter systems. The goal of biofilter modeling was to understand the physical processes involved in "black box" system of biofilters. The first biofilter model was developed by Ottengraf and Oever (1983), and was fully described by Ottengraf (1987). The steady state homogenous biofilter model employed a Michaelis-Menten expression for zero order biodegradation. Ottengraf's model has been experimentally verified in many studies and can be used to at least estimate treatment rates for several compounds. However, the model is simple and has some limitations, including not accounting for oxygen limitation. Shareefdeen and Baltzis (1994) extended the model conceptualization of Ottengraf and coworkers by distinguishing among gas, solid, and liquid phases in biofilters. Their expression included diffusion limitation by methanol, and biokinetic limitation by oxygen. Deshusses et al. (1995) have developed a model to describe both steady-state and transient-state dynamics of a biofilter to describe biodegradation of Methyl Ethyl Ketone (MEK) and Methyl Iso Butane Ketone (MIBK), but did not account for biomass growth. Subsequently, Hodge and Devinny (1995, 1997) introduced axial dispersion coefficient in their first order, variable input concentration kinetics model for biofilter treating ethanol. Chitwood et al. (2002) developed a steady-state computational fluid dynamics model to study the effect of flow heterogeneity on the removal efficiency. The model predicted a reduction in removal with higher flow heterogeneity. This model also did not account for the effects of biofilm growth.

35

The models discussed above showed a good predictive capability for their respective model compounds. However, they were limited by employing flat plate structure for the biofilm. Traditional biofilter models also make use of effective properties including average bed porosity and pore size, therefore; for the most part they are incapable of accounting for the geometry and topology of the porous medium, i.e., its pore size distribution and connectivity. Both of these are means to understand non-uniform biomass growth, and the clogging that result in channeling of flow.

Alonso et al. (1997, 1998) developed a model that accounts for biomass growth in biofilters and biotrickling filters. The biofilter was described as a plug flow reactor, and the pore space was considered to form of parallel tubular pores, parallel slit-type pores, or uniformly packed solid spheres. This model accounts for the importance of the changing biofilm surface and the thickness, which are particularly important when biodegradation is controlled by diffusion in the biofilm. However, they were unable to predict large-scale flow inhomogeneities, which are often faced in biofilters.

Several models tried to predict biofilter performance by molecular aspects of the treated compounds (Choi et al. 1996; Johnson and Deshusses, 1997; Govind and Briggs, 1997; Devinny et al. 1997). These quantitative structure activity relationship (QASR) models seek to describe elimination of particular chemicals based on their chemical bond structure, partition coefficient, and diffusivity. However, reactor

36

properties such as porosity, pore structure, and humidity are entirely neglected. By recognizing the significance of pore size distribution and connectivity, network models of porous medium are capable of describing unique characteristics of biofilters.

This study uses Shariati's percolation model, including continuous mathematics, as a base and develops discrete forms of the formulation so that any pore size distribution can be included in the model. Because the pore structures in biofilters can be very different, depending on the support material used for biomass growth, and because they can be determined exactly, this model will open the possibility for more rational design of the biofilters.

3.3 Characterization of Biofilter Media in Numerical Percolation Model

The proposed study has applied percolation theory to biofilters by considering the air-filled space in the packing to consist of nodes connected by pores. A new biofilter is a single cluster of nodes, connected by open pores, that spans the distance from the input to the output of the biofilter. As biofiltration proceeds and biomass accumulates, the smaller pores are filled with biomass. Further, some pores that have not been filled become isolated from the airflow because the surrounding pores are filled (Figure 3-1).
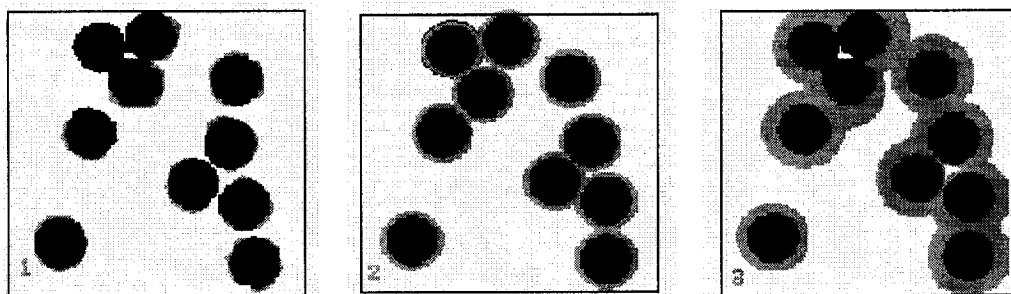
Figure 3-1: Evolution of pores in the biofilter process. 1) at time (t=0), all the pores are open, and accessible to flow with initial biofilm layer surrounding the particles, 2) Biofilm starts to grow on surfaces, 3) Some pores become filled, some become isolated, as remaining stay open.

Blocked and isolated pores cannot carry air or contribute to treatment, so pollutant removal efficiency declines and flow resistance increases. As biomass growth proceeds, more of the biofilter becomes unavailable, and ultimately there is no cluster of open pores spanning the biofilter medium—the biofilter is completely clogged.

Understanding the process requires a means to calculate the number of filled and isolated pores, i.e. population balances, and the surface area or volume of biofilm that remains available to contribute to treatment.

38

3.4 Modeling of Biofilter Using Percolation Theory

3.4.1 Numerical Model for Population Balances

A model that closely followed models developed by Shariati et al. (2000) and Yortsos and Sharma (1986) was created to numerically solve the equations of percolation theory. It divides the pores in the biofilter medium into N size classes, with a normalized pore-size distribution function, f (n), describing the fraction of pores in each class. Biofilm growth was modeled in time steps chosen such that the increment in biofilm thickness is equal to the increments in pore radius. Thus, at each time step, pores in the smallest size class that are available to air flow are filled with biomass. The size distribution of the remaining pores is adjusted to reflect the accumulation of biomass. Throughout the calculation, pores may be open, filled, or isolated. Isolated and filled pores are permanently removed from the calculation and they make no further contribution to treatment (Figure 3-2).

The portion of the total number of pores that is available, A(n), is the same for all size classes at a given time, but declines as time passes and pores are filled, increasing the likelihood that an unfilled pore will be surrounded by filled pores.

39
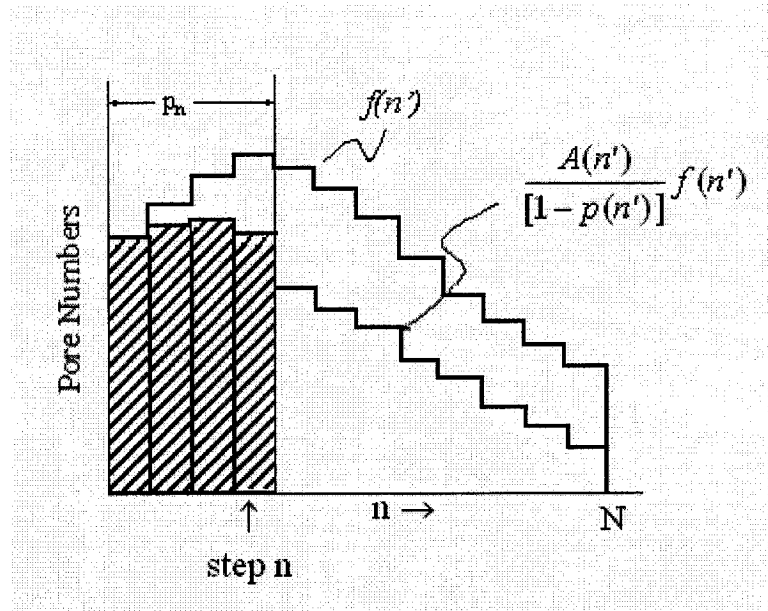
Figure 3-2: Schematic of calculation for pore distribution as the biofilm thickens.

p(n) is the number of pores with radius less than or equal to the biofilm thickness—the number that would be filled if none had been made inaccessible. Thus the fraction of pores available to contribute to the treatment process, $X_a(n)$, is

$$X_a(n) = A(n) \sum_{n'=0}^{N} f(n') = A(n) \qquad (3.2)$$

A(n) depends on the number of connections each pore has with others. For the calculations done here, the coordination number (Z) was assumed to be six, as it is for a cubic lattice of pores. The number of isolated pores as a function of p(n) cannot be calculated directly, but has been determined through computer

40

simulations. For this calculation, the function for A(n) was developed by using the data in Kirkpatrick (1973).

A(n) can be defined in three sections of p(n):

$p(n) > p_c;$ $\quad A(n) = 0$
$0.6 < p(n) \le p_c;$ $\quad A(n) = -201.55p(n)^3 + 394.39p(n)^2 - 258.36p(n) + 56.97$ $\quad$ (3.3)
$p(n) \le 0.6;$ $\quad A(n) = 1 - p(n)$

Once pores are isolated, no more biofilm growth can occur within them. The number of pores filled at each step is equal to the number that is available in size class n. The total number of filled pores is the sum of f(n) multiplied by the fraction of pores that was available at each step:

$$X_f(n) = \sum_{n'=0}^{n} \frac{A(n')}{[1 - p(n')]} f(n') \qquad (3.4)$$

where the notation n' indicates that a sum over other values of n is being calculated to determine values at step n.

Finally, the pores that are not available are all of those that are neither filled nor available:

$$X_{na}(n) = 1 - X_a(n) - X_f(n) \qquad (3.5)$$

41

One advantage of the percolation model is that the sub models for biomass growth and pore clogging are essentially separate. Biofilm thickness is determined as a function of time, while clogging is determined as a function of biofilm thickness. Thus any model for biofilm growth that relates growth to time can be coupled with the clogging model. This study has employed two different biofilm growth models.

3.4.2 Biofilm Growth Models

3.4.2.1 Surface Area Limited and Volume Limited Models

As the first trial, two assumptions for biomass growth were used for separate calculations. In one case the growth rate was assumed to be proportional to the available surface area of biomass, as would be appropriate for phase transfer limitation, or if only the biomass very near the biomass-air interface were active (Figure 3-3). Biofilm thickness increases linearly with time. In the second case, biofilm growth was presumed to be proportional to the volume of biomass present, as would be appropriate when there is no transfer limitation and all of the biomass is equally active. In this case, biofilm thickness increases exponentially. It was also necessary to assume a small initial "inoculum" of biomass, because an initial value of zero would have produced no growth.

42
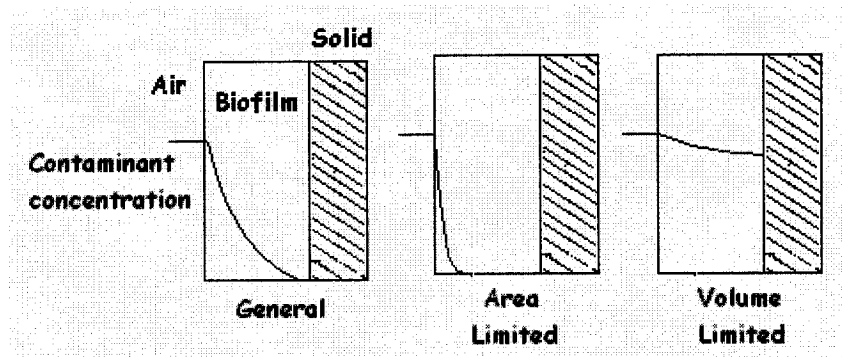
Figure 3-3: General case, where at any point in the biofilm, the rate of consumption is proportional to contaminant concentration (first order), therefore the result is an exponential decline in concentration. The other cases represent area limited, and volume limited biofilm growth models, respectively.

Typical values for growth constants in the case of ethanol degradation and porous packing surface areas were taken from Deshusses and Cox (2000) and Shareefdeen et al. (1993), Table 3-1.

Table 3-1: Percolation Model Parameter Values

Parameter	Description	Value	Unit
r	Pore radius	0.003-0.3	cm
K	Ethanol degradation constant for surface limited case	9.72×10^{-9}	cm/s
K_v	Ethanol degradation constant for volume limited case	8.33×10^{-7}	1/s
Z	Coordination number	6	-
p_c	Percolation threshold	0.75	-

Two pore conformations were investigated. Pores were first modeled as parallel plates with biofilm growing on both surfaces, so that the pore was filled

43

when the biofilm thickness (r_i) equaled one-half the separation between the plates (r_o). In the second case, pores were taken as cylinders with growth occurring on the curved surfaces, so that the pores filled when the biofilm thickness (r_i) equaled the radius of the cylinder (Figure 3-4).
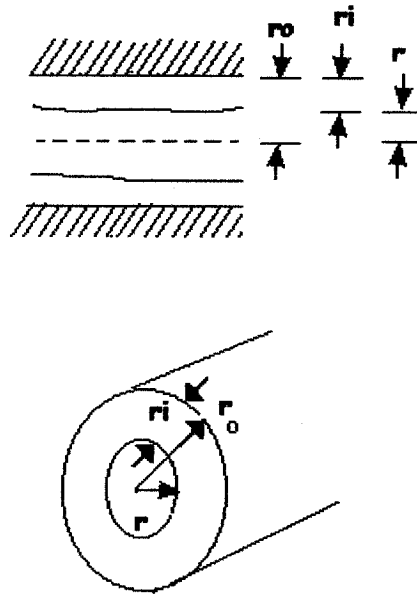
Figure 3-4: Pore configurations used in numerical model, top is flat plate pore and the bottom is cylindrical pore

The two cases of pore conformation were combined with the two cases for biofilm growth rate to create four models presented here. For surface-limited growth on flat plate pores, growth was linear. This was also true for surface-limited growth in cylindrical pores, because the decline in available surface that occurs as the pore narrows is matched by the decline in amount of biofilm growth needed to increase

44

film thickness. In the biomass volume-limited case, both pore conformations produced exponential growth. For the details of the numerical calculations please see appendices.

Comparisons of model characteristics were made for a series of lognormal pore size distributions of the form:

$$f(n) = \frac{1}{n\sigma\sqrt{2\pi}} \cdot \exp{-\frac{1}{2}\left[\frac{(\ln(n) - \mu)}{\sigma}\right]^2} \qquad (3.6)$$

where μ is the location parameter and σ is the shape parameter. In each case, the distribution was truncated at $n = 100$ and renormalized so that the sum of f(n) = 1.

Biofilters are less prone to clogging when the pores are uniform in size. To illustrate the effects of pore size distribution, a hypothetical biofilter was modeled in which all of the pores were cylinders of the same radius, 0.3 cm. It was presumed that the ends of the pores made no contribution. For this case, biofilm surface area declines as the biofilm grows, because the air-filled radius of the pores declines, and all of the pores are blocked simultaneously when the thickness of the biofilm equals the radius of the pores. No isolation of pores occurs because no pores were filled until the last instant. The derivations of the equations used in the model can be seen in Appendix I.

45

3.4.2.2 Cellular Automaton Model

Recent work by Song and Kinney (2002) has shown biomass growth and its effect by introducing a model including cellular automata (CA) algorithm that was previously developed by other groups (Noguera et al. 1999; Picioreanu et al. 1998, 2000; Pizarro et al. 2001). Song and Kinney (2002) assumed that the total biomass can be divided into active and inactive fractions, and used CA algorithm to describe the developing biofilm, including details of how film activity changes as a function of depth in the biofilm.

In our work, the CA model was linked to the percolation model in a way that allows modeling of growth and activity within the biofilm in conjunction with the effects of changes in the pore size distribution and pore blockage. This model was run for the same pore size distributions used previously, but for the cylindrical pores case only and published in a conference proceeding (Ozis et al. 2004c).

The biofilm growth model described in this study follows closely on that developed by Song and Kinney (2002). The biofilm was treated as a series of layers, in which the active biomass is presumed to grow according to the Monod equation and also dies at a rate proportional to the amount present:

$$\frac{\partial X_{act}}{\partial t} = \frac{\mu_m C}{K_s + C} X_{act} - k_d X_{act} \qquad (3.7)$$

46

where X_{act} is active biomass density, μ_m is the growth constant, K_s is the half

saturation constant, C is the concentration of the substrate and k_d is the death rate

constant. Inactive biomass is formed at a rate proportional to the rate of death of the

active biomass. Net growth accumulates, and when total biomass in the existing

layers exceeds a chosen limit, a new layer is formed (Figure 3-5).
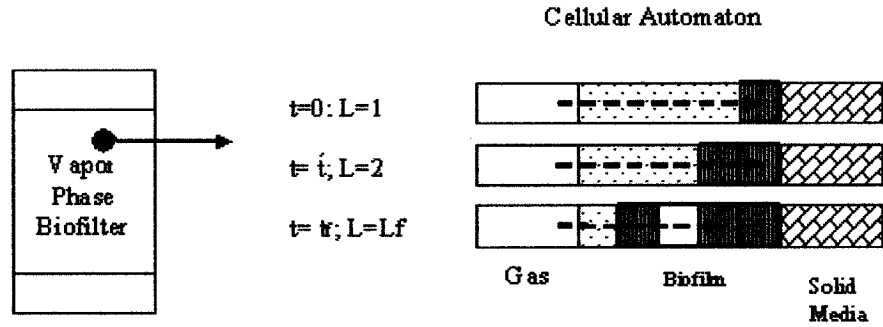
Figure 3-5: The description of the numerical domain used for the cellular automaton approach, adapted from Song and Kinney (2002). The dashed arrows represent the pollutant diffusion into biofilm layers.

Contaminant diffuses into the biofilm from the surface, while degradation

consumes contaminant within the layers, so that concentrations are highest in the

surface layers and lower in deeper layers. The change in concentration in any layer

is given by:

$$\frac{\partial C}{\partial t} = D \frac{\partial^2 C}{\partial d^2} - \frac{\mu_m C}{K_s + C} \frac{X_{act}}{Y} \qquad (3.8)$$

47

where D is the diffusion coefficient, d is depth in the biofilm, and Y is the biomass yield.

Inactive biomass is created at a rate proportional to the rate of death of active biomass. As the biofilm thickens, diffusive resistance prevents penetration of contaminant to the deeper layers, so that the biomass growth rate falls below the death rate. Only the outer layers of the biofilm make significant contributions to treatment. The kinetic parameters, derived by Song and Kinney (2002) for toluene, were used, and it was presumed that the incoming concentration of toluene was 25 ppm (Table 3-2).

Table 3-2: Cellular Automaton Model Parameter Values

Parameter	Value	Units
μ_m	0.05	1/h
K_s	0.10	mg/L
Y	0.76	mg biomass/mg Toluene
k_d	0.016	1/h
$C_{initial}$	25	ppm

48

3.4.3 Sensitivity Testing of Numerical Model

Sensitivity testing of mathematical model was performed on the version of the model that utilized a log-normal pore size distribution. Two selected pore size distribution parameters and three primarily microbiological variables were tested to determine, which are most critical to model predictions.

Determination of the sensitivity to each will provide an estimate of model reliability and show which parameters should be investigated further. The effect of a single parameter was estimated from the results produced when only that parameter was changed ($\pm$ 10%) while others are kept constant.

The sensitivity analyses tested the impact of (1) R (maximum pore radius), (2) μ_L (location parameter of pore size distribution), and the variables that are functions of the substrate and cell physiology including (3) K_S (Monod half saturation constant), (4) μ (maximum growth rate), and (5) D_f (diffusion coefficient of contaminant in biofilm) on time of clogging, initial elimination capacity, average elimination capacity, maximum elimination capacity, initial surface area, and useful life of the medium. Useful life was estimated by determining the time when the elimination capacity was reduced to less than half of the average value.

Ten runs were performed. Simulations of biofilters with one parameter changed by 10% were compared to the initial configuration. Percentage differences in predicted results are tabulated in Table 3-3 and 3-4.

49

Table 3-3: Effect of substrate related parameters on model predictions

	Df+10%	Df-10%	μ+10%	μ-10%	Ks+10%	Ks-10%
Time to Clogging(hrs)	-3%	5%	-10%	14%	1%	-1%
Initial EC (g/m³/hr)	0.03%	-0.04%	11%	-11%	-0.33%	0.34%
Average EC (g/m³/hr)	5%	-6%	5%	-5%	-0.45%	0.47%
Maximum EC (g/m³/hr)	2%	-4%	7%	-9%	-1%	1%
Initial Surf Area (m²/m³)	0%	0%	0%	0%	0%	0%
Useful Life (hrs)	-4%	5%	-10%	14%	1%	-1%

Table 3-4: Effect of Pore size distribution parameters on model predictions

	μ_L+10%	μ_L -10%	R+10%	R-10%
Time to Clogging(hrs)	0%	0%	10%	-9%
Initial EC (g/m³/hr)	-7%	11%	-0.08%	0.07%
Average EC (g/m³/hr)	-5%	10%	-10%	12%
Maximum EC (g/m³/hr)	-7%	10%	-10%	9%
Initial Surf Area (m²/m³)	-7%	11%	-9%	11%
Useful Life (hrs)	1%	-3%	9%	-9%

The sensitivity testing of the model also tells us how accurately we have to know the data which are used in the model, and what can be changed to make better biofilters. According to the results, K_S (Monod half saturation constant) has the least impact on model predictions. This suggests that much of the removal in this biofilter is being done at high local concentrations of ethanol, so that the Monod rate constant is approximately equal to its maximum value. D_f (Diffusion coefficient of contaminant in biofilm), over which the designer has little control, also has a small effect on the results. All the biofilter characteristics other than initial surface area have a high sensitivity to μ (maximum growth rate), organisms that grow 10% faster can increase initial Elimination Capacity (EC) by 11%, and increase the average EC by 5%. None of these variables has an effect on initial surface area because they do

50

not change the pore size distribution. On the other hand, μ_L (location parameter of log-normal distribution) and R (maximum pore radius) have significant effects on initial surface area and therefore on elimination capacity. The results seem to be more sensitive to R, which is readily controlled by the biofilter designer. One interesting thing to notice here is that μ_L does not change the time to clogging, and has a very little effect on the useful life of biofilter; therefore using lower μ_L can lead better design of biofilter with higher elimination capacity.

3.5 Theoretical Findings of Numerical Model

3.5.1 Predicted Effects of Pore Size Distribution on Clogging Time and Treatment Efficiency

Results for the surface area limited and volume limited biofilm growth models, for f(n), X_a, X_f, and X_{na} were plotted for two distributions with $\sigma = 1$ and $\mu = 4$ or 7 (Figure 3-6). Calculations compared hypothetical packing materials with differing pore size distributions, but with the same total pore volume, as is likely to be the choice faced by biofilter designers. The distributions with more small pores had a higher total surface area and so the available surface area at time t= 0 was larger than in the uniform pore case (Figure 3-7).

In the first distribution, with more pores in the small size classes, some pores were filled or isolated earlier, and X_a began to decline earlier, while X_f rose

51

gradually. X_{na} remained near zero for much of the time, but rose sharply near the end. When the process was complete, all the pores had been moved from the accessible class to become filled or isolated ($A_n = 0$, $X_f = 0.71$ and $X_{na} = 0.29$). For the case in which $\mu = 7$, the fraction of available pores remained near one for a longer time and the clogging process was more abrupt.

Overall, the time available before final clogging was about twice as long for the pore size distribution with $\mu = 7$.

It was presumed that biofilm growth, and therefore the amount of contaminant removed from the airflow, varied either with biofilm surface area or biofilm volume (Ozis et al. 2002). The variation of these quantities with time therefore indicates variation in biofilter performance (Figure 3- 7). As might be expected, the general trend is that at as the pore distribution becomes more uniform, the surface area and biomass volume curves more closely approximate the curves of the case in which the pores are all the same size.

Where $\mu = 4$, the higher initial surface area had a marked effect on the surface-limited treatment model. Initial treatment rates were twice as high in the parallel plate model, and four times higher in the cylindrical pore model than for the uniform case. Correspondingly, however, clogging occurred more rapidly, with the biofilter being blocked in about half of the time at $\mu = 4$ than at $\mu = 7$. For $\mu = 7$, the performance of the non-uniform case was only moderately different from that of the uniform-pore case. The same effect, while less pronounced, was seen in the results

52

for the biomass volume limited case. The same initial biofilm thickness was assumed as an inoculum, but the greater initial surface area in the $\mu = 4$ case meant there was more biofilm and subsequent growth was more rapid. Again, clogging occurred sooner where μ was 4.
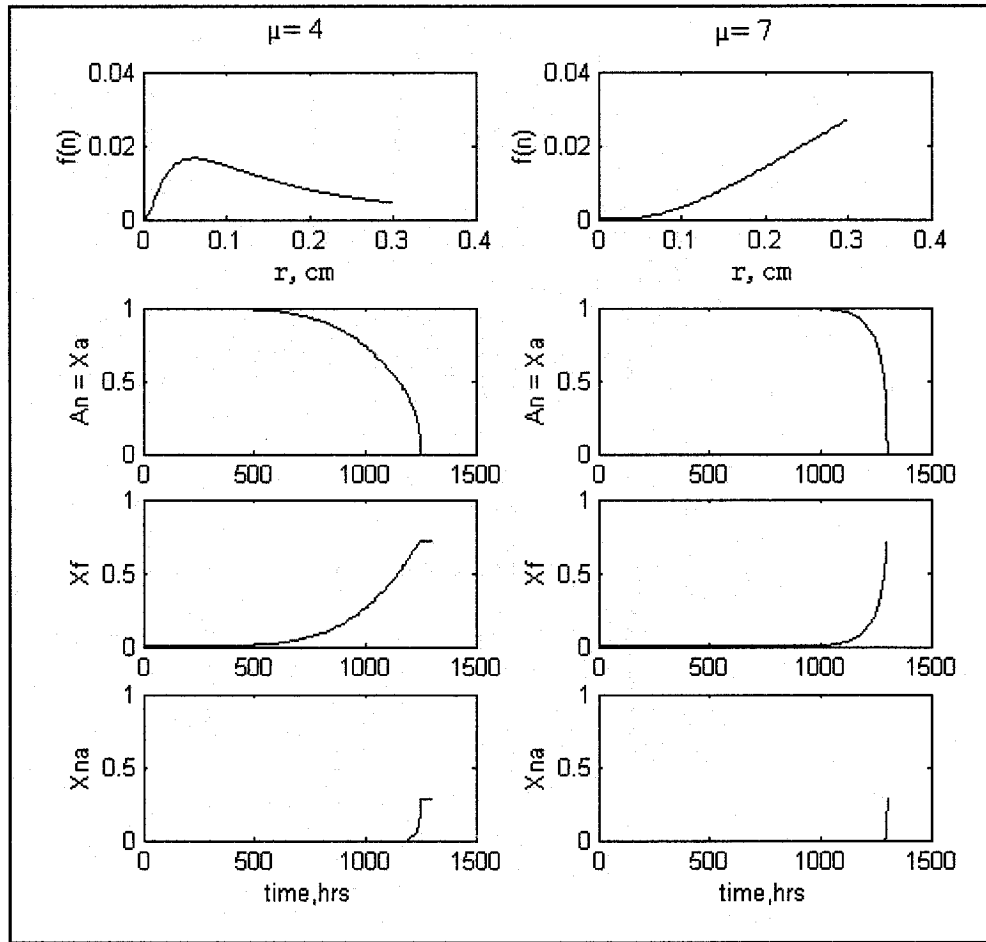
Figure 3-6: Model results for lognormal distributions with $\mu = 4$ and $\mu = 7$, for the case of biomass-limited growth in cylindrical pores. The top plots [f(n)] show the pore size distribution in each case. The plots on the second line show the decline in pore accessibility [A(n)], and the third pair shows the increase in the number of filled pores [(Xf)]. The number of pores that are not filled, [(Xna)], but are inaccessible, rises sharply as clogging occurs.
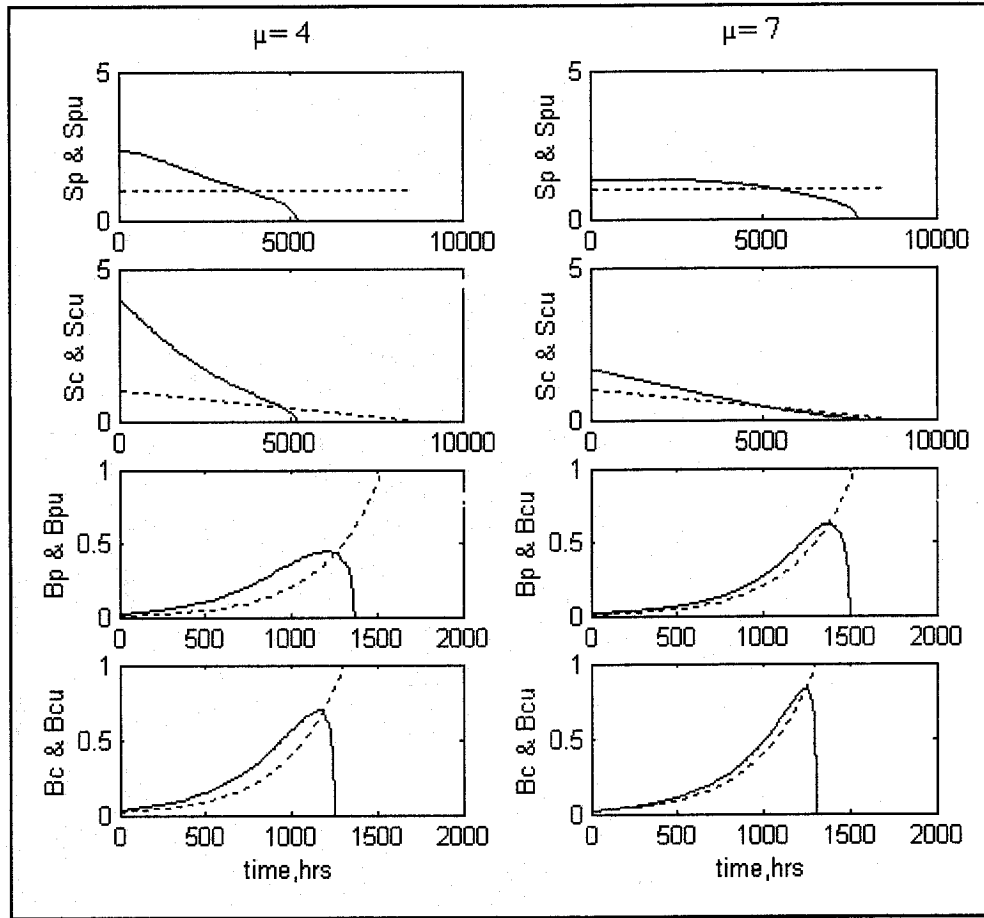
Figure 3-7: Available surface area and available biomass volume evolution for two pore size distributions with equal pore volume. The top plots show biomass surface areas for plate pore distributions [Sp, solid line] and for plate pores of uniform size [Spu, dotted line]. The second pair shows the corresponding values of biomass surface areas in cylindrical pores. The third pair of plots shows biomass volumes for plate pore distributions [Bp, solid line] and uniform plate pores [Bpu, dotted line]. The fourth set of plots shows the corresponding values of biomass volumes in cylindrical pores.

54

3.5.2 Predicted Effects of Pore Size Distribution on Permeability

By applying Effective Medium Approximation (EMA), and solving the integral equation stated in Kirkpatrick (1973), the effective pore radius (r_m) that reproduced the overall effective permeability was calculated.

Figure 3-8 shows that as the time progresses the biofilm grows and the effective pore radius (r_m) becomes smaller. It is notable that r_m points to zero at the same time treatment effectiveness reaches zero (Ozis et al. 2002).
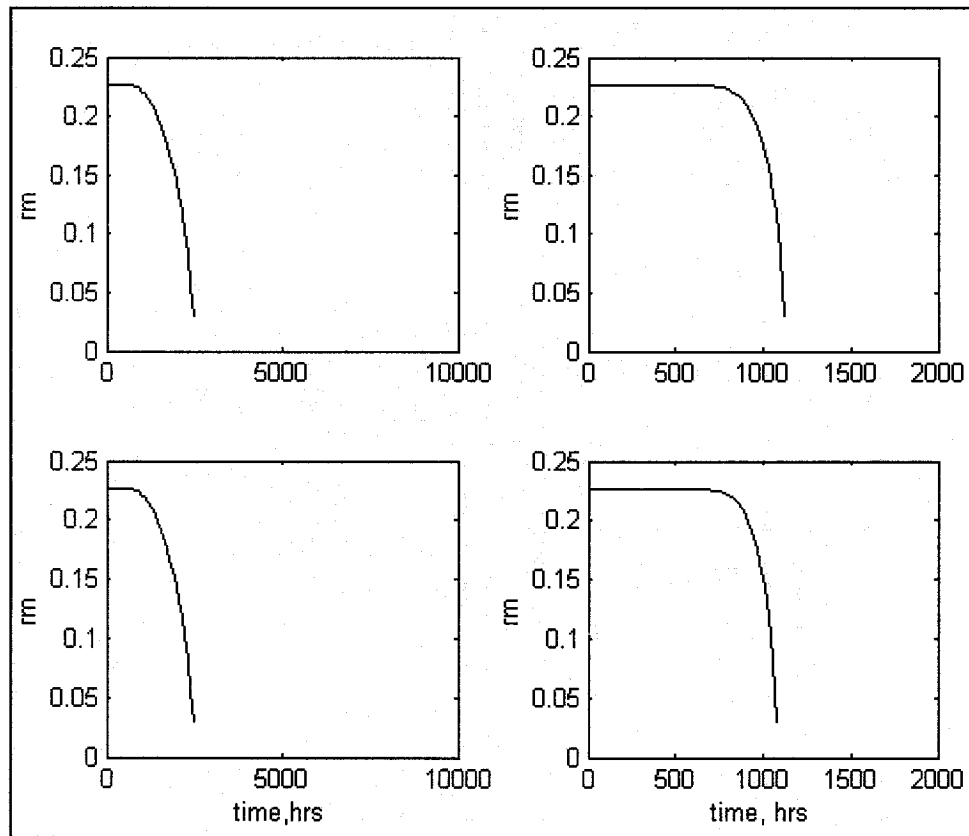
Figure 3-8: Effective Pore Size, rm change with time. On the left, the plots showing biomass surface area limited case and on the right biomass volume limited case. The top plots for parallel plate pore distribution, and the bottom pair show the corresponding values for cylindrical pores.

3.5.3   The Results from Cellular Automaton Model

Three cases were examined using the combined percolation and cellular automaton models (Ozis et al. 2003). In the first, the pores were presumed to be uniform cylindrical pores of radius 0.3 cm. In the second, the pore distribution was assumed with a location parameter $\mu = 7$. In the third, μ was taken as 4. The cases thus represent examples of successively less uniform pores of smaller average diameter, but with fixed volume and increasing total surface area. Growth parameters and contaminant concentrations were chosen such that the biofilm expanded rapidly, and clogging occurred in a short time, in order to provide conveniently short time periods for calculation. Most parameters, however, were those determined by Song and Kinney (2002) for Toluene.

For the uniform pore size case, it was presumed that the total pore volume was 50% of the biofilter volume. This implies an active surface area of 313 m^2 of surface area per m^3 of biofilter packing. This number was multiplied by relative surface area values coming from numerical percolation model.

In each case, the specific activity of the biofilm, measured in grams of toluene consumed per m^2 per hour, rose sharply in the first two hundred hours, and then reached a steady-state value (Figure 3-9). At this point, only the surface of the biofilm was active, and continued growth was matched by continued inactivation of deeper layer so that the net effect was to just increase the number of underlying layers of inactive biomass. The overall elimination capacity, which was the product

56

of the biofilm specific activity and the available area of biofilm, also initially rose rapidly, in response to the increase in activity. Once the biofilm had reached its steady-state specific activity, elimination capacity declined gradually as the reduction in pore size and clogging reduced available surface area.
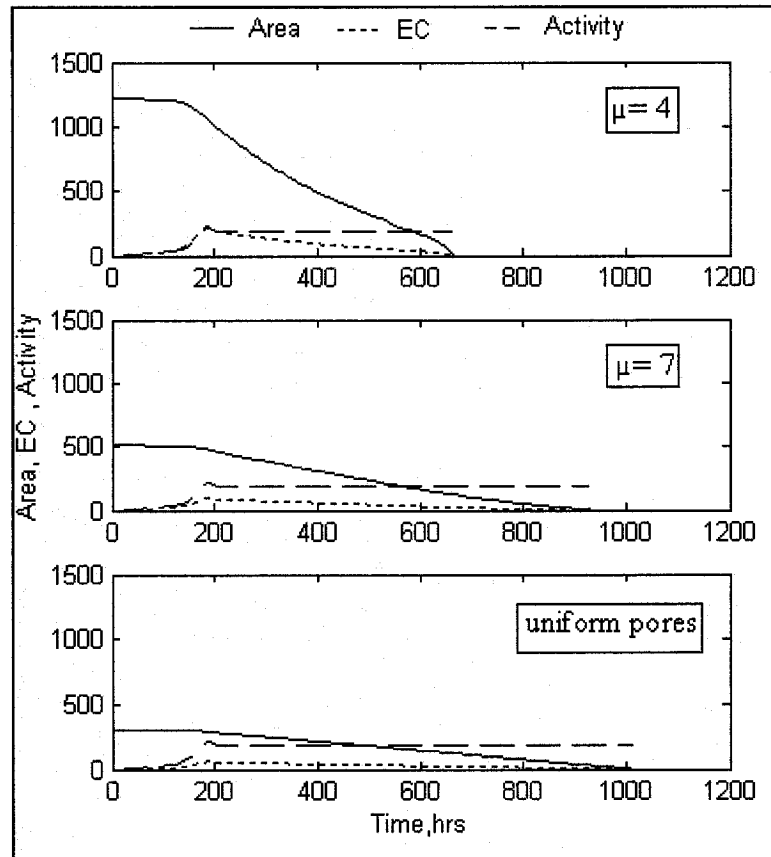
Figure 3-9: Top, simulation for $\mu = 4$. Middle, Simulation for $\mu = 7$. Bottom, simulation for uniform pores. [Solid line]: surface area, m^2/m^3, [dotted line]: biofilter elimination capacity, g/m^3-h, [dashed line]: biofilm activity, mg/m^2-h.

The simulated biofilters with smaller pores provided higher initial elimination capacities, but correspondingly clogged more rapidly (Table 3-5).

Table 3-5: Results of Numerical Percolation-CA Model Calculations

Pore Distribution	Initial Surface Area, m^2/m^3	Maximum Elimination Capacity, $g/m^3/h$	Time to Clogging, d
Uniform pores	313	55	44
$\mu = 7$	516	90	40
$\mu = 4$	1236	200	29

The biofilm growth model calculated the specific activity of the biofilm. It also determined the activity of each layer within biofilm as a function of depth (Figure 3- 10). Essentially all of the contaminant degradation occurred in the outer 70 layers of the biofilm, corresponding to the outer 210 microns of the biofilm. Thus overall activity rates rose as the first 70 layers accumulated, but were essentially constant thereafter.

This suggests that an appropriate biofilm thickness for an ideal biofilter is 210 microns, which is comparable with the values reported previously (Cox et al. 1997; Ottengraf and Diks, 1992). At the steady state activity of 190 mg/m^2-h, $\mu = 4$ biofilter would have an elimination capacity of 200 g/m^3-h, or more than two times the peak elimination capacity of the $\mu = 7$ biofilter. However, $\mu = 4$ biofilter clogged in just 29 days, and for most of that period provided elimination capacities well below the maximum.
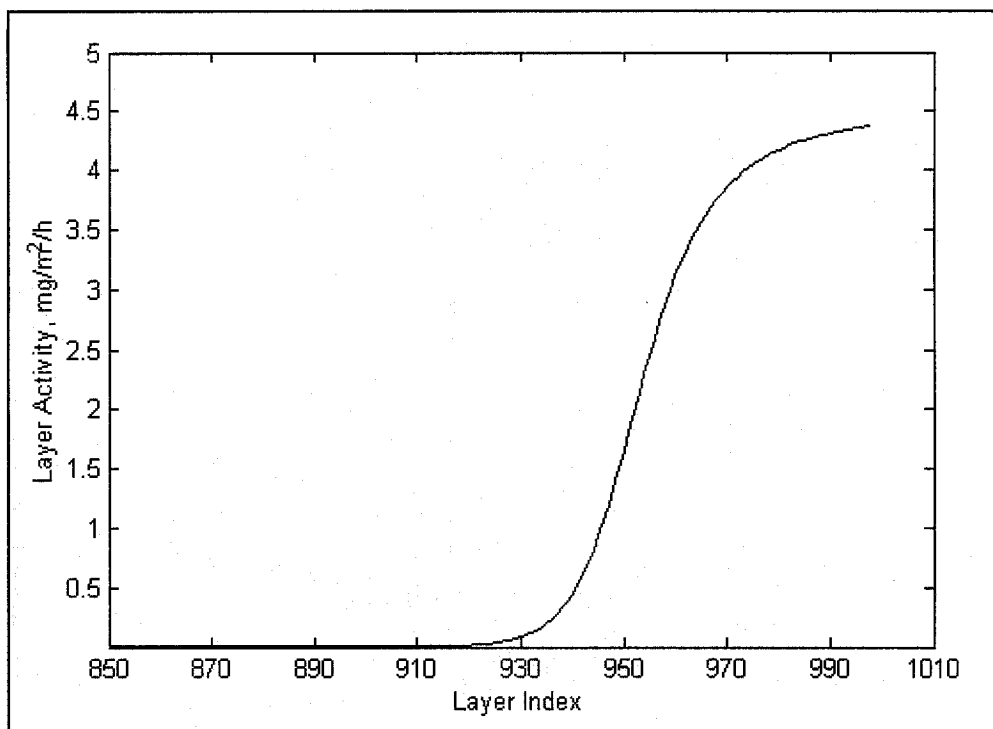
Figure 3-10: Specific activity (mg/m^2-h) of layers within the simulated biofilm. Layers are 0.003mm thick.

A better comparison might be between $\mu = 7$ biofilter and uniform pore biofilter, which ran for 40 and 44 days respectively before clogging and maintained a somewhat more constant treatment rate. The elimination capacity of the $\mu = 4$ biofilter was about two times higher than the maximum in uniform pore case (Ozis et al. 2003).

59

4 MATERIALS AND METHODS

4.1 Objective

The numerical clogging model developed by this work was tested by comparison with bench scale biofilter experiments. A main objective of this experimental study was analysis of the clogging of biofilters; to this end, biofilters were tested on heavy loads of highly biodegradable ethanol.

4.2 Continuous Flow Bench-Scale Studies

Two acrylic plastic column biofilters, each with 7cm inner diameter and 25cm length, were used in parallel to evaluate ethanol degradation (Figure 4-1). Sand and lava rock, with median grain sizes of 2.2 and 4.7 mm, were selected as support media. In order for a biofilter to operate at its best, the filter material must meet the following requirements. (1) Provide optimum environmental conditions for the resident microbial population in order to achieve and maintain high degradation rates, (2) filter particle size distribution and pore structure should provide large reactive surfaces and low pressure drops, (3) compaction should be kept to a minimum, reducing the need for maintenance and replacement of the filter material.

The particle shape and size distribution of the media were analyzed by Camsizer® Digital Image Processing Particle Size Analyzer (Horiba Instruments Inc, Irvine, CA).

60

Figure 4-1: Schematic of experimental set up

The air flow rate was 1.5 liters per minute (LPM), producing an EBRT of 20 seconds. The contaminated vapor was generated by passing air through a cylinder where liquid ethanol was injected by a syringe pump. Air was moisturized by passing it through a flask, where distilled water was nebulized by a fogger (Artistic Delights, Milpitas, CA). The nebulizer supplied the packed beds with a total of approximately 6 ml/h humidified air. These two airflows were metered separately, and then mixed to produce the desired concentration of influent to each biofilter. The head loss across the biofilter bed was measured by a U-tube water manometer. The air samples were taken twice a day in the first two weeks and then daily using disposable syringes (1 ml). Four replicates were taken per sampling port.

61

4.3 Methods

4.3.1 Inoculum Preparation

Preparation of the inoculum began with mixing 10 ml raw sludge (pH = 6.2) and 300 μl ethanol with 1 liter of nutrient solution including 1.0 g/L KH_2PO_4, 1.0 g/L K_2HPO_4, 1.0 g/L KNO_3, 1.0 g/L NaCl, 0.2 g/L $MgSO_4$ and 0.02 g/L $CaCl_2$ and 0.5 ml of trace elements solution. The trace elements solution contained 12.2 g/L $FeCl_2.4H_2O$, 4.09 g/L $MnCl_2.4H_2O$, 0.927 g/L $CoCl_2.6H_2O$, 2.37 g/L ZnCl, 0.616 g $CuCl_2.2H_2O$, 0.579 g/L $NaMoO_4.2H_2O$, 0.16 g/L H_3BO_3, 0.148 g/L KI, 0.067 g/L $NiCl_2.6H_2O$ and 6.5 g/L $EDTANa_2.4H_2O$ (Nukunya, 2004). Ethanol addition continued on every 4th day while increasing the amount to 1000 μl in two consecutive steps. The mixture was kept for 4 weeks and aerated continuously. The pH gradually increased to 7.1 just before the acclimated inoculum was transferred to the biofilters. The packing grains were first flooded with the nutrient solution and then with inoculum and then drained. The biofilters were flooded with fresh nutrient solution once a week during the experiments.

4.3.2 Gas Concentration Determination

Analysis of gas concentrations was performed by gas chromatography. An SRI Model 8610 Gas Chromatograph equipped with a flame ionization detector (FID) and interfaced with a Hyundia 386 computer with SRI's Peaksimple II data

62

system-integrator was used. A stainless steel column, 10 cm. long x 1 mm I.D. with no internal packing material, was used for sample analysis. Response from the FID was immediate after the sample injection, which allows for large number of analyses in a short period. Each determination was the average of four replicates. The carrier gas had 10:1 ratio of air to hydrogen at total flow rate of 20 ml/min. The detection limit for the GC was evaluated by having serial dilutions of ethanol in nitrogen gas; the detection limit of the instrument was determined as 10 ppb.

4.4 Operating Conditions

The flow rates through the biofilters were 1.5 LPM, to yield an empty bed detention time (EBRT) of 20 sec in the biofilter. Ethanol was supplied continuously at a rate of 0.06 ml/h to yield an inlet gas phase concentration of approximately 100 ppm_v. The temperature was room temperature, and relative humidity was kept close to 100%.

4.5 Analysis

4.5.1 Porosity

The initial porosity of the biofilters was estimated by following the procedure given by Hodge (1993). It was done as following:

63

- Determine volume of sample with a graduated cylinder (50 ml).

- Determine weight of sample and graduated cylinder.

- Add water to sample and graduated cylinder, periodically tapping cylinder to dislodge air bubbles, until sample is completely saturated.

- Determine weight of sample, graduated cylinder and water.

$$\% \text{ Porosity} = \text{Void Space Volume} / \text{Volume of Sample} \qquad (4.1)$$

$$= \frac{(\textit{Weight of sample} + \textit{Cylinder} + \textit{Water}) - (\textit{Weight of sample} + \textit{cylinder})}{\textit{Density of water} / \textit{Volume of sample}} \qquad (4.2)$$

According to this procedure the initial porosity was 51% for the lava rock and 39% for sand.

4.5.2   Pore Size Distribution from Particle Size Distribution

Typically, support particles are not uniform in size. Hence, when they are packed within a biofilter they result in a non-uniform pore size distribution (PSD). In modeling flow through porous media, it is essential that a realistic porous medium model is used to properly account for the interaction between the solid matrix and the fluid within the pore space. Knowledge of the pore size distribution of a biofilter bed, therefore, is crucial to analyze its performance.

64

However, there is no straightforward experimental technique that can provide the pore structure characteristics for packed-bed reactors (Nukunya et al. 2005). A number of studies reported methods to generate PSD based on experimental particle size measurements. Nolan and Kavanagh (1994) produced a computer algorithm to investigate PSD of random spheres whose size distribution obeyed the log-normal distribution. They concluded that as the standard deviation of the particle size increased the PSD became broader and less ordered. A probabilistic approach that determines PSD in packed spheres was employed by Ronault and Assouline (1998). The approach was applied to power-function, Gaussian and log-normal distributions of spheres that were assumed to have tetrahedral symmetry. Their results revealed that, in case of bell-shaped particle size distributions, the type of PSD is similar to particle size distribution; however, there is no mathematical similarity between the two. Chan and Ng (1988) have studied the PSD of computer-generated random packing of spheres by applying tetrahedral tessellation and statistical analysis. It was shown that the pores linked by a common constriction were rather close in size, while constrictions of the same pore tend to have more different sizes.

The approach we employed for generating the PSD is based on a model developed for cohesionless soils and similar granular materials by Aberg (1992, 1996). Nukunya (2004, 2005) was the first to use the Aberg's method developed for cohesionless soils and similar granular materials to predict the pore size distribution

as a function of grain size distribution for a biofilter. This study followed the same procedure to determine pore size distribution in experimental biofilters.

4.5.2.1 Theory

Aberg (1992) has developed a theory describing the packing of irregularly shaped grains. Each particle is assumed to have an intersection with an imaginary straight line. Then, AB is called grain chord, and a void chord lies in between two adjacent grain chords.
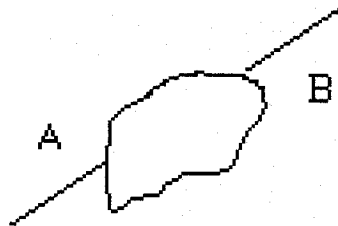
Figure 4-2: Grain chord and Void chord definition

Aberg (1992) states the average length of the grain chord is proven to be

$$g = 4v/s \quad (4.3)$$

where v is volume of the particle, and s is the geometric surface area. Assuming that the particle just passes through a square mesh with apertures of size x, Aberg sets

$$g = 4ax \quad (4.4)$$

66

It is assumed that the cross-sectional area of the line passing through each grain forms a square and the area is dA. There are Ng grain chords and Nv void chords and if the total length of the line is L, and the porosity of the material is ε, then

Total volume of grains is

$$V_g = (1-\varepsilon)\, L\, dA \qquad (4.5)$$

and the total volume of the voids is

$$V_v = \varepsilon\, L\, dA \qquad (4.6)$$

The total number of grain chords is taken as:

$$N_{gy} = \frac{(1-\varepsilon)L}{4a} \int_{y}^{d} \frac{dy}{x(y)} \qquad (4.7)$$

The number of total grain chords mapping particles of size between x and x+dx is dN_g. The probability that a void chord is in between a particle of this size and the maximum size is equal to

$$p = \frac{N_{gy}}{N_g} \qquad (4.8)$$

The total number of such void chords is 2pdN$_g$.

By assuming the average length of void chord (i) is proportional to the grain chord, one can say

$$i = cg = c4ax \qquad (4.9)$$

where c is a coefficient that depends on the shape of the grains.

67

Then, the total volume void chords

$$dV_v = 2pdN_g cgdA = 2c\frac{N_{gy}}{N_g}dV_g \qquad (4.10)$$

The void volume, dV_v, that corresponds to the void chords of lengths $i = cx/2$ to $c(x+dx)/2$ is

$$dV_v = 2c\frac{B_y}{B_0}V_g dy \qquad (4.11)$$

where y, takes values between zero and one, is the ordinate of the gradation curve corresponding to the grain size x, and V_g is the total solid volume of the material.

$$B_y = \int_y^1 \frac{dy}{x(y)} \qquad (4.12)$$

B_0 is given by above equation when $y = 0$ (Aberg, 1996).

Integration of dV_v from $y = 0$ to $y = 1$ gives to total void volume, Vv of the material, whereas integration between $y = y_b$ to $y = 1$ gives the void volume that corresponds to the void chords with lengths between $i_b = cxb/2$ and $i_{100} = cx100/2$, x_b is the grain size corresponding to y_b.

Consequently, the ordinates, z_b of the cumulative distribution curve for the void volume are given by

$$z_b = 1 - \frac{A_b}{A_0} \qquad (4.13)$$

68

where

$$A_b = \int_{y_b}^{1} \frac{y}{x(y)} dy - y_b \int_{y_b}^{1} \frac{dy}{x(y)} \qquad (4.14)$$

A_0 is given by above equation by taking $y_b = 0$ (Aberg, 1996).

The void ratio is defined as the ratio of void volume to grain volume;

$$\Phi = \frac{V_v}{V_g} \qquad (4.15)$$

which can be rewritten as

$$\Phi = \frac{dV_v}{V_g} = 2c \frac{A_0}{B_0} \qquad (4.16)$$

and c can be calculated from this equation for a specific material.

In short, from the porosity of the bed and therefore the volume of the grains, the model estimates the total number of grain chords. It is assumed that the average length of void chord is proportional to a grain size x, and the void volume corresponding to a number of void chords that depend on the grain length in a definite interval were calculated. The calculations provide a cumulative distribution curve of void volume.

69

4.5.2.2 Lava Rock Biofilter Pore Size Distribution

The Camsizer® was employed by Horiba Instruments (Irvine, CA) to determine the particle size distribution of the lava rock particles. The Camsizer® is equipped with two cameras that capture images as the dry samples are fed into the observation zone of the instrument. Approximately 1 liter of lava rock particles was analyzed three times and the average of the particle size and their corresponding average fractions in the sample were used in calculations (Horiba Report can be seen in Appendix IV). The maximum particle size was 6.7 mm (Figure 4- 3). The initial porosity of the lava rock biofilter was estimated as 51% by following the procedure described by Hodge (1993).

The relationship between the particle size and the cumulative fraction was obtained by fitting it to a fifth degree polynomial. The equation was:

$$x = 242.8315y^5 - 625.241y4 + 580.0602y^3 - 232.6478y^2 + 40.5798y + 1.234 \qquad (4.17)$$

Where x = particle size (mm), and y = fraction
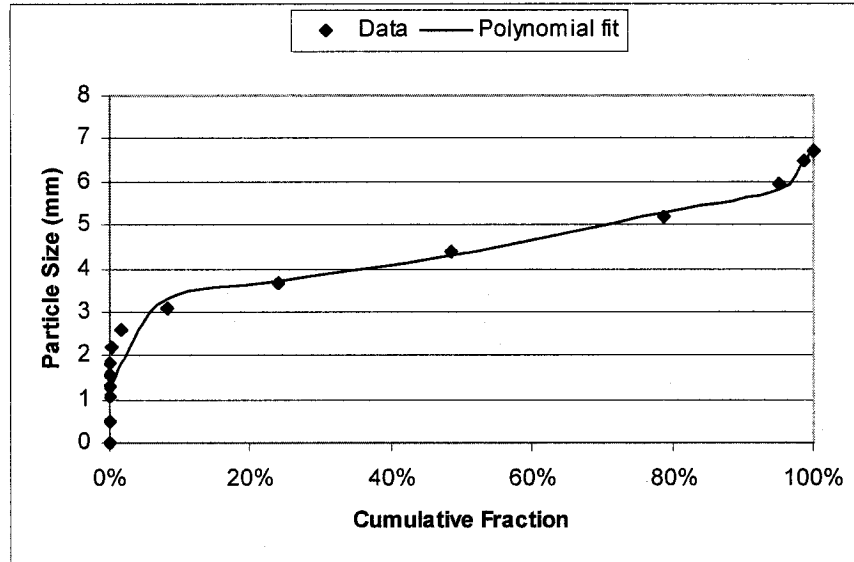
Figure 4-3: The particle size versus cumulative fraction of particle size in lava rock sample

The pore size distribution of the lava rock bed was calculated using the approach defined by Aberg (1996) and published in Ozis et al. (2004c). First, the cumulative pore fraction as a function of the pore size was obtained (Figure 4-4). From this, the graph of the pore fraction versus pore size was generated (Figure 4-5). A third order polynomial was fitted to the graph for pore sizes between 0.08 and 0.196 cm. The equation representing the relationship between the pore radius (cm) and its fraction (f) in the lava rock bed is,

$$r < 0.08 \rightarrow \quad f = 0$$
$$0.08 \leq r < 0.196 \rightarrow f = 731.42\,r^3 - 379.28\,r^2 + 60.075\,r - 2.72 \qquad (4.18)$$
$$r \geq 0.196 \rightarrow f = 0$$
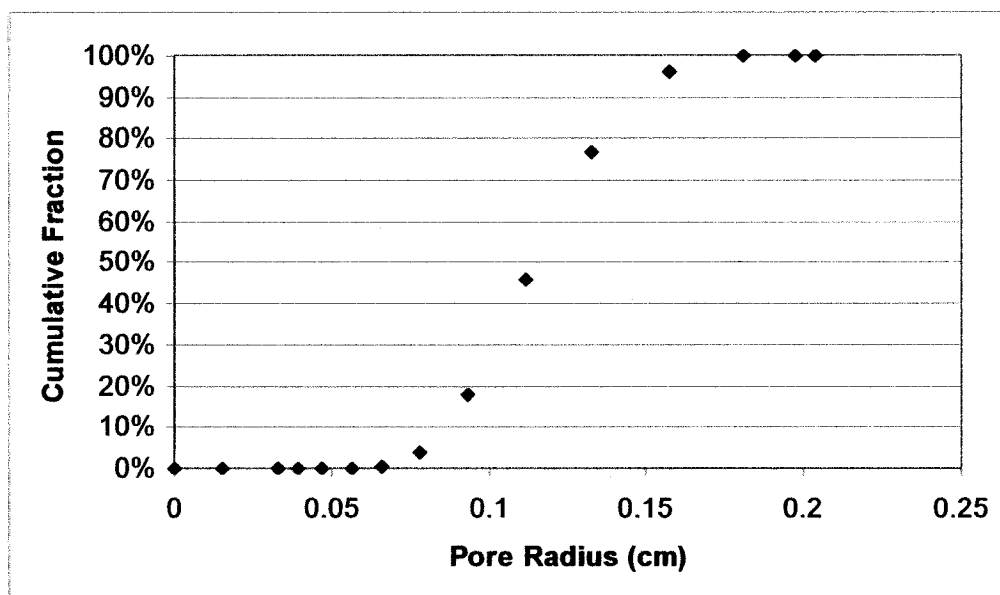
Figure 4-4: The cumulative fraction versus pore radius in lava rock biofilter
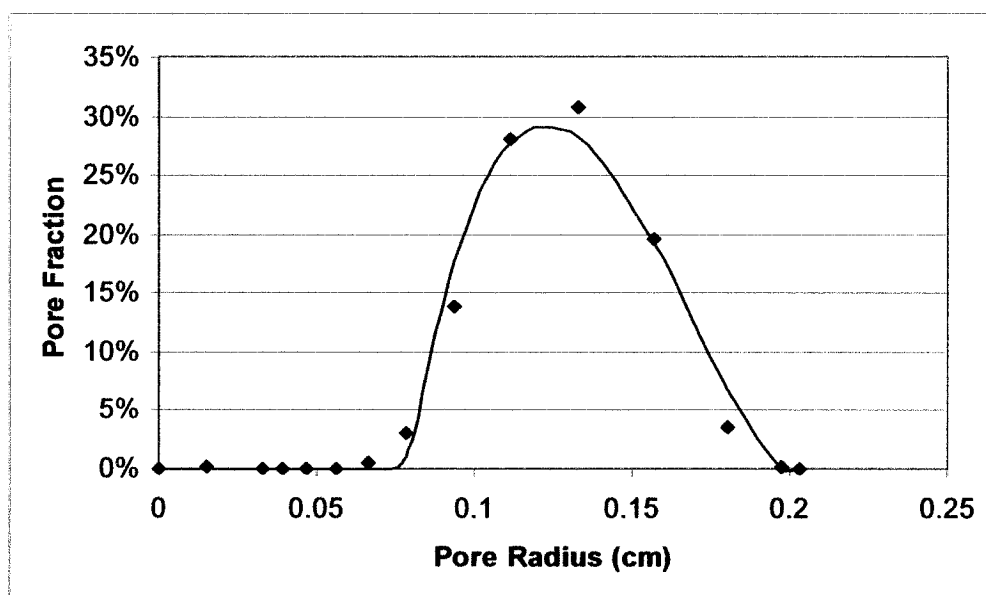
Figure 4-5: The pore fraction versus pore radius in lava rock biofilter; points are calculated values, and line is the polynomial fit.

72

4.5.2.3 Sand Biofilter Pore Size Distribution

The same procedure was applied to sand media. The maximum particle size was 3.68 mm (Figure 4-6). The relationship between the particle size and the cumulative fraction was obtained by fitting it to a fifth degree polynomial. The equation was:

$$x = 122.22y^5 - 319.19y^4 + 304.84y^3 - 127.34y^2 + 22.298y + 0.6031 \qquad (4.19)$$

Where x = particle size (mm), and y = fraction)
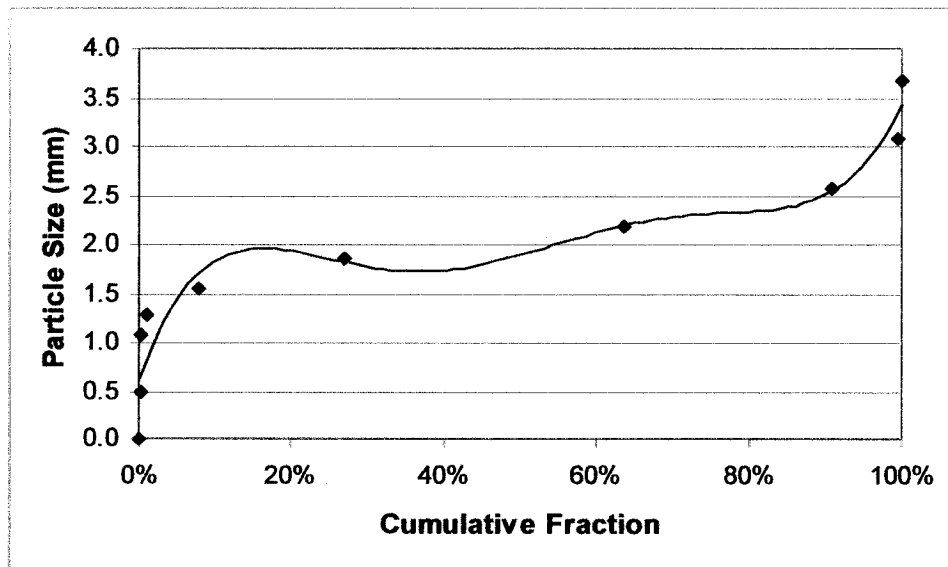
Figure 4-6: The particle size versus cumulative fraction of particle size in sand sample

73
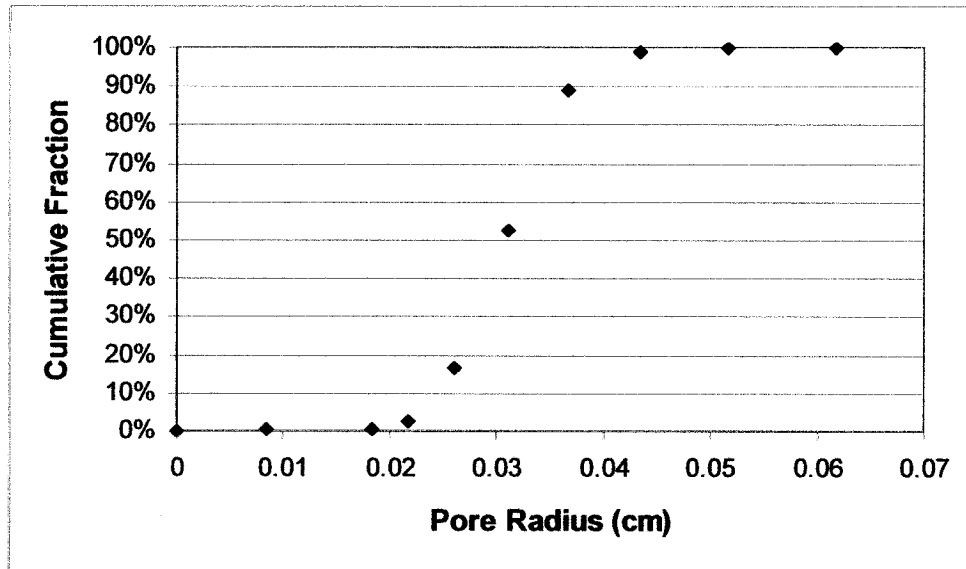
Figure 4-7: The cumulative fraction versus pore radius in sand biofilter
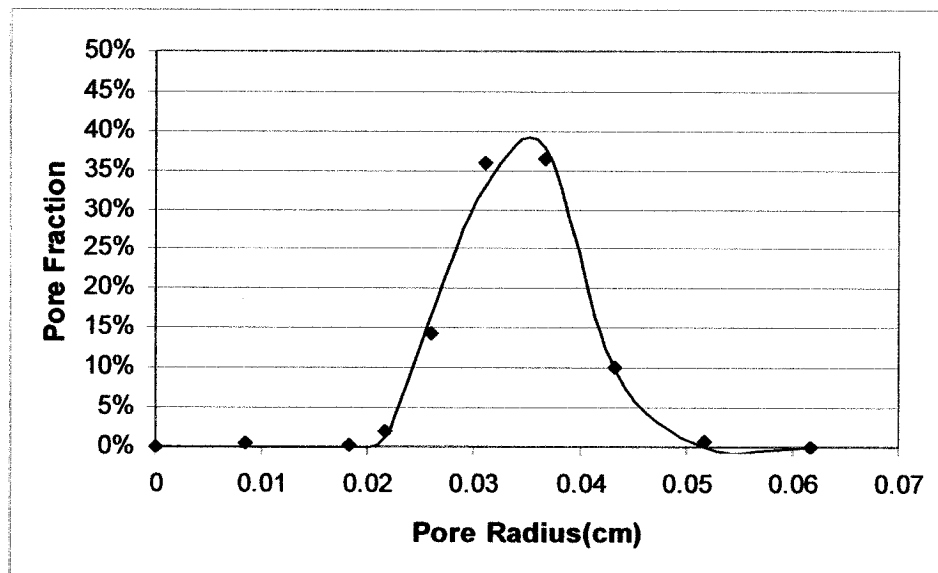
Figure 4-8: The pore fraction versus pore radius in sand biofilter; points are calculated values, and line is the polynomial fit.

74

First the graph of cumulative pore fraction was generated (Figure 4-7), then a third order polynomial was fitted to the graph of pore fraction versus pore size for pore sizes between 0.022 and 0.044 cm (Figure 4-8). The equation representing the relationship between the pore radius (cm) and its fraction (f) in the sand medium is:

$$r < 0.022 \rightarrow \qquad f = 0$$
$$0.022 \leq r < 0.044 \rightarrow f = -119080\,r^3 + 9028.8\,r^2 - 191.52\,r + 1.1339 \qquad (4.20)$$
$$r \geq 0.044 \rightarrow \qquad f = 0$$

The functions were directly included into the corresponding version of the model where pore size distribution was defined.

4.5.3 Head Loss

Head loss data were gathered when testing for removal was done during the useful life of the biofilters. Head loss readings were done by having U-tube water manometer, which compares pressure difference right before and after the medium.

4.5.4 pH

During the experiments, the leachate collected from the bottom of the biofilter and its pH was measured by pH indicator papers for the range of 0-14 and 6-7 (VWR Scientific) regularly.

75

4.5.5 Removal efficiency and elimination capacity

Removal efficiency and elimination capacity are general terms to describe the performance of biofilters. Removal efficiency (RE) is the fraction of the contaminant removed by the biofilter, expressed as a percentage:

$$RE = \frac{\text{Inlet Concentration - Outlet Concentration}}{\text{Inlet Concentration}} \times 100\% \qquad (4.21)$$

Elimination capacity (EC) is expressed as the mass of contaminant degraded per unit volume of the filter material per unit time.

$$EC = \frac{(\text{Inlet Concentration - Outlet Concentration})}{\text{Filter Bed Volume}} \times \text{Flow Rate} \qquad (4.22)$$

4.5.6 Clogging and Channeling

As time progresses, the growing biomass were expected to clog the pores and create higher pressure drops across the filter bed. It was also expected to lead to channeling, letting contaminated air by-pass the medium untreated.

After operation was ceased, the lava rock biofilter was tested with air carrying red-dyed microspheres with nominal mean diameter 0.17 μm (Bangs Laboratories, Fishers, IN) to identify the clusters of open and closed pores. Highly concentrated aqueous microsphere solutions (about 5 mg of particles in 1 mL of

76

deionized water) were nebulized using room air at 20 psi (Figure 4-9). The generated aerosols passed through a 2-L cylindrical chamber where they were mixed with room air at 20 LPM (relative humidity: 20-30%) to reduce their size back to the original value. The particles then pulled through the lava rock biofilter at a flow rate of 1.5 LPM.
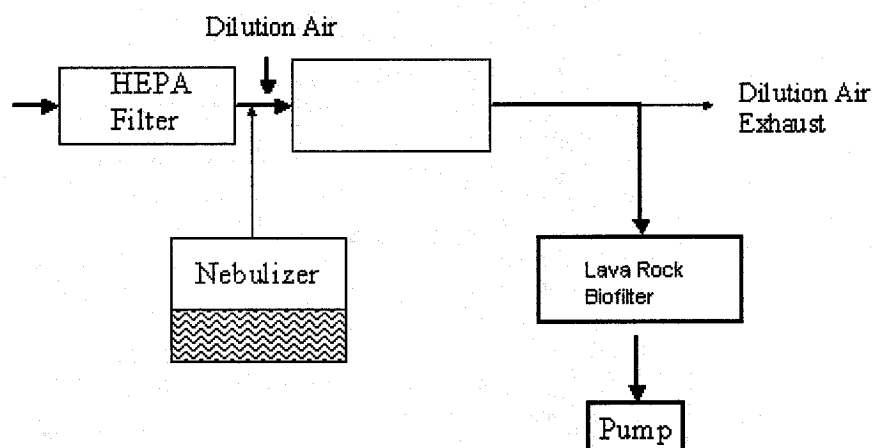
Figure 4-9: Schematic of the test for identifying channeling in Lava Rock Biofilter

The medium was kept in the refrigerator overnight. Then, the media was pushed out of the cylinder at certain distances, and each interval cross-section was photographed to identify the pattern of channeling.

4.5.7 Swimming Pool Cleaner Tests

After clogging observed in sand biofilter, a set of experiments with pool cleaner, natural enzyme product biodegrading organic contaminants, were performed. Pool cleaner was presumed to be effective on exopolysaccharides (EPS) by degrading the excess amounts. Therefore, it would be possible to restore the biofiltration process.

Distilled water having certain concentration of pool cleaner flooded the biofilter for a period of time (3 or 30 min). After each treatment, the biofilter flooded with distilled water only for one minute and drained slowly by gravity. Head loss was measured after 24 hours of each application. This procedure was repeated by increasing the concentration by a factor of ten till the observed reduction in head loss was satisfactory.

78

5 LABORATORY BIOFILTRATION OF ETHANOL VAPOR

This chapter presents the results of laboratory studies investigating the applicability of the clogging model. Experiments were performed using two bench-scale biofilters operating in parallel for the removal of ethanol vapors. Two different packing materials with different grain sizes, lava rock and sand, were chosen as media to evaluate model's simulations for overall performance and duration of operation before the air is impeded due to biofilm clogging. All the experimental data for ethanol biofilters can be seen in Appendix III.

5.1 Lava rock Biofilter

5.1.1 Biofilter Performance

The inlet and outlet concentrations of lava rock biofilter during the experimental period are shown in Figure 5-1. The average inlet concentration of ethanol was 67 ppm$_v$.
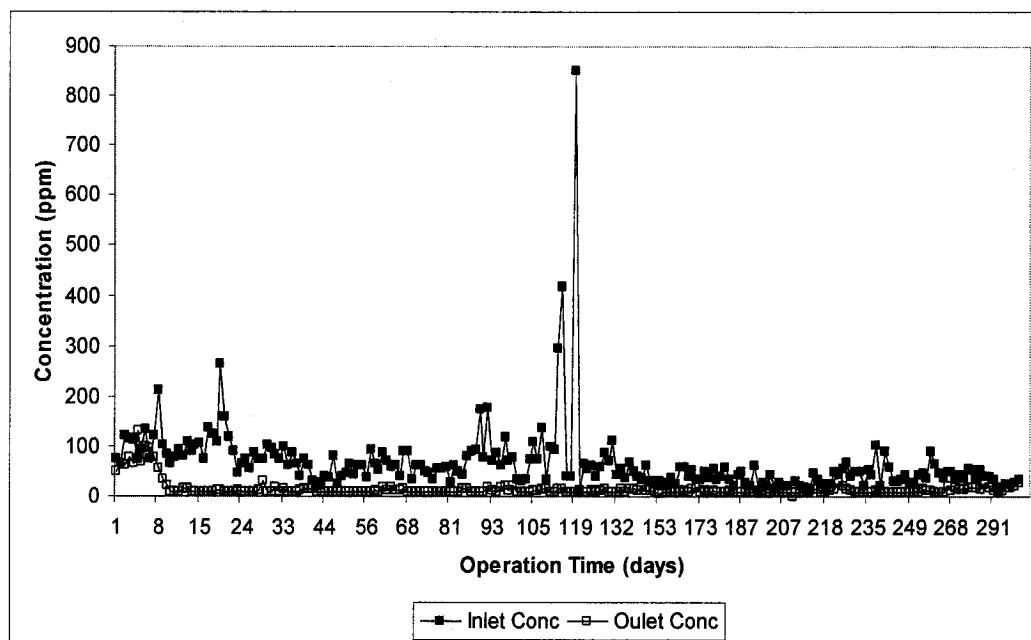
Figure 5-1: Inlet and outlet concentrations of ethanol for lava rock biofilter

At the beginning of the experiment, the removal efficiency changed rapidly between negative and positive values because of absorption of ethanol into the water or media (Figure 5-2). This change was not attributed to the microbial acclimation for two reasons: (1) ethanol is a readily biodegradable compound, and (2) the inoculum preparation was expected to already have experienced extensive selection for ethanol degraders. After the initial period, the biofilter performance gradually improved and then, more effective and steady removal was observed (81% on average). Although there were a few problems with drying and inlet concentration instability, the operation was smooth till day 113, when the inlet concentration started to increase because of a moisture problem and jumped to 851 ppm$_v$ on day

80

118. The higher ethanol concentrations were correlated with the low moisture levels in the air. Ethanol concentrations in the air phase increased because ethanol was released as the water phase evaporated. On day 119, the inlet concentration was very low because of syringe pump maladjustment, and this reduced the removal efficiency. Between day 136 and 214, the average inlet concentration of ethanol in the lava rock biofilter was lower than the long-term average concentration (37 ppm$_v$), and that corresponded to a decrease in removal efficiency. After the concentration was stabilized at the original value, a modest recovery in removal efficiency was observed starting from day 214. The period between day 240 and 260 showed the same pattern of decreased removal efficiencies due to low inlet concentrations. After day 260 the removal declined significantly, and was between 15 to 20% in the last four days of the operation. The process was terminated on day 303.
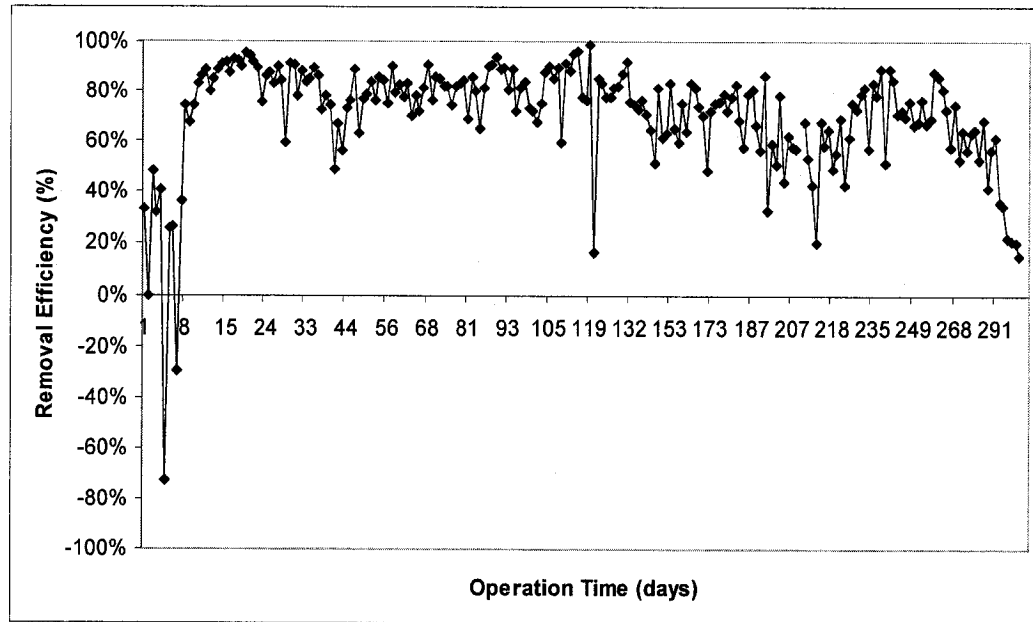
Figure 5-2: Removal efficiency for the lava rock biofilter over the duration of the experiment

5.1.2 Head Loss

Headloss was measured with a U-tube water monometer. When the operation just started 2 mm of water head loss was observed (Figure 5-3). It stayed as 2 mm till day 22, and then started increasing slowly. The increment was very small until day 144, then the increases became significant, and on day 215 the head loss was measured as 40 mm of water. After that there was a problem in the manometer and it was not possible to see any pressure difference. Although the tubing and connection hoses were cleaned, and replaced, and the whole system checked for the leaks, the cause could not be identified. This may represent channeling; however because the removal efficiency was still good, this was not

82

identified as the cause before the biofilter was taken down and analyzed for channeling later.
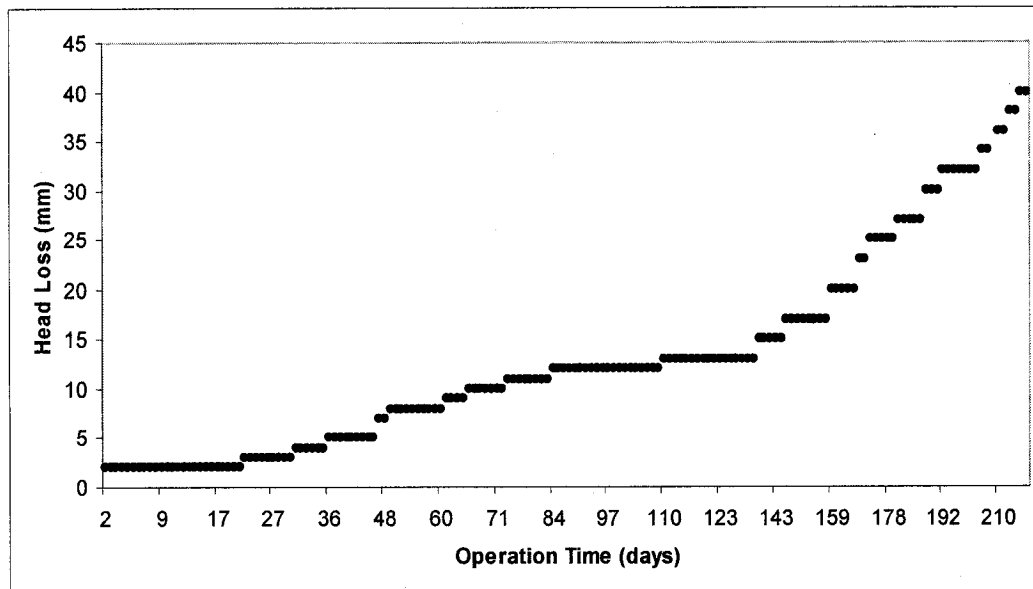
Figure 5-3: Headloss profile for the lava rock biofilter

5.1.3 pH

The pH profile of the lava rock biofilter was almost unchanged during the operational period (Figure 5-4). On day 40, and 43 the pH was observed as 7.5, and stabilized back to 7 on day 84. Another episode of higher pH observation was seen between day 116 and 120 of the operation, when the pH was 7.6 and 7.4 respectively. After that the pH was neutral, and stayed as neutral till the end of the operation.

83
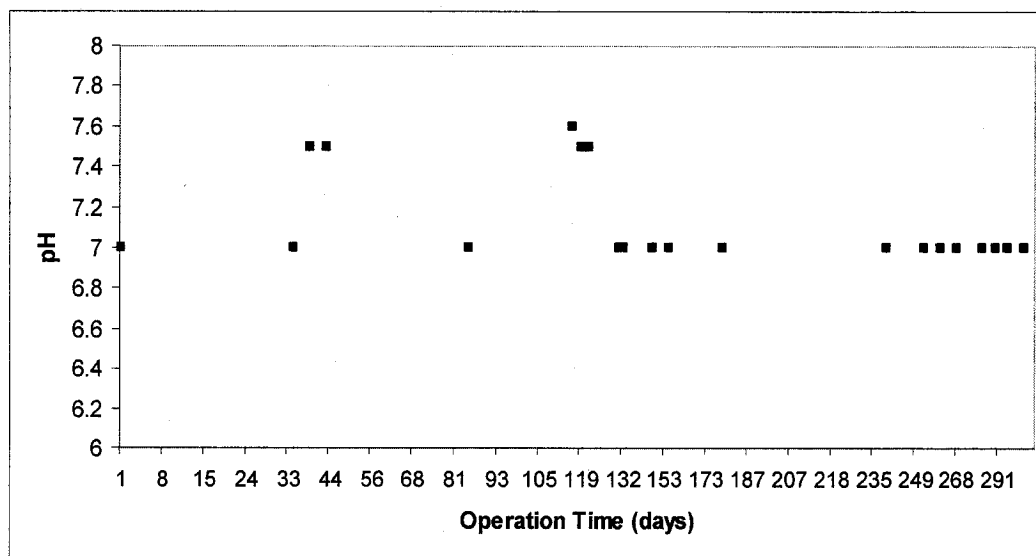
Figure 5-4: pH profile over the operational time of lava rock biofilter

5.1.4 Bacteria and Viral Enumeration

Bacteria and viruses were enumerated by SYBR Green I staining and epifluorescence microscopy following the Noble and Fuhrman Method Noble (Noble and Fuhrman 1998).

Leachate samples from biofilters were taken to investigate the organisms being removed from the biofilters. The SYBR Green I counting procedure for viruses and bacteria included first placing the anodisc filter over a pre-wetted 0.8 μm millipore filter in the glass filter unit. Then, a vacuum was applied to moisten and stick the anodisc filter in place completely flat and smooth without any air bubbles beneath. After that the filter was placed on 100 μl drop of SBYR on the bottom of a

84

plastic petri dish. The anodisc filters were laid sample side up on the drops of the staining solution for 15 minutes in a dark drawer. Any water on the back of the anodisc filters was blotted with a paper tissue so that the filter was uniformly dry and looked opaque when held up to the light for examination. After the filter was transferred on a glass slide with 30 µl drop of antifade mounting solution; it was viewed with blue excitation. Most of this work was done by Josh Steele, graduate student in biology who was cooperating with the project.

Counts showed 5.15 (+/- 1.7) x 10^6 bacteria and 6.85 (+/- 0.1) x 10^7 viruses per ml leachate from the lava rock biofilter. Therefore, the virus to bacteria ratio was 14.79 (Steele et al. 2004).

5.2 Sand Biofilter

5.2.1   Biofilter Performance

The inlet and outlet concentrations of sand biofilter during the experimental period are shown in Figure 5-5. The average inlet concentration of ethanol was 100 ppm$_v$.
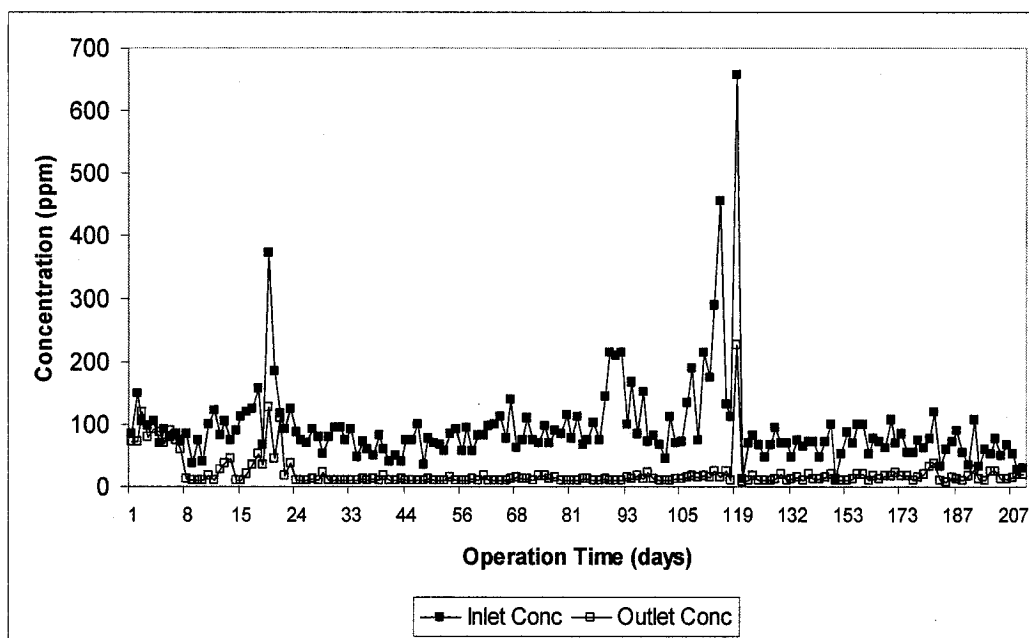
Figure 5-5: Inlet and outlet concentrations of ethanol for sand biofilter

The sand biofilter performed very poorly during the start-up period. Improvement in performance was seen after approximately 6 days, and then the removal efficiency increased rapidly (Figure 5- 6).

86
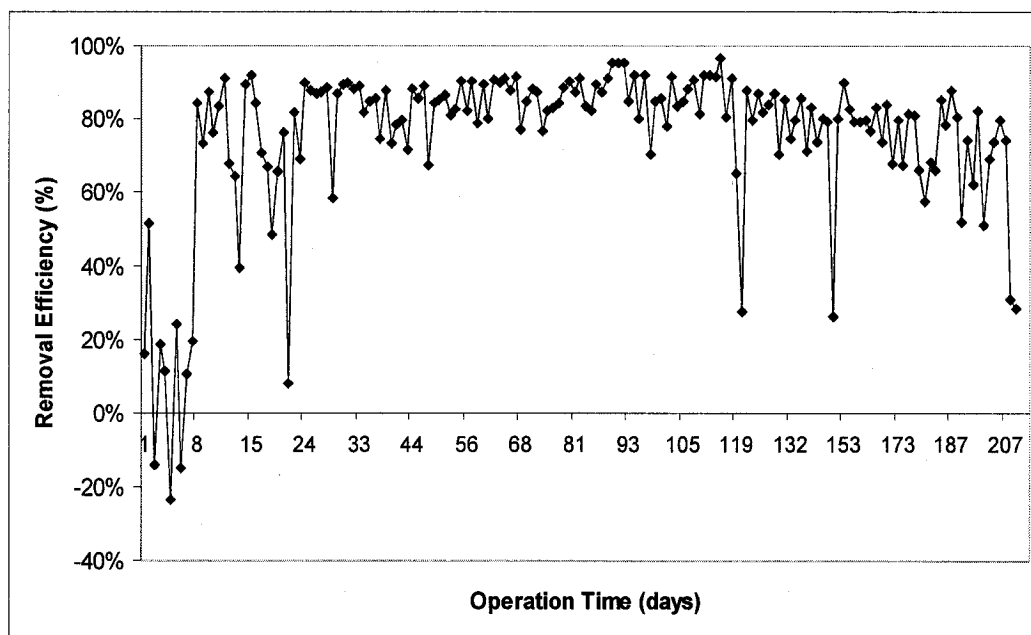
Figure 5-6: Removal efficiency for the sand biofilter over the duration of the experiment

After the initial phase, the sand biofilter seemed to work appropriately. On days 10 and 17 there was a little drying problem observed at the top of the biofilter due to the nebulizer malfunction, and nutrient solution addition helped to restore normal conditions. On day 20 of operation drying was very serious, and almost half of the biofilter depth was observed as dry. The removal efficiency was as low as 8% on that day. Again, nutrient solution was added. After the problem was fixed, ethanol was adequately treated and removal efficiency was stable at around 85%. This improvement may have occurred because microbial density increased and a mature microbial population developed. There were periods when stabilizing the inlet ethanol concentration was troublesome, from day 88 to 97 and from day 106 to

87

day 120 of operation. On day 118, the inlet concentration increased abruptly to 656 ppm_v and the syringe pump rate had to be readjusted. The next day the inlet concentration was really low because of the low pumping rate.

After approximately 100 days of operation the removal efficiency of the sand biofilter started to show a downward trend. This might have been caused by the partial clogging in the biofilter; however, the other parts available to air flow were still contributing to the overall treatment. On day 150, 26% removal efficiency was observed again due to the low inlet concentration of ethanol (12 ppm_v). The average removal during the last 50 days declined to 70%. The operation was terminated on day 208 because of high headloss.

5.2.2 Head Loss

The initial headloss was 2 mm, and stayed the same through day 25 of operation. Then, every 10 days period on average the headloss increased by 2 mm and reached at 8 mm on day 60 (Figure 5-7). After day 110, the headloss showed steady increase and did not stay constant over long periods of days like before. On day 177 the headloss was measured as 50 mm and from there on the increases were more abrupt. It reached 80 mm in two weeks. On the last day of operation, the headloss reached its maximum (110 mm), and the experiments were terminated after this point.

88
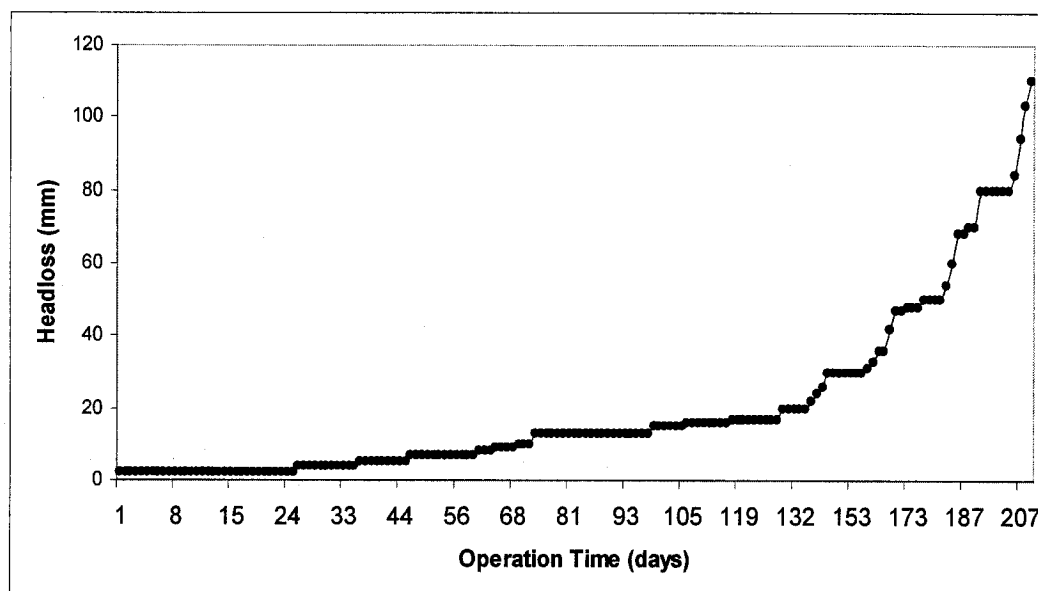
Figure 5-7: Headloss profile for the sand biofilter over the duration of the experiment

5.2.3   pH

The pH of the ethanol biofilters was one of the most significant signs that assure the successful operation. Ethanol due to its degradation pattern can create very low pH and that can interrupt the operation (Devinny and Hodge, 1995). There was a sensitive relationship between the moisture level, pH and the removal efficiency in the biofilter. Acidity was regularly checked, and adjusted to neutral by regular addition of nutrient solution including phosphate buffer. There were periods when low pH (pH=3 on day 116 of operation, and pH= 4 on day 120) was observed. During those periods nutrient solution was added more frequently and sometimes

89

phosphate buffer solution was applied to the sand biofilter. After day 123 of operation, pH was stabilized between 6 -7 (Figure 5-8).
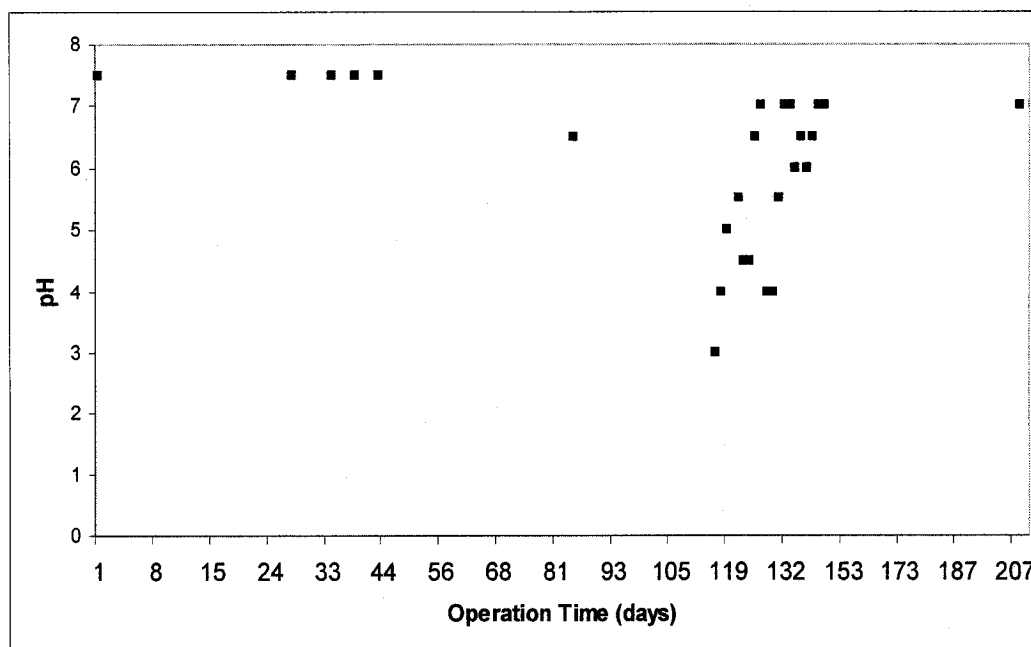
Figure 5-8: pH profile over the operational time of sand biofilter

5.2.4   Bacteria and Viral Enumeration

The bacteria count for the sand biofilter leachate was 9.14 (+/- .18) x 10^7 bacteria per ml, and the viral count was 3.99 (+/- 0.9) x 10^8 per ml (Steele et al. 2004). The virus to bacteria ratio was 3.37 in the sand biofilter.

5.3 Model Simulations for Biofilters

The biofilter pore structure was described by a pore network of cylindrical pores with varying diameters following an experimental pore size distribution. The numerical program combines percolation theory that is used to predict pore characteristics and surface area with biofilm growth cellular automaton (CA) algorithm, which determines the change in the biofilm thickness with time.

First, the initial pore size distribution that was experimentally determined and assigned to the whole network of pores. This was followed by the calculations of concentration and various characteristics including active, inactive and total biomass density in each discrete grid forming biomass. Biofilm growth was simulated by relocating excess microbial component to the next available grid (Song and Kinney, 2002). While CA algorithm predicted the spatial heterogeneity of biofilm in the network, the percolation part calculated fluid flow properties, changes in the pore sizes, and the cluster of the connected pores that were either filled or isolated, which therefore cannot contribute to the overall treatment process. Percolation model, where the effective medium approximation included, was also used to determine effective pore radius, and therefore the head loss profile along the biofilter with time. The program written in MATLAB can be seen in the Appendix II.

Ethanol was chosen as the model contaminant to be biodegraded in our experimental assessments because it was readily biodegradable, studied commonly and had many relevant parameters available in the literature.

91

Although there are variations in cellular composition with different types of organisms, according to Shuler and Kargi (2001) a typical cellular composition can be represented as $C\,H_{1.8}O_{0.5}N_{0.2}$. Therefore, the simplified biological conversion of ethanol can be written as

$$C_2H_6O + 2.475\,O_2 + 0.1\,NH_3 \;\rightarrow\; 0.5\,CH_{1.8}O_{0.5}N_{0.2} + 2.7\,H_2O + 1.5\,CO_2 \quad (5.1)$$
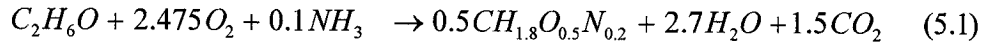
The degradation of ethanol was presumed to follow Monod kinetics (Nukunya et al. 2005). In the laboratory, ethanol biodegradation took place under aerobic conditions. The oxygen concentration in most waste gases is several orders of magnitude higher than the contaminant concentration. However, because of the low solubility of oxygen, the process may be limited by mass transfer of oxygen into the biofilm and/or diffusion in the biofilm (Kennes and Veiga, 2001). To determine whether oxygen was limiting, the criteria derived by Williamson and McCarty (1976) and used by Shareefdeen et al. (1993) and Nukunya et al. (2005) were employed. Oxygen will be limiting if the following two conditions are satisfied:

$$S_O < \frac{\upsilon_O D_{eth} MW_O}{\upsilon_{eth} D_O MW_{eth}} S_{eth} \qquad (5.2)$$

$$X_O < \frac{K_{SO}}{K_{Seth}} X_{eth} \qquad (5.3)$$

where υ_O and υ_{eth} are the stoichiometric coefficients for oxygen and ethanol in the ethanol degradation reaction, D_O and D_{eth} are the diffusion coefficients, MW_O and

MW_{eth} are the corresponding molecular weights, K_{SO} and K_{Seth} are the half-saturation constants, and S_O and S_{eth} are the experimental substrate concentrations. X_O and X_{eth} are the oxygen and ethanol concentrations in the biofilm, respectively.

When parameters describing experimental conditions were used in eq 5.2, it was determined that the concentration of ethanol in the air phase should be greater than 2.85×10^{-6}. This relationship was satisfied within our system up to the point where concentration of ethanol dropped to about 2% of its original value, which is the case in our experimental biofilters.

Williamson and McCarty (1976) have related all these by suggesting

$$\frac{S_{eth} - X_{eth}}{S_O - X_O} < \frac{\upsilon_{eth} D_O MW_{eth}}{\upsilon_O D_{eth} MW_O} \qquad (5.4)$$

Eq 5.3 was found to be satisfied by using eq 5.4 and assuming that X_O can be equal to oxygen solubility in the water at maximum. Therefore, oxygen was limiting; the biodegradation equations used in the model were described by considering oxygen only as suggested by Shareefdeen et al. (1993).

5.3.1 Model Simulations for Lava Rock Biofilter

The model was run for the oxygen limited kinetics for ethanol removal. The whole depth of the biofilter was modeled in five consecutive vertical segments to account for the depth of the filter. Because it was observed that the top parts of the biofilter were showing heavy growth of biofilm while deeper parts were available

93

and contributing to the overall treatment. The input parameters used in the simulations for lava rock biofilter were tabulated in Table 5-1.

Table 5-1: Input parameters used in the model for lava rock biofilter

	Parameter	Units	Value
estimated	$X_{initial}$ (initial biofilm density)	mg/L	30,000
	X_{set} (maximum biomass density)	mg/L	45,000
	μ (maximum growth rate)	1/h	0.03
	Y_o (yield coefficient)	mg biomass/ mg Oxygen	0.1
	C_o (oxygen concentration)	mg/L	3.4
	r_i (initial biofilm thickness)	m	20×10^{-6}
	k_d (biomass decay rate)	1/h	0.016
	β (inactive biomass formation)	mg/mg	0.17
known	C_e (ethanol concentration)	mg/L	0.126×10^{-3}
	H_o (Henry's law constant, oxygen)	Dimensionless	29.5
	H_e (Henry's law constant, ethanol)	Dimensionless	0.00025
	D_o (oxygen diffusion constant)	m^2/s	2.41×10^{-9}
	D_e (ethanol diffusion constant)	m^2/s	0.99×10^{-9}
	K_{s-o} (half-saturation constant)	mg/L	0.26
	V (total volume of biofilter)	L	1
	V_b (packed bed volume)	L	0.6
	ε (clean bed porosity)	Dimensionless	0.51
	R (maximum pore radius)	m	2.03×10^{-3}

Two parameters including k_d (biomass decay rate) and β (inactive biomass formation from active biomass) were taken from Song and Kinney (2002). The others were estimated by optimizing the model simulations for the experimental data. The typical biomass densities reported in literature for biofilters range from 23 to 220 kg m^{-3} (Shareefdeen et al. 1993). Therefore, the values (30 and 45 g/L) used in this simulation were comparable. Schwarz et al. (2001) reported typical range for maximum growth rates observed in biofilters range from 0.0036 to 36 h^{-1}. The value $\mu = 0.03$ h^{-1} was used in the calculations for lava rock biofilter in the absence of a

94

better estimate for simulations. When considering ethanol as substrate, theoretical biomass yields based on energetic relationships have been reported to reach 0.3 g biomass/g ethanol and 0.15 g biomass/ g oxygen (Nukunya et al. 2005). However, yield coefficients are not constants, since they are dependent on the substrate loading, biological parameters (X, μ), and chemical parameters including pO_2, C/N ratio and P content of the medium (Crueger and Crueger, 1990; Christen et al. 2002). Two studies Pérez et al. (2002) and Christen et al. (2002) reported two different yield coefficients for ethanol degradation in biofilters; the range was from 0.04 to 0.41 g biomass/ g oxygen consumed. The value used in this work, 0.1 g biomass/ g oxygen, is at about the middle point of the reported values and reasonable with respect to low growth rate used. Consumption of substrate by microorganisms for functions other than the production of new biomass (called maintenance metabolism) explains the lower growth rate constants associated with lower yield coefficients (Abbott et al. 1974). Initial biofilm thickness is usually assumed to be formed by a few layers of microorganisms ranging from 1- 10 μm (Schwarz et al. 2001), this work assumed a single layer to start with and the thickness of the layer was 20×10^{-6} m, comparable to the values reported in the literature (Shareefdeen et al. 1993; Song and Kinney, 2002; Nukunya et al. 2005; Schwarz et al. 2001). The oxygen concentration in the biofilm estimated as 3.4 mg/L, lower than the values used previously for oxygen solubility at room temperatures (Shareefdeen et al. 1993; Nukunya et al. 2005). Although the biofilter was operated in room temperature ranging between 23-26° C, the

95

temperature within the biofilm could have been several degrees higher, due to biological activity, thus resulting in decreased oxygen availability to the biofilm layers. Additionally, Plessis et al. (1998) suggested that less metabolic heat is lost from the biofilm in an aerosol biofilter, where the nebulizer supplied the bed with the moisture like in our case, due to heat transfer properties, resulting in lower oxygen solubility in the biofilm. It is recognized that the oxygen concentration of 3.4 mg/L used in the model simulations is likely lower than the actual concentrations. An explanation for this could not be firmly established. It is interesting to speculate whether this may reflect some factor retarding the transfer of oxygen to the biofilm.

The cumulative effects of the segments were compared to the bench scale lava rock biofilter experimental results. The model simulations for head loss, elimination capacity and the removal efficiency of the sand biofilter treating ethanol approximated the experimental data (Figure 5-9).

The model predicted that the head loss stays at the initial value of 2 mm till day 202, and very slowly increased to 4 mm on day 326, after that it became 10mm on day 347 which was followed by sudden infinite increase as clogging occurred.

96
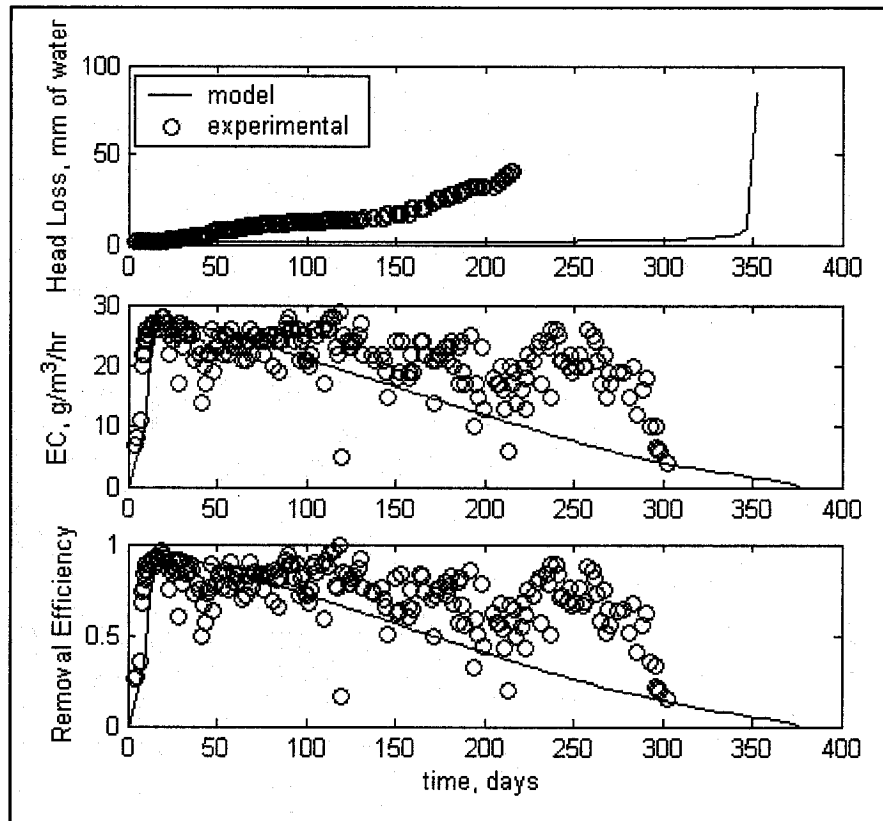
Figure 5-9: The simulated results for head loss, elimination capacity and the removal efficiency of the lava rock biofilter

In the early phase of the biofilter operation, exponential increase in removal of ethanol was observed. The model simulation clearly demonstrated the initial increase in removal efficiency and elimination capacity. The model was also able to simulate the gradual decline in removal efficiency and elimination capacity followed by clogging. The model predicted the clogging of the filter about 70 days after it occurred in the experiment.

97

5.3.2 Model simulations for Sand Biofilter

The model with five vertical segments and oxygen limitation for ethanol biodegradation was also run for the sand biofilter. The input parameters used in the simulations were summarized in Table 5-2.

Table 5-2: Input parameters used in the model for sand biofilter

	Parameter	Units	Value
estimated	$X_{initial}$ (initial biofilm density)	mg/L	25,000
	X_{set} (maximum biomass density)	mg/L	30,000
	μ (maximum growth rate)	1/h	0.02
	Y_o (yield coefficient)	mg biomass/ mg Oxygen	0.1
	C_o (oxygen concentration)	mg/L	3.4
	r_i (initial biofilm thickness)	m	6.75×10^{-6}
	k_d (biomass decay rate)	1/h	0.016
	β (inactive biomass formation)	mg/mg	0.17
known	C_e (ethanol concentration)	mg/L	0.188×10^{-3}
	H_o (Henry's law constant, oxygen)	Dimensionless	29.5
	H_e (Henry's law constant, ethanol)	Dimensionless	0.00025
	D_o (oxygen diffusion constant)	m^2/s	2.41×10^{-9}
	D_e (ethanol diffusion constant)	m^2/s	0.99×10^{-9}
	K_{s-o} (half-saturation constant)	mg/L	0.26
	V (total volume of biofilter)	L	1
	V_b (packed bed volume)	L	0.6
	ε (clean bed porosity)	Dimensionless	0.39
	R (maximum pore radius)	m	6.75×10^{-4}

Two biofilters were operated under the same conditions; therefore the values related with the process were selected as the same. The sand biofilter had smaller pore size distribution; hence, the typical biomass densities used in sand biofilter simulations were less than the lava rock simulations. However, they were still comparable with those in the literature (Shareefdeen et al. 1993).

98

The value for the maximum growth rate constant was used as 0.02 h^{-1}, which lies in the range reported in the literature. Initial biofilm thickness was assumed as 6.75×10^{-6} m as comparable to the pore size characteristics of the sand biofilter. The oxygen concentrations in the biofilm as well as the yield coefficient were used as the same for lava rock biofilter model.

The cumulative effects of the five segments were compared to the bench scale biofilter results. The simulated results for head loss, elimination capacity and the removal efficiency of the sand biofilter treating ethanol approximated the experimental data (Figure 5-10).

The model predicted that the head loss stays at the initial value of 2 mm till day 161, and very slowly increased to 5mm on day 196, after that a sudden increase to 10mm on day 199, followed by an infinite increase at the time of clogging.

Initially, exponential removal of ethanol was observed. The model simulation clearly demonstrated the initial increase in removal efficiency and elimination capacity, and shift to steady state after 50 days. The model also successfully simulated the gradual decline in removal efficiency and elimination capacity followed by clogging. The model predicted clogging about 6 days after it occurred in the experimental biofilter.

99
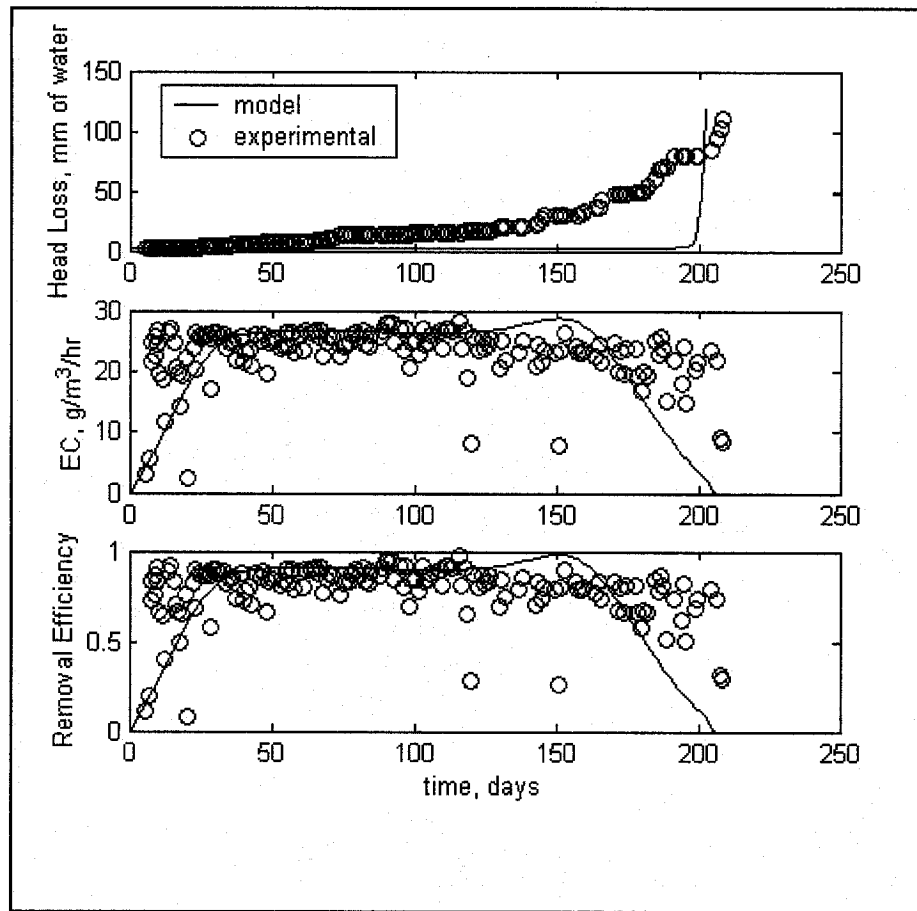
Figure 5-10: The simulated results for head loss, elimination capacity and the removal efficiency of the sand biofilter.

5.4 Clogging and Channeling Tests

After the red-dyed microsphere particles were run through the media for 5 hours, the lava rock biofilter was placed in the refrigerator overnight. The bottom of the filter was cut off, and the biofilter was inverted. A piston was used to push the media out of the acrylic cylinder in stages marked on the photographs as 0, 2, 4, 6, 8,

100

10, 12, 13, 14, 14.5 that is showing the distance from the bottom of the media, those numbers corresponded to bottom, 13, 11, 9, 7, 5, 3, 2, 1, and 0.5 cm from the top of the filter. At each stage, the protruding portion of the media was removed to reveal a cross-section of the pack. This was done by scraping away the media with a ruler. While this caused some minor disruption of the revealed cross–section, it is believed that the photographs are accurately representative of conditions in the media.

The image for top of the filter that was photographed before the media was turned over, and is shown here in mirror image to demonstrate alignment with the deeper sections (Figure 5- 11). The top of the filter was heavily clogged and showed only two spots for red particle deposition. Those two spots were probably the only spots for air to flow into the media; the biofilm has developed along these pathways down into the media. Air carrying red particles flowed the same way and the particles were deposited to appear in the cross sections, that was why red particles were observed in the areas where biofilm growth was obvious.
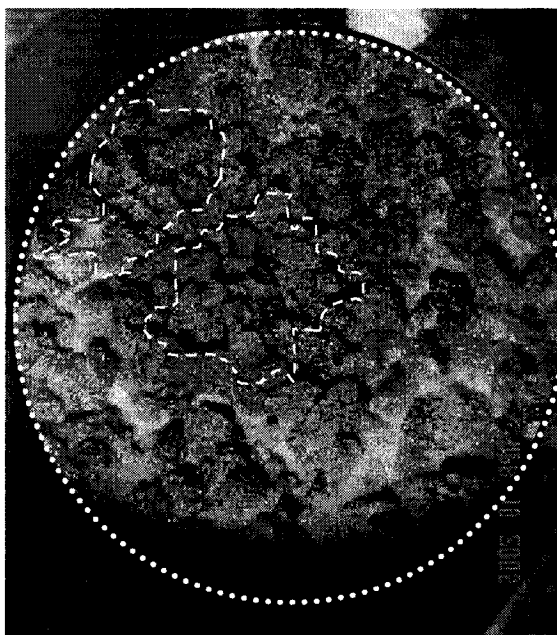
Figure 5-11: The top view of the biofilter, [black circle]: the media circumference, [white dotted line]: biofilm coverage, [white dashed line]: red particle spots
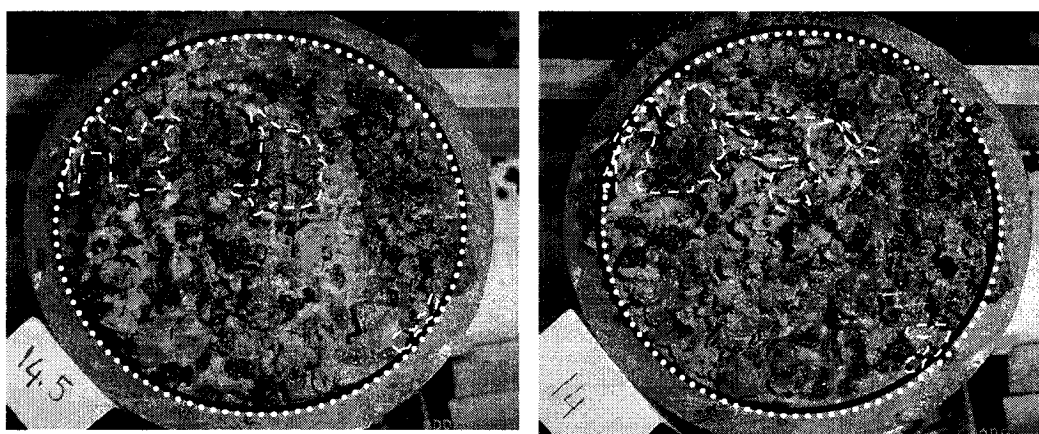
Figure 5-12: The photographs of cross-sections at 0.5 and 1 cm from the top of the lava rock filter, [black circle]: the media circumference, [white dotted line]: biofilm coverage, [white dashed line]: red particle spots

102

At 0.5 and 1 cm from the top, the coverage of heavy biofilm was 100%, and there was a third extra spot adjacent to the side of the acrylic cylinder (Figure 5-12).

At 2 cm from the top of the filter which was also mostly covered by heavy biofilm, the center spot for red particles became more significant with very brilliant color (Figure 5-13). At 3 cm from the top of the filter, dense glue-like biofilm was observed on 75% of the cross-section. At 5 cm (10 on the photograph), half of the cross-section was covered by heavy biofilm where red particles were observed in scattered small areas. At the cross-section that is 7 cm from the top of the filter, partial coverage—about one-third by brownish heavy biofilm was observed. Red particles were again observed at two spots within the area where the biofilm grown. At the top 3 cm of the filter the biofilm coverage was throughout the cross-section, however; further down showed partial coverage.

103
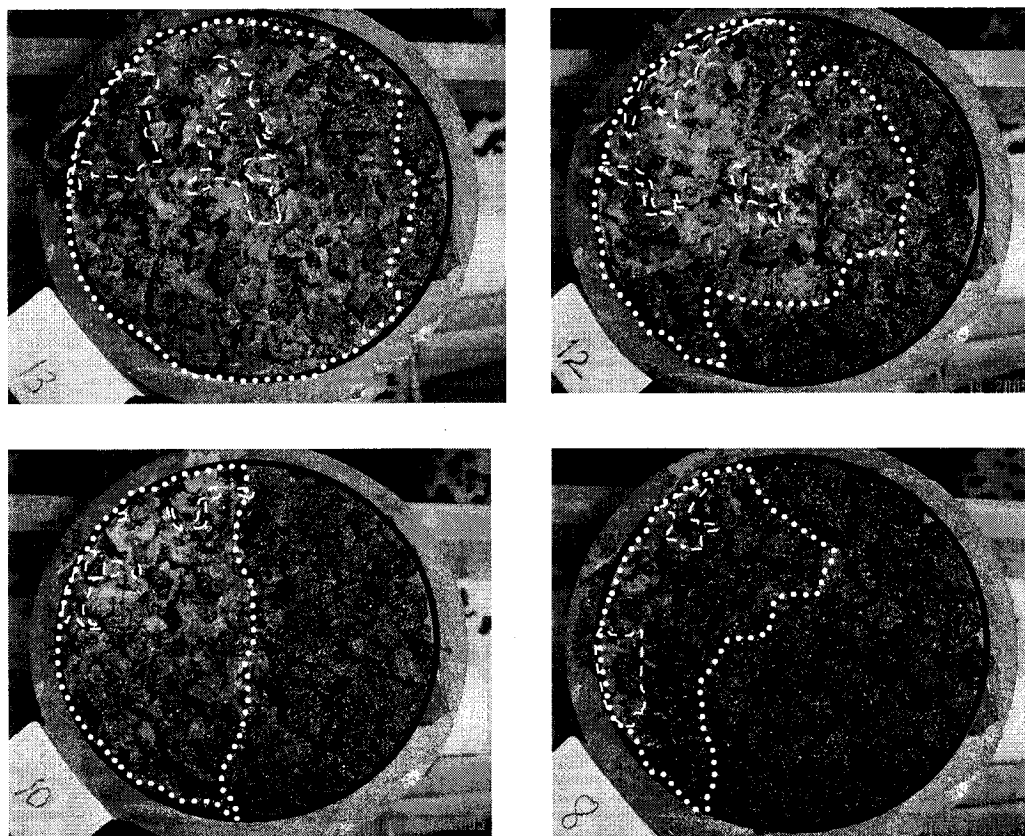
Figure 5-13: The photographs of cross-sections at 2, 3, 5 and 7 cm from the top of the lava rock filter, [black circle]: the media circumference, [white dotted line]: biofilm coverage, [white dashed line]: red particle spots

The cross-sections taken at 9, 11, 13 cm from the top and the bottom of the media (6, 4, 2, and 0 on the photograph) showed neither visual brownish biofilm nor red particles (Figure 5-14). However, the lava rock particles were slimy. This 6 cm-deep section at the bottom of the filter was probably the only part of the filter that was removing significant amounts of ethanol when treatment was ceased. The red

104

particles were not observed in this section, possibly because all of them were captured in the overlying sections of the filter.
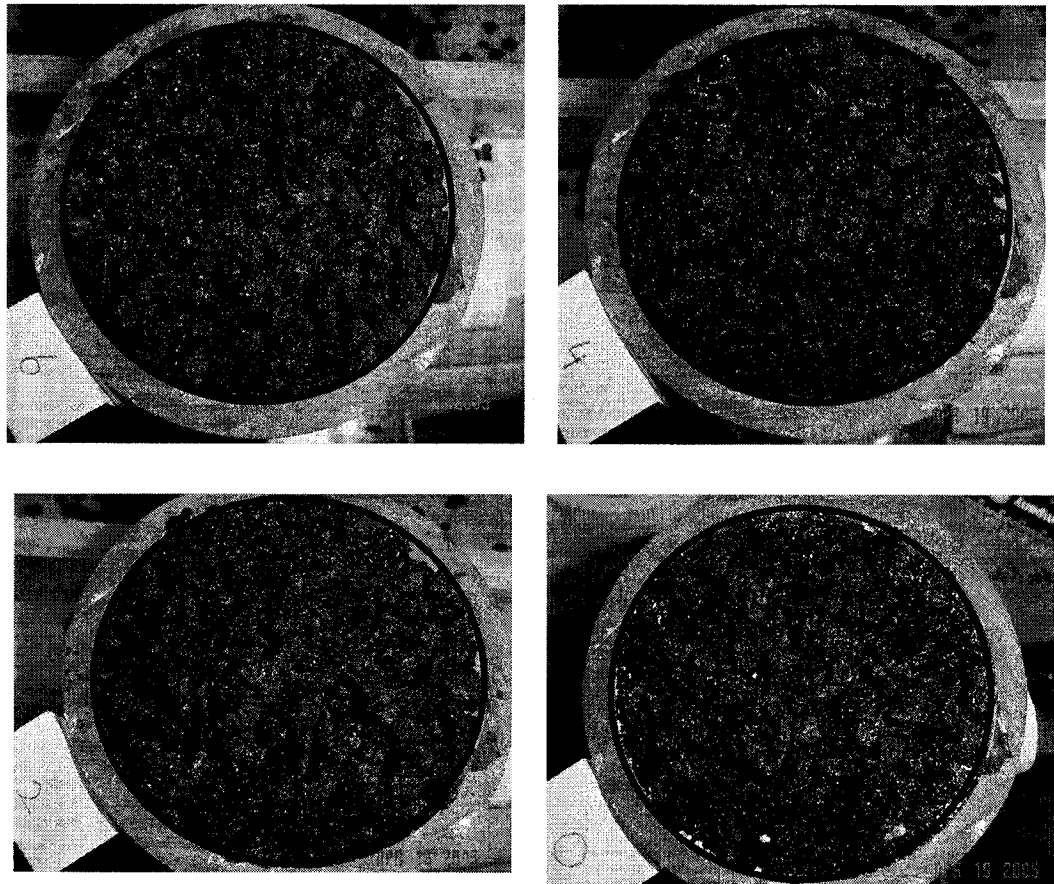
Figure 5-14: The photographs of cross-sections at 9, 11, 13 cm from the top of the biofilter and at the bottom of the lava rock filter, [black circle]: the media circumference (white particles on the bottom were acrylic plastic left by cutting the column)

The clogging and channeling tests demonstrated heavy clogging on the top 3 cm of the biofilter. Observation of red-dyed particles in certain areas including the center and two other spots adjacent to the side wall of the cylinder proved that there

105

was channeling in the filter. The channels could be seen extending through the first 9 cm of the biofilter. Below this, the biofilm was apparently much more uniform.

5.5 Swimming Pool Cleaner Tests

Tests were performed to see if a swimming pool cleaning product containing biofilm-destroying enzymes would be effective at degrading the excess exopolysaccharides (EPS), and restoring the biofiltration process in a clogged biofilter.

The tests were numbered from 1 to 9, with 1 referring to the control test having no pool cleaner. Test 2 started with the recommended dosage of enzyme for pool cleaning and increased stepwise. The concentration of cleaner, the holding time for flooding, inlet and outlet concentrations of ethanol, the removal efficiency and head loss results were shown in the Table 5- 3. (The density of the pool cleaner as it comes from the manufacturer is 1 g/ml.)

Table 5-3: The results for tests with pool cleaner

Test #	Pool Cleaner Concentration (mg/L)	Duration (min)	Inlet (ppm)	Outlet (ppm)	RE (%)	HL (mm)
1	Control – 0	3	70.70	21.64	69%	88
2	4	3	61.43	14.21	77%	90
3	40	3	31.95	10.41	67%	87
4	400	3	30.16	11.16	63%	90
5	4×10^3	3	50.61	10.74	79%	88
6	4×10^4	3	45.14	9.11	80%	70
7	4×10^5	3	35.21	9.36	73%	50
8	4×10^4	30	76.92	10.37	87%	60
9	4×10^5	30	43.60	9.07	79%	50

The control experiment was performed by flooding the biofilter with nutrient solution first for 3 minutes, and draining, then flooding again with distilled water only. The head loss was measured 24 hours after application. Tests 6 and 7 were repeated to test for the effects of duration of exposure. It seems that longer duration of flooding did not play a significant role on effectiveness of the enzyme, although it had some effect on condition 6 by further reducing the head loss from 70 to 60 mm of water (Figure 5 -15). While removal efficiency was somewhat steady between 60 and 80%, 43% decrease in head loss was observed when 4×10^5 mg/L pool cleaner was applied.
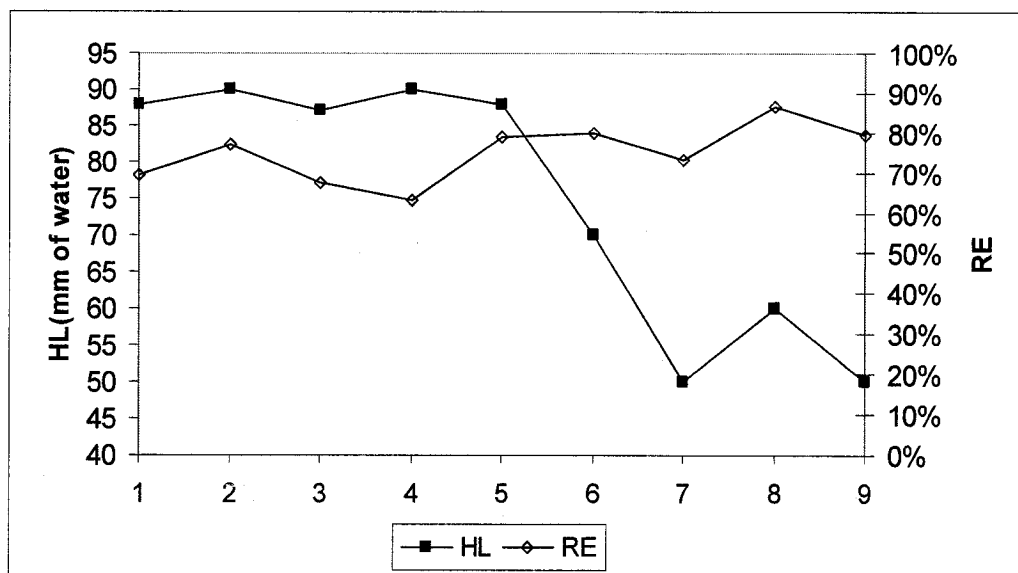
Figure 5-15: The results of the pool cleaner tests

107

After the last application of enzyme, the biofilter was operated like before, and analyzed for operation once a week by recording removal efficiency and head loss data.

It was planned to repeat the procedure for biodegradation tests when the head loss reached 80 mm again. According to the previous run, the head loss was 40 mm on day 164 of operation and increased to 80 mm in 28 days. After use of the pool cleaner, head loss increase was less rapid (Figure 5- 16). The headloss was observed as 60mm 24hr after the last application of the enzyme, and decreased to 40mm in two weeks; this decrease was probably due to the slow drainage of the excess degraded EPS or to continued activity of enzyme that that was not entirely removed. Then the head loss remained at 40 mm for 75 days after the cleaner application and removal efficiency was almost stable at 85% (Figure 5-17) for the inlet concentration profile over this period (Figure 5-18).

108
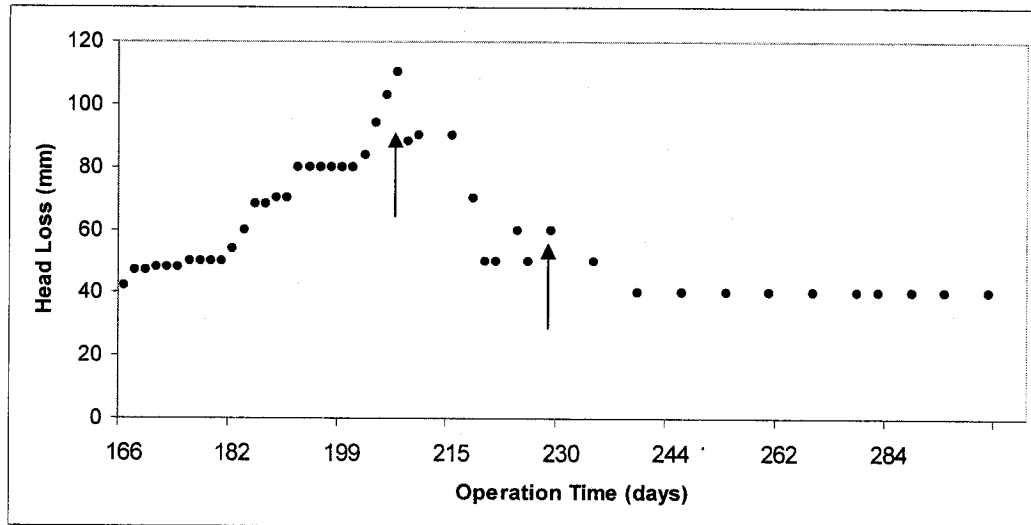
Figure 5-16: [Left of the first arrow]: Head loss profile of the sand biofilter before the application of enzyme, [between the arrows]: the head loss profile observed for different concentrations of enzyme, [Right of second arrow]: Head loss profile of the sand biofilter over a period after the application of pool cleaner
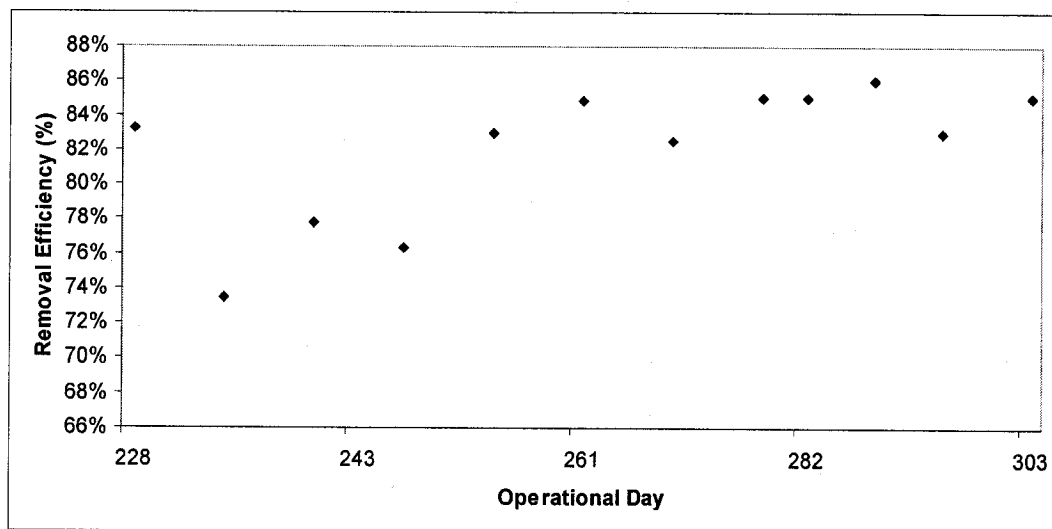
Figure 5-17: Removal efficiency profile of the sand biofilter over a period after application of pool cleaner

109
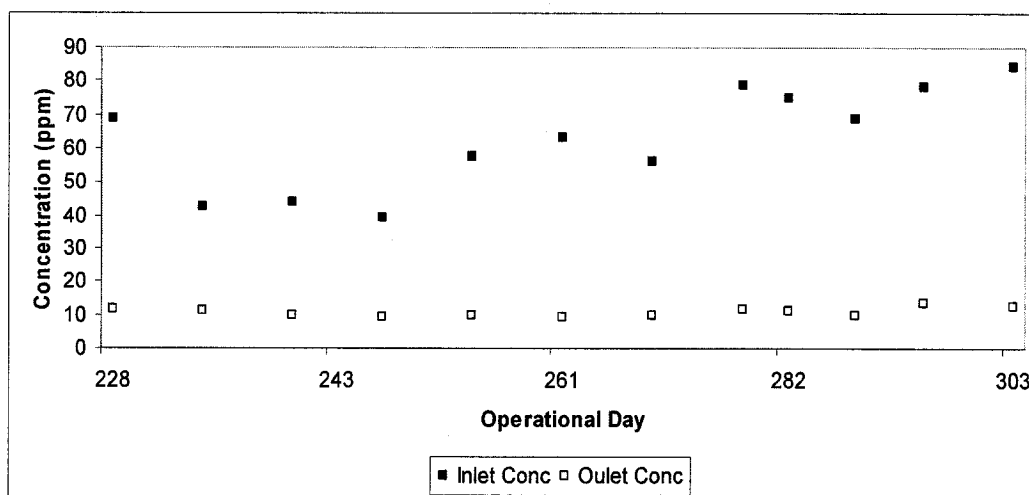
Figure 5-18: The inlet and outlet concentration of sand biofilter over a period after application of pool cleaner.

A final test was performed just to see the effect of enzyme on the sand biofilter with 40 mm head loss. 4×10^4 mg/L of pool cleaner solution was used to flood the biofilter for 3 minutes, and then distilled water was used for 1 min. The head loss declined from 40 mm to 30 mm the next day and to 20 mm in two weeks.

These experiments must be considered preliminary. Because the concentration of the pool cleaner was increased in steps, subsequent applications were not truly controlled demonstrations of how the cleaner might work in a single application on a biofilter. However, the results indicate that the process shows promise. It is of particular note that the removal efficiency was not reduced by the treatment. Other proposed clogging remedies, such as nutrient deprivation, heat treatment, or hypochlorite, all reduce treatment efficiency for a time (Nukunya 2004; Van Lith et al. 1994; Weber and Hartmans, 1994).

110

5.6 Discussion

The size and shape of the filter material determines the surface area to volume ratio. Smaller particles have higher surface area to volume ratios that promote increased adsorption of pollutants on the filter material and promote increased dissolution and absorption of pollutants into the water phase (Hodge et al. 1991). This was evident in the elimination profile of the sand biofilter. The removal efficiency of sand biofilter was much more sensitive to the inlet concentrations of ethanol and moisture content in the media, while lava rock biofilter performed more smoothly. Small particle sizes, on the other hand, decreases the permeability of the material, leading to increases in head losses and energy requirements (Ottengraf, 1986). The results from sand biofilter experiments suggested that smaller particles are more susceptible to biomass clogging than the larger lava rock particles.

Buffer capacity of the material must be sufficient to maintain pH values within a range that is optimum for microbial degradation efficiency. The pH may have been reduced due to the accumulation of carbon dioxide and/or acidic intermediates resulting from biodegradation of ethanol in the water phase. The experiments showed that the sand biofilter had deficient alkalinity concentrations as compared to lava rock biofilter, so required addition of chemical buffers more often.

The virus to bacteria ratio in the sand biofilter (3.37) was one fourth of the ratio observed for lava rock biofilter (14.79). This is an interesting distinction that could suggest a greater number of lysis events within the lava rock biofilter

community. Alternatively, this could merely reflect the inability of the virus particles to stick to the packing material in the more loosely packed lava rock. The relatively high virus to bacteria ratio suggests a dynamic interplay between bacteria and viruses in the biofilter community (Steele et al. 2004).

Preliminary tests have been performed on the clogging model for two packing materials with ethanol as the contaminant showed that five-segment approximation for the biofilter depth was effective to describe the process. Initial conditions of exponential increase followed by gradual decrease in the removal efficiency that is typical for biofilter applications were modeled satisfactorily. A complete understanding of the clogging process, and ultimately its control, would increase biofilter efficiency and broaden the range of applications. It is possible to imagine biofilters in which excess biomass is removed by washing, chemical dissolution, or mechanical removal. Each of these processes, however, requires expensive operating techniques or equipment on top of an inexpensive and simple packed bed system. This model may be able to predict the attendant improvement in efficiency and associated reduction in biofilter size for the additional expense of more elaborate biofilm control systems, and help guide development of new biofilter designs with appropriate packing.

The channeling tests showed that although top of the filter was heavily clogged, the air was channeled deeper into the media, where ethanol was treated effectively by the active part of the biofilter.

112

The pool cleaner tested showed that further testing of the enzyme is a promising avenue. It can be speculated that application of pool cleaner helps controlling the biomass overgrowth and prevent clogging.

113

6 REMOVAL OF ULTRAFINE AND FINE PARTICULATE MATTER IN GRANULAR FILTER WITH POSSIBLE APPLICATIONS TO BIOFILTRATION

6.1 Introduction

Several epidemiological studies have shown airborne particulate matter (PM) to increase mortality and morbidity rates in exposed populations (Dockery et al.1993; Pope at al. 1995). Atmospheric ultrafine particles ($100<$ d_p (particle diameter)< 150 nm) have recently received significant attention as toxicological investigations have indicated their potential for causing adverse respiratory health effects (Oberdörster et al.1992; Oberdörster et al. 1995; Donaldson and MacNee, 1998). Epidemiological studies conducted by Peters et al. (1997a-b) have demonstrated a stronger association between health effects and exposure to ultrafine particles than for fine or coarse particles. A study by Pekannen et al. (1997) found associations between the incidence of asthma in children and fine and ultrafine particles. Laboratory studies by Ferin et al. (1991) indicated that, for deposition of a given mass of PM in the lung, toxicity increases as the particle size decreases. Li et al. (2002) demonstrated that when epithelial cells from human airways were exposed to the different size categories of atmospheric PM, based on an equal mass basis, ultrafine PM caused a greater response. More recent studies in Southern California

114

(Li et al. 2003) demonstrated increased biological potency of the spatially inhomogeneous urban ultrafine particles, which was related to their high content of oxidant organic chemicals and their ability to damage mitochondria. These emerging findings from both the toxicological and epidemiological studies suggest further development and application of control technologies to reduce the emission rates of ultrafine PM.

Granular bed filtration has been extensively examined by many researchers for treatment of air containing large particles. Some studies have employed granular bed filters either for aerosol size distribution measurements or for analyzing the effect of electrostatic charges on filtration of particles (Boulaud, 1991; Shapiro et al. 1988; Fo et al. 2000). Results from these studies have shown that the presence of electrostatic charges can alter significantly the filtering behavior of the granular bed, but the relationship between charge and removal efficiency was not linear (Fo et al. 2000). Shapiro et al. (1988) has reviewed the state of the art of aerosol filtration by granular filters (by covering approximately 130 references) in the presence of electrostatic forces. Different types of electrostatic interactions were described, namely charging of aerosol particles, charging of filter granules and application of an external electrostatic field to the filter bed. This work does not employ electrical charging. Instead it investigates removal efficiency for electrically neutral particles by uncharged granular filters.

115

The removal efficiency of granular filters packed with lava rock and sand was studied for collection of airborne particles 0.05 to 2.5µm in diameter in anticipation of the possibility that either inert granular filters or biofilters could be used for treatment of fine particles. The effects of filter depth, packing wetness, grain size and flow rate on collection efficiency were investigated. Two packing grain sizes (0.3 cm and 0.15 cm) were tested for flow rates of 1.2, 2.4 and 3.6 liters per minute (LPM), corresponding to empty bed residence times (EBRT, equal to the bulk volume of the packing divided by the air flow rate) in the granular media of 60, 30 and 20s, respectively.

If granular filters are to be used for removal of particles from air, some mechanism must also be devised for cleaning or disposing of the filters. This might be accomplished by physical or chemical methods, but this work also anticipates the possibility of using biofilters, in which the granular packing is covered with a biofilm that degrades captured contaminants. Experiments used wet and dry media and grain sizes appropriate for biological treatment systems (Ozis et al. 2004a). However, no experiments involving biodegradation were done, and the removal efficiencies measured are applicable to a variety of conceivable filter designs.

116

6.2 Materials and Methods

The ultrafine airborne PM used in the experiments was polydisperse ammonium sulfate aerosols generated by a nebulizer (HOPE, B & B Medical Technologies, Inc., Orangevale, CA, Figure 6-1). Aqueous ammonium sulfate solutions (about 1 mg of ammonium sulfate in 1 mL of deionized water) were nebulized using room air at 20 psi. The generated aerosol passed through a 1-L chamber with ten Polonium-210 ionizing units (Staticmaster, NRD Inc., Grand Island, NY) to reduce particle charge to the Boltzmann equilibrium. The neutralized aerosol was mixed with room air (relative humidity: 20-30%) in a 35 L chamber and passed through the granular bed being tested.

For particles 0.05 to 0.8 μm in diameter, removal efficiency was determined by measuring their number concentration upstream and downstream of the filter with a Scanning Mobility Particle Sizer (SMPS, Model 3936, TSI Inc., St. Paul, MN). The SMPS sampled 0.3 liters per minute (LPM) of the total flow rates of 1.2, 2.4 and 3.6 LPM through the filter. The granular filter bed flow rate was monitored continuously throughout the experiments using a calibrated in-line direct-reading flow meter (Model A-32457-44, Cole-Parmer Instrument Company, Vernon Hills, IL). When wet packing was tested, a diffusion dryer was placed directly upstream of the particle analyzers to remove water vapor and dry the particles to restore them to their original size distribution.
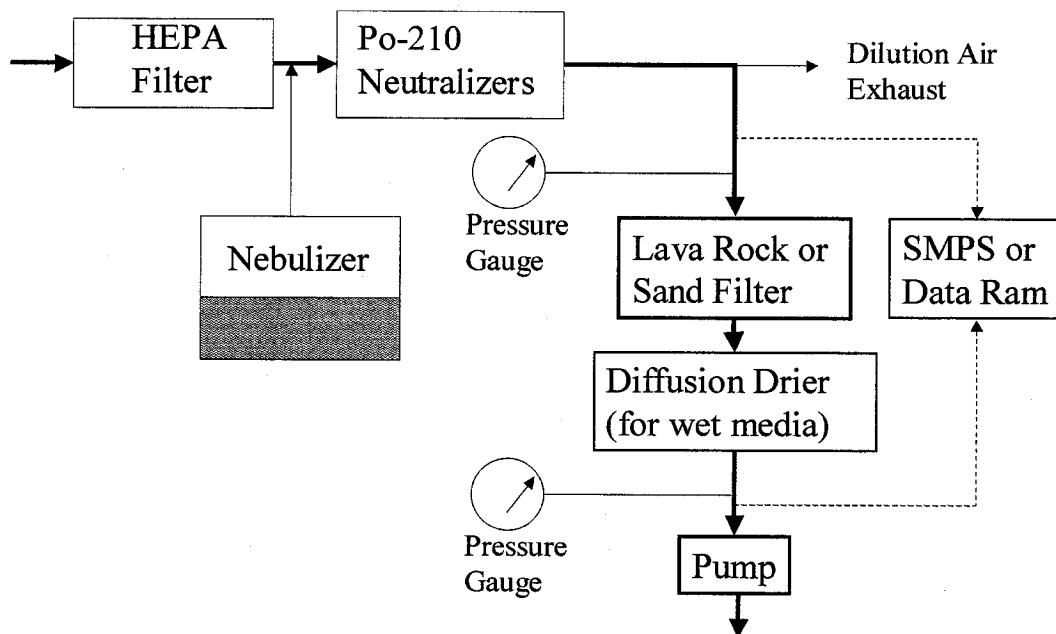
Figure 6-1: Schematic of the experimental set-up

In addition to the SMPS, the DataRAM (RAM-1, MIE Inc., Billerica, MA) was used to evaluate collection efficiency for particles in the 0.5 to 2.5 μm range, using laboratory-generated monodisperse polystyrene latex (PSL) particles (Bangs Laboratories Inc., Fishers, IN). The DataRAM was used for larger particles, while the SMPS was used for small particles, in order to optimize accuracy (Ozis et al. 2004a).

An acrylic plastic column filter, 7 cm inner diameter and 37 cm length, contained the packed bed. One packing was lava rock (Black Cinder, Sunburst Rock

118

Inc, Irwindale, CA), with a 0.3 cm median grain diameter after sieving. The second was quartz sand with a 0.15 cm median grain size. A single column was used, and experiments were run sequentially. Packing was added in three successive steps, producing packed beds 9, 18, and 27 cm deep (Table 6-1).

Table 6-1: Operating Conditions of the Experiments

Flowrate (LPM)	EBRT[a] (sec)	Filter Media	Filter Bed Configuration
1.2	60	Wet[b]/Dry	9cm, 18cm, 27cm
2.4	30	Wet[b]/Dry	9cm, 18cm, 27cm
3.6	20	Wet[b]/Dry	9cm, 18cm, 27cm

a Empty Bed Residence Time

b Wet media was only tested for full bed scenario.

6.2.1 Analysis

The density of the ammonium sulfate particles was 1.77 g cm^{-3} and that of the PSL particles was 1.05 g cm^{-3}. The aerodynamic diameters were calculated by multiplying each size by the square root of the particle density. In this work the terms "size" and "aerodynamic diameter" were used interchangeably (Ozis et al. 2004a).

The removal efficiency for the granular filter was determined by measuring inlet and outlet aerosol mass or number concentrations. For each particle size, removal efficiency was calculated from the inlet and outlet measurements:

119

$$RE\ (\%) = \frac{\left(C_{inlet} - C_{outlet}\right)}{C_{inlet}} \times 100 \qquad (6.1)$$

where RE is the removal efficiency; C_{inlet} is the inlet aerosol concentration; C_{outlet} is the outlet aerosol concentration.

Yoshida and Tien (1985) have developed an empirical equation describing the probability of particle adhesion for particles contacting surfaces at high gas velocities. They found that when the Stokes number exceeds 0.01, the collection efficiency decreases as particle "bounce off" rates become significant. For this work, the case in which the rebound probability is highest is for the lava rock media (porosity 47%, grain size 0.3 cm), the highest flow rate (3.6 LPM), and the largest particle size (2.5 µm). The Stokes number in this case, S, can be calculated with eq 6.2:

$$S = \frac{\rho_p\, d_p^2\, U}{9\, \mu\, D_G} = 0.0004 \qquad (6.2)$$

where ρ_p is the particle density, d_p is the particle diameter, U is the approach velocity, μ is the air viscosity, and D_G is the grain size. This value for the Stokes number is far below those at which particles are expected to bounce off of the packing surface. Therefore, removal efficiency calculations in this study presume that all contacts between the airborne particles and the filter grains result in permanent deposition of the particles.

120

The collection efficiency (1- P, where P is the penetration) for a given aerosol can be expressed in terms of the dimensionless single grain collector efficiency (Tardos et al. 1978; D'Ottavio and Goren, 1983; Boulaud et al. 1989), η_j.

$$\eta_j = \frac{frequency\ of\ deposition\ on\ a\ filtering\ element\ j}{n\ U\ A_j} \qquad (6.3)$$

where n is the local aerosol concentration, and A_j is the cross-sectional area of the particle normal to the direction of flow.

For a bed depth of L, of uniform packing porosity ε, and filtering elements of volume V_j, penetration can be written as (Boulaud et al. 1989):

$$-\ln P = (1-\varepsilon)\ L \sum_j \eta_j\ A_j \Big/ \sum_j V_j \qquad (6.4)$$

Experimental results obtained for neutral filters were insensitive to granule shape (Tardos et al. 1978), so the bed was assumed to consist of identical spheres of diameter D_G, and eq 6.4 becomes:

$$-\ln P = 3/2\ (1-\varepsilon)\ L\ \eta/D_G \qquad (6.5)$$

where η is single grain collection efficiency. If eq 6.5 is rewritten:

121

$$P = \exp(-3\,(1-\varepsilon)\,L\,\eta/2D_G) \qquad (6.6)$$

Thus the penetration through the granular bed is related to the single-grain collection efficiency by geometric parameters only, namely porosity, bed depth, and grain size.

The main mechanisms responsible for removing aerosols on a single grain—impaction, sedimentation, interception, and diffusion—and the theoretical calculations of collection efficiencies for those mechanisms were summarized by Boulaud (1991), Mann and Goren (1984) , Shapiro et al.(1988) , Yoshida and Tien (1985), Gal et al.(1985), Alonso and Alguacil (2002).

The equations of Boulaud (1991) were used in this study to calculate collection efficiencies. Equations were derived for the single grain collector efficiency for each removal mechanism and the overall collection efficiency of the bed was presumed to be their sum:

$$\eta = \eta_I + \eta_S + \eta_\Gamma + \eta_D \qquad (6.7)$$

where the subscripts I, S, Γ, and D refer to impaction, sedimentation, interception and diffusion, respectively (Ozis et al. 2004a).

Impaction removal efficiency (η_I) was correlated with effective Stokes number (S_{eff}) by Gal et al. (1985) and Otani et al. (1989):

122

$$\eta_I = \frac{S^3_{eff}}{1.4 \times 10^{-2} + S^3_{eff}} \qquad (6.8)$$

where S_{eff} is based on Ergun's equation and relates the single collector efficiency to the inertial parameters of the particles:

$$S_{eff} = \left(1 + \frac{1.75\,R_e\varepsilon}{150(1-\varepsilon)}\right) S \qquad (6.9)$$

where R_e is the Reynolds number of flow around the grain, and

$$S = \tau \times U / D_G \quad \text{, and } \tau = D_p^2 \times \rho_p \times C_p / 18\mu \qquad (6.10)$$

where τ is the particle relaxation time, ρp is the density of the particles, Cp is the Cunningham slip correction factor, and μ is the air viscosity.

Some particles are removed when they settle under the effects of gravity, and contact the packing surface below. The equation for sedimentation efficiency is (Boulaud, 1991):

$$\eta_S = 0.0375\,(G_r)^{0.5} + 0.21(G_r)^{0.78} \qquad (6.11)$$

where G_r =Vs/U, the particle sedimentation velocity divided by the approach velocity.

123

Interception is a geometric mechanism that occurs when the trajectory of a particle of diameter Dp moves within a distance of less than half of Dp from a grain diameter D_G. The interception parameter, R, is:

$$R = D_P / D_G \qquad (6.12)$$

and the single-grain collection efficiency (η_Γ) is:

$$\eta_\Gamma = H(\varepsilon)R^2 \qquad (6.13)$$

where H(ε) is a hydrodynamic factor and is a function of the bed porosity (Boulaud, 1991).

$$H(\varepsilon) = 6.3\varepsilon^{-2.4} \qquad (6.14)$$

For smaller sizes of aerosol particles Brownian motion becomes more significant as a mechanism of removal. Otani et al. (1989) have developed an equation for the diffusional efficiency of a single grain:

$$\eta_D = B(R_e)S_c^{f1(R_e)}R_e^{f2(R_e)} \qquad (6.15)$$

where Sc is the Schmidt number (v/Di where v is the kinematic viscosity of air, and Di is the Stokes-Einstein diffusion coefficient), and:

124

$$f_1(R_e) = -\frac{2}{3} + \frac{R_e^3}{6\left(R_e^3 + 2.0 \times 10^5\right)}$$

$$for\ R_e < 30: \qquad B(R_e) = 8 \quad and \quad f_2(R_e) = -2/3$$

$$for\ 30 \le R_e \le 100: \quad B(R_e) = 40 \quad and \quad f_2(R_e) = -1.15 \qquad (6.16)$$

Over the particle size range of interest, 0.05 μm to 2.5 μm, the contribution of these mechanisms changes. Diffusion is dominant for small particles, which are moved easily by Brownian motion. For larger particles, Brownian motion is less significant, but settling velocities are larger, so sedimentation dominates. Diffusion and sedimentation removal are equal at about 1.2 μm under the conditions of this study. Interception is negligible throughout the range. Impaction is negligible for the small particles because of their low mass, but it accounts for about 10% of removal for particles of 2.5 μm (Ozis et al. 2004a).

It is valuable to note that the diffusion collection efficiency depends on the Reynolds number for flow through the packing. In turn, the means that treatment success increases with air velocity, and therefore decreases with the cross-sectional area of the granular filter. Biofilter designers are accustomed to accepting reactor volume as the primary determinant of removal efficiency for a given contaminant and packing conditions, with the appropriate combination of reactor depth and cross-sectional area determined by secondary factors such as the ability of the packing to resist crushing under its own weight or the allowable reactor footprint. For the interception of fine particles, however, two granular beds of the same volume (and

125

EBRT) but different cross-sectional areas are predicted to have different removal efficiencies.

The effect is not strong—in some cases doubling the diameter of a cylindrical bed can decrease removal efficiency by 20%—but it will in sometimes dictate that multiple reactors should be operated in series rather than in parallel. Ultimately, design will involve a tradeoff between the higher efficiencies resulting from higher flow rates and the associated higher head losses (Ozis et al. 2004a).

6.3 Results and Discussion

The experimentally determined particle removal efficiencies for the filters using lava rock packing (0.3 cm median) showed that particle collection increases with increasing depth of the filter media for depths from 9 to 27 cm (Figures 6.2 to 6.4). As expected, greater time of exposure allowed for more particle removal by either diffusion or sedimentation (Ozis et al. 2004a).

For all flow rates, the relationship between removal efficiency and particle size was similar, with a minimum for particles with diameters between 0.5 μm and 0.7 μm (Figures 6-2 to 6-4). The observation that particle removal decreases as flow rate increases for larger particles is consistent with the conclusion that impaction was not a significant removal mechanism. Lower flow rates (hence higher residence times in the filter bed) result in higher removal efficiency for the entire range studied

126

that is again consistent with the conclusion that diffusion and sedimentation dominate removal and the effect of impaction is smaller. Removal efficiency increases with decreasing particle size for particles smaller than 0.5 μm and increases with size for particles larger than 0.7 μm. This supports the hypothesis that the dominant removal mechanism for the smaller size range is diffusion, that a combination of diffusion and sedimentation are seen in the middle size range (neither of which is fully effective), and that sedimentation dominates for the higher particle size range (Ozis et al. 2004a). All the experimental data can be seen in Appendix V.
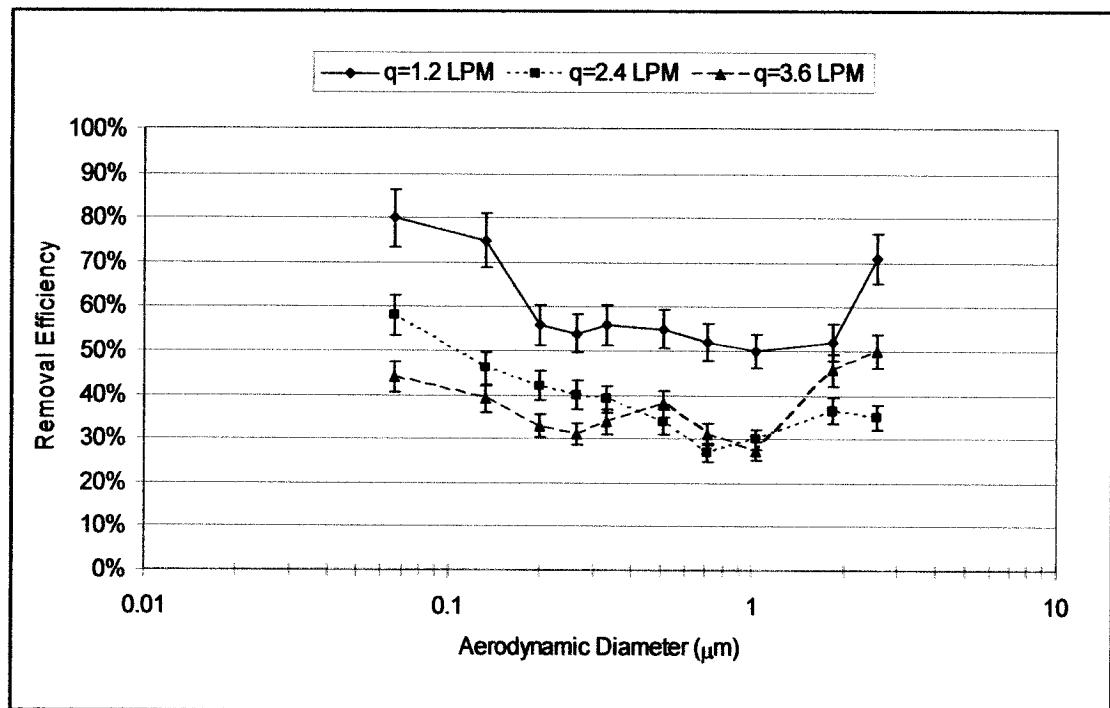
Figure 6-2: Removal Efficiency vs. Aerodynamic Diameter for three flow rates on 9 cm of dry lava rock
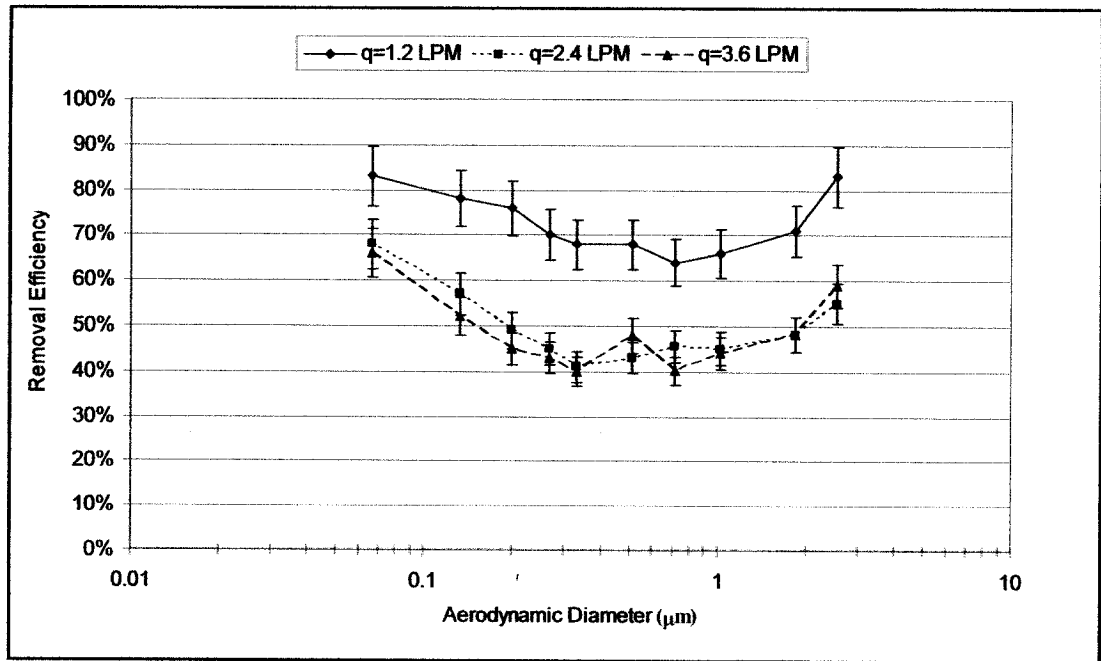
Figure 6-3: Removal Efficiency vs. Aerodynamic Diameter for three flow rates on 18 cm of dry lava rock
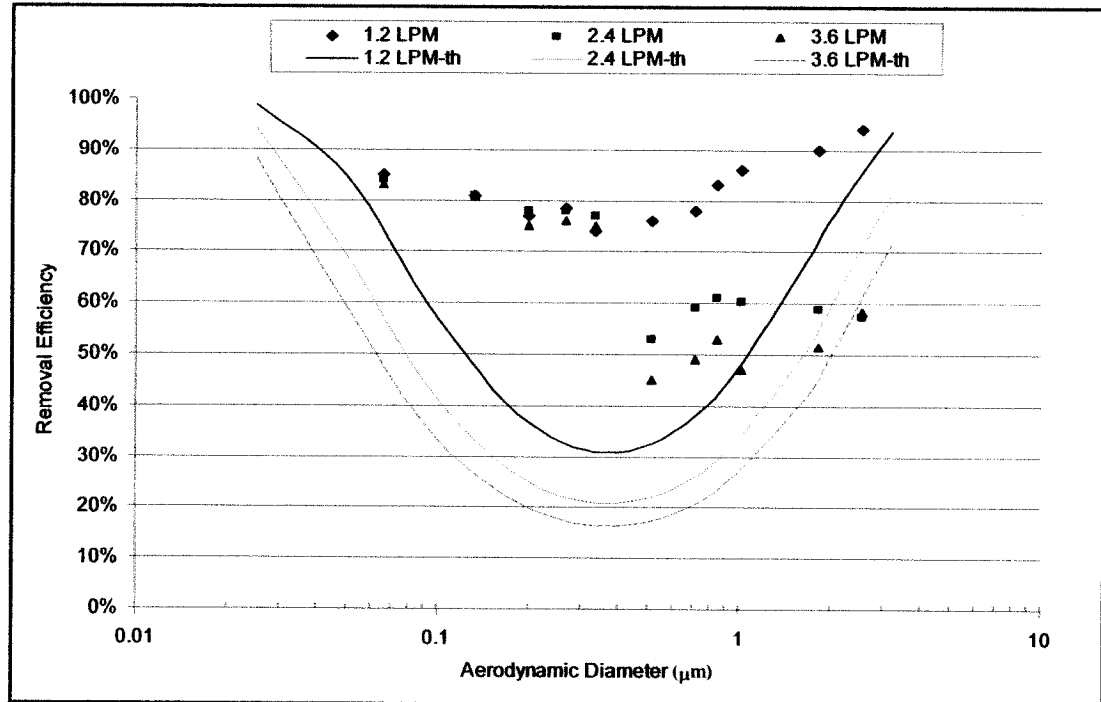
Figure 6-4: Removal Efficiency vs. Aerodynamic Diameter for three flow rates on 27 cm of dry lava rock. (Experimental data shown as points, model calculations lines)

128

Excepting a few results for small particles in the 3.6 LPM case, the removal efficiencies measured in the sand-filled bed (0.15 cm grains, Figure 6-5) were higher than those in the comparable lava rock experiment (0.3 cm grains, Figure 6-4). This presumably occurred because the sand medium has smaller pores and the distances over which the particles diffused or settled before contacting the packing grains were shorter (Ozis et al. 2004a).

Theoretical and experimental data showed similar trends: removal efficiency curves were U-shape, with removals lower for the middle size range and higher for the smallest and largest particles (Figures 6- 4 and 6- 5). In the case of lava rock media, theoretical calculations predicted somewhat lower removal values than the experimental results (Ozis et al. 2004a).
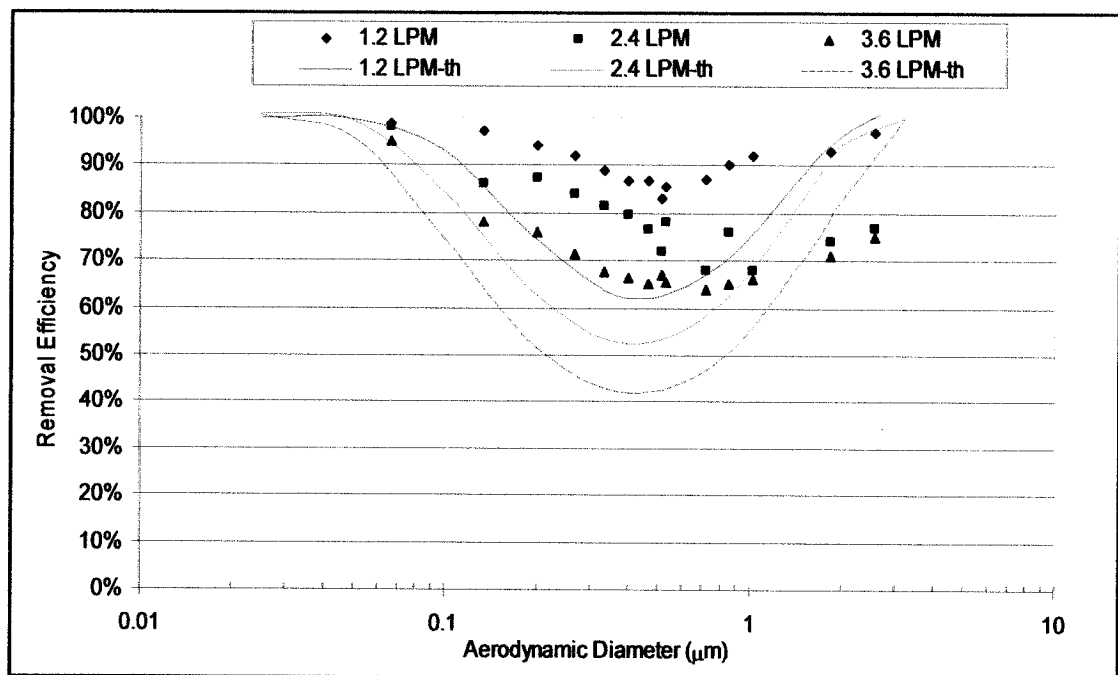
Figure 6-5 : Removal Efficiency vs. Aerodynamic Diameter for three flow rates on 27 cm of dry sand. (Experimental data shown as points, model calculations lines)

129

Particles, especially in the middle size range, were removed more effectively than calculations indicated for all flow rates. This presumable reflects the effects of additional factors like electrostatic forces that were not included in the theoretical calculations. Moreover, the estimation of total filtration efficiency for a granular filter using theoretical models of single bodies must be viewed cautiously because the current theoretical description of the effect of neighboring collectors on particle trajectories is inadequate (Shapiro et al. 1988). This may also account for the error in the estimation of removal efficiencies on lava rock. On the other hand, in the case of sand media, theoretical calculations approximated experimental removals more closely. The greatest divergence between theoretical and experimental data occurred in the middle size range; again, factors not included in the model may have had some effect.

The comparison of removal efficiencies between dry and wet media at different flow rates for 27 cm of media (Figure 6-6 and 6-7) shows that dry media removal efficiencies for ultrafine particles were higher than those observed for wet media. At least two factors may have contributed to this difference. Added water forms a film on the media granules that reduces the size of the larger pores and fills the smallest pores. This decreases the total porosity and the actual contact time and surface area available for contact by particle diffusion. It also raises the relative humidity for air in the pores to a value very close to 100%. Hydrophilic particles may act as condensation nuclei, gaining a film of water from the humid atmosphere

130

that effectively increases their size and thus reduces their diffusion rates (Ozis et al. 2004a). However, the removal efficiency for the larger particles was not much affected by water on the medium. Because the dominant mechanism of removal is sedimentation rather than diffusion, any effects of reduction in pore volume could be countered by accumulation of a water film on the particles, because it would increase their mass and thus their sedimentation velocities. Additionally, the decreased pore volume and the resulting higher interstitial velocities may also enhance particle impaction, which is just beginning to have some effects at the largest particle sizes. This phenomenon has also been suggested by Raynor and Leith (2000).
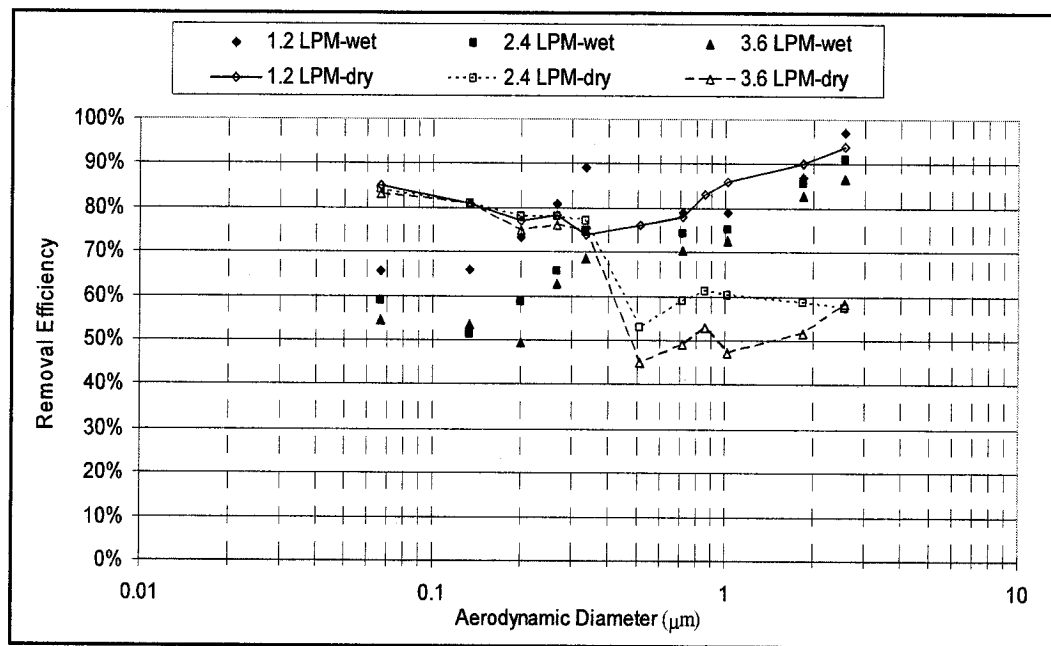
Figure 6-6: Removal Efficiency vs. Aerodynamic Diameter for 27 cm wet and dry lava rock. Filled symbols are removal on wet media; lines with empty symbols refer to dry media (repeating data of Figure 6-4).

131
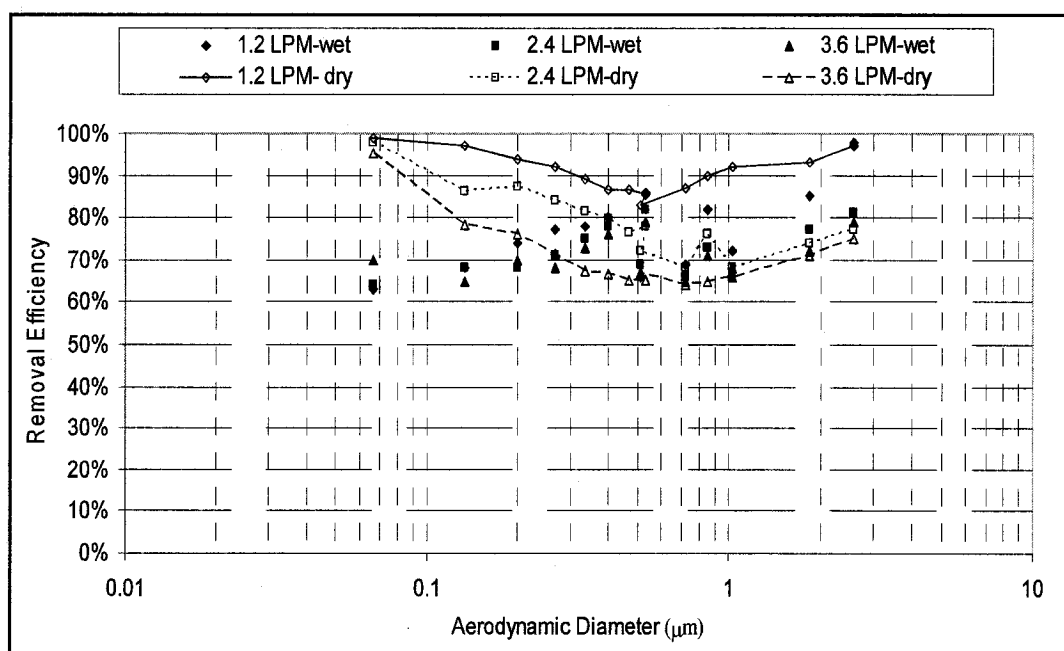
Figure 6-7: Removal Efficiency vs. Aerodynamic Diameter for 27 cm wet and dry sand. Filled symbols are removal on wet media; lines with empty symbols refer to dry media (repeating data of Figure 6-5)

Finally, an additional experiment was run to provide a head-to-head comparison of the polystyrene latex beads and the ammonium sulfate particles in the size range of 0.1 to 0.4 μm. The polystyrene latex particles are hydrophobic, and are expected to be unaffected by condensation on the particles. The hydrophilic ammonium sulfate particles will increase in size as humidity promotes condensation. When tested under identical conditions, removal efficiencies for PSL beads were essentially unaffected by the addition of water to the media (Figure 6-8). But the removal efficiencies for small ammonium sulfate particles were clearly higher on dry media than on wet. Thus we conclude that condensation on the particles and the

132

associate reduction in diffusion rates is the important factor in reducing removal efficiencies in wet media. Effects are important for ultrafine particles, but not for fine particles (Ozis et al. 2004a).
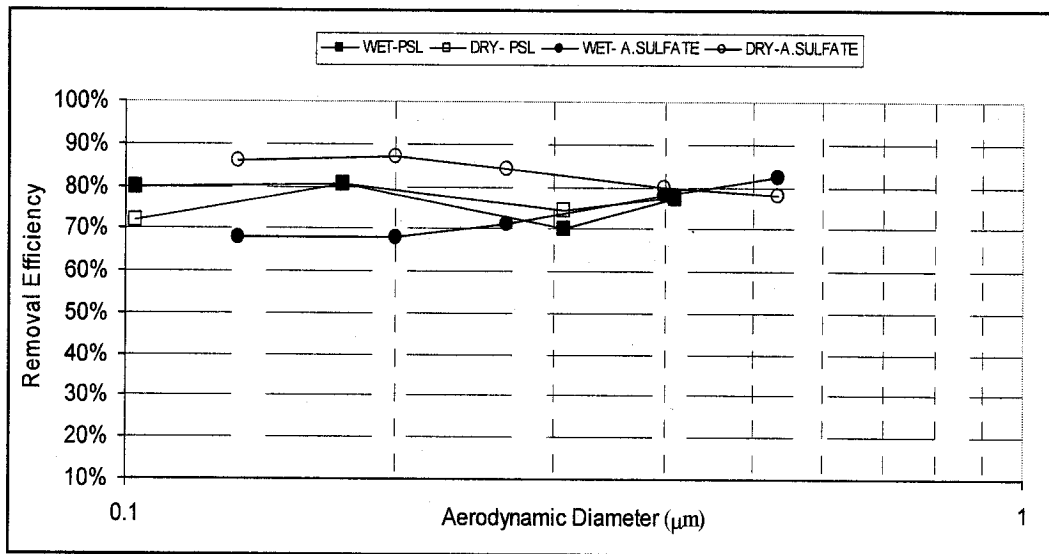
Figure 6-8: Comparison of removal efficiencies of PSL and Ammonium Sulfate particles on 27 cm of sand bed at 2.4 LPM. (Data for ammonium sulfate are repeated from Figures 6-5 and 6-7.)

The pressure differences across the filter packing were measured with pressure gauges. The pressure drops measured during experimental studies were very low, well within the range of values typically seen for economically viable biofilters (Table 6-2 and 6-3).

133

Table 6-2: Pressure drop data measured during the experimental studies with lava rock media

| | Pressure Drop (mm of water) | | | |
| | 9 cm deep bed | 18 cm deep bed | 27 cm deep bed | |
Flowrate (LPM)	Dry	Dry	Dry	Wet
1.2	0.127	0.381	0.508	0.127
2.4	0.254	0.508	0.762	0.381
3.6	0.381	0.635	1.016	0.508

Table 6-3: Pressure drop data measured during the experimental studies with sand media

| | Pressure Drop (mm of water) | |
| | 27 cm deep bed | |
Flowrate (LPM)	Dry	Wet
1.2	1.397	1.016
2.4	2.286	1.778
3.6	5.08	2.032

6.4 Application of the Model

The data were in fair agreement with predictions of previously developed model for collection efficiencies in granular bed filters. This model allows conceptual design of granular filters that can be effectively applied to major sources of particulate matter (Ozis et al. 2004b). A granular filter that could remove 91% of heavy-duty diesel truck emissions (2000 – 5000 LPM) could be small enough for use on-board. The size of a granular filter for emissions from Caldecott Tunnel located in Berkeley, California was also determined. The calculations are certainly

134

preliminary and approximate, but allow a general assessment of the feasibility of granular beds for removing particulates in real-world applications.

In use, granular filters will gradually fill with particles, limiting their useful lifetime. The time to clogging for the hypothesized filters was shown to be acceptable for practical use.

6.4.1 Heavy Duty Diesel Truck

Heavy-duty diesel vehicles are substantial contributors of particulate matter, and as health effects of fine PM have become more apparent; EPA is developing stricter regulations (EPA, 2000).

Diesel particles are a complex mixture of elemental carbon, a variety of hydrocarbons, sulfur compounds and other species (Burtscher, 2001). The particulate emissions from vehicles can be easily affected by vehicle class and weight, driving cycle, vehicle use patterns, fuel type, engine exhaust after treatment, vehicle age, and the terrain traveled (Holmen and Ayala, 2002). Zhi et al.(2002) have studied the characteristics of the diesel exhaust particulate for S195 diesel engine (at a speed of 2000 rpm, and engine load range of 0 - 0.7 MPa) and found average particle exhaust concentrations of 200 mg/m^3 in cooled exhaust. However, for the purpose of this paper we have assumed steady state conditions of operation, so that PM emissions were insensitive to the vehicle weight (Clark and Gajendranand, 2003). The fine particle size distribution of heavy-duty diesel truck emissions has been determined

135

by EPA's On-road Diesel Emissions Characterization by sampling directly from the plume (Brown, 2001).

Assuming 3500 LPM average flow rate for the exhaust, a granular filter that can remove 91% of particulate matter emissions from a heavy duty diesel truck specified by the study conditions of Zhi et al.(2002), could be a cylinder 115 cm long and 100 cm in diameter (or three cylinders 115 cm long and 70 cm in diameter). The design EBRT is 16 seconds. The total volume of particles (m^3) per cubic centimeter of air is 1.59x10-13. Assuming 40% initial porosity in quartz sand packing (0.15 cm average grain size), that clogging occurs when the initial porosity is reduced by half, and 10 hours of operation per day, the time-to-clogging for this granular filter was calculated as 564 days (Ozis et al. 2004b).

While this filter is large, it is still within range of practical use on a typical diesel tractor, where it could be placed behind the cab, or on top, behind the aerodynamic fairing. Cleaning or replacement of the media would be required about once every 18 months, but this seems a workable maintenance schedule.

6.4.2   Caldecott Tunnel

Caldecott tunnel, which has three bores, runs in the east-west direction through the Berkeley hills and connects Oakland and Berkeley with inland communities in Contra Costa County (Miguel et al. 1998). Each bore is approximately 1.1 km long, 8 m wide and 10 m high.

136

The tunnel has been the object of several studies because it has bores reserved for heavy-duty and light-duty traffic. These bores are divided by concrete walls, and air is not mixed between them. Allen et al. (2001) has sampled particulate matter mass concentration in the tunnel during the passage of 37,500 vehicles in four sampling events, each of which ran for 3 hours. They reported 102 $\mu g/m^3$ as the average PM 1.9 mass concentration in Bore 1, where the heavy-duty vehicle contribution is much greater than that for light-duty vehicles. The bores are fitted with CO sensors and a fiber optic system for tracking traffic flow and triggering the ventilation system when toxic gases build up. For the calculation here it was presumed that the ventilation system replaced the air in the tunnel 10 times per hour, so that the total flow rate of the air is 9500 m^3/min. The mass concentration of particulates was presumed to be 1452 g/day.

Assuming 40% porosity in 0.15 cm quartz sand grains, the granular filter that can remove 90% of the total particulates is 125 cm long and 50 m in diameter. The EBRT is 15 seconds, and the clogging time is 373 days. Such a system could be designed, for example, as 25 stacked tanks 1.25 m deep and 10 m in diameter, or in some other configuration convenient for land availability at the site. The installation would again be very large but within the range of practicality (Ozis et al. 2004b).

137

7 CONCLUSION

Important transport, topological and biological reaction processes observed in biofilters were combined to form a set of differential equations that provided a description of constituent concentration, change in the pore characteristics, and biofilm growth. The differential equations were solved numerically, and given initial conditions, the model predicted removal efficiency, elimination capacity and head loss profiles throughout the useful life of the biofilters. Both theoretical and experimental biofilters were modeled for different substrates. Experimental biofilters were modeled under oxygen-limitation kinetics. The applicability of the model was evidenced by its ability to model two different types of biofilters having different pore sizes.

Results from bench scale studies suggest that the use of biofiltration for control of ethanol emissions is feasible as a control alternative. The loading rate was 30 g/m^3/hr, selected to be lower than the values reported in literature to avoid accumulation of acidic intermediates (Pérez et al. 2002; Christen et al. 2002; Hodge, 1993). Biofilters can reduce ethanol emissions in a safe, natural and sustainable way. Biofilter systems work at room temperature without toxic chemicals. They are safer than incineration or chemical scrubbing; they use less energy, do not produce hazardous end products, and characterized as a "natural" process (Ozis et al. 2005).

Packed-bed granular filters proved effective, for practical filter sizes and flow rates, for removal of fine and ultrafine particles from air. The grain sizes used and

138

the observation that operation with wet grains was effective are consistent with the eventual development of biological treatment systems for airborne particles composed of biodegradable materials. A biofilter of this kind could simultaneously remove biotransformable compounds such as unburned hydrocarbons and nitrogen oxides. A recent study by Higuchi et al. (2004) showed that it is possible to reach 100% PM removal for the size range of 0.03-0.5 μm in a compost-woodchip biofilter where MEK was supplied as organic compound.

Granular filters utilizing other means of removing accumulated particles from the filter bed might also be used. However, for the ultrafine particles, removal efficiencies may be somewhat reduced in a wet bed because of the increase in particle size resulting from condensation.

This work also demonstrated the conceptual feasibility of granular filters for the on-road emissions of a truck and for emissions of a fleet of diesel vehicles in a tunnel. Such filters would be large, but not impossibly large, and the time-to-clogging would be acceptable. Additional work is needed to identify the best mechanism for cleaning or replacing the media.

139

REFERENCES

- Abbott, B.J.; Laskin, A.I.; McCoy, C.Y. Effect of Growth Rate and Nutrient Limitation on the Composition and Biomass Yield of Acinetobacter Calcoaceticus; *App. Microb.* **1974**, 28(1), 58-63.

- Aberg, B. Void Ratio of Non-cohesive Soils and Similar Materials; *J. Geotech. Eng.* **1992**, 118, 1315-1334.

- Aberg, B. Void Sizes in Granular Soils; *J. Geotech. Eng.* **1996**, 122, 236-239.

- Allen, J.O.; Mayo, P.R.; Hughes, L.S.; Salmon, L.G.; Cass, G.R. Emissions of Size-segregated Aerosols from On-road Vehicles in the Caldecott Tunnel; *Environ. Sci. Technol.* **2001**, 35(21), 4189-4197.

- Alonso, C.; Suidan, M.T.; Sorial, G.A.; Smith, F.L.; Biswas, P.; Smith, P.J.; Brenner, R.C. Gas Treatment in Trickle-Bed Biofilters: Biomass, How much is Enough?; *Biotechnol. Bioeng.* **1997**, 54(6), 583-594.

- Alonso, C.; Suidan, M.T; Kim, B.R; Kim, B.J. Dynamic Mathematic Model for the Biodegradation of VOCs in a Biofilter: Biomass Accumulation Study; *Environ. Sci. Technol.* **1998**, 32(20), 3118-3123.

- Alonso, M.; Alguacil, F.J. Electrostatic Precipitation of Ultrafine Particles Enhanced by Simultaneous Diffusional Deposition on Wire Screens; *J. Air & Waste Manage. Assoc.* **2002**, 52, 1342-1347.

- Arulneyam, D.; Swaminathan, T. Biodegradation of Ethanol Vapor in a Biofilter; *Bioprocess Eng.* **2000**, 22, 63-67.

- Auria, R.; Aycaguer, A.C.; Devinny, J.S. Influence of Water Content on Degradation Rates for Ethanol in Biofiltration; *J. Air & Waste Manage. Assoc.* **1998**, 48(1), 65-70.

- Barton, J.W.; Klasson, K.T.; Davison, B.H. Extended Operation and Control of Biomass Overgrowth in Biofilters Designed for VOC Removal. In *Proceedings of A&WMA's 90th Annual Meeting & Exhibition*, Toronto, Ontario. *June 9-13, 1997*; A&WMA: Pittsburgh, PA, 1997; Paper 97-WA71A.06.

- Bohn, H.L.; Bohn, K.H. Moisture in Biofilters; *Environ. Prog.* **1999**, 183, 156-161.

140

- Boswell, G.P.; Britton, N. F.; Franks, N. R. Habitat Fragmentation, Percolation Theory and the Conservation of a Keystone Species; *Proceedings: Biological Sciences*. **1998**, 265 (1409), 1924-1925.

- Boulaud, D. Use of Granular Beds in the Inertial Impaction Regime for Aerosol Size Distribution Measurement; *J. Aerosol Science,* **1991**, 22, 273-287.

- Boulaud, D.; Comper, C.; Diouri, M. Comparison between the SDI and Electrical Methods for the Measurement of Fine Aerosols; *J. Aerosol Science.* **1989**, 20, 1505-1508.

- Broadbent, S.R.; Hammersley, T.M. Percolation Processes, Crystals and Mazes; *Proc. Camb. Phil. Soc.* **1957**, 53, 629-641.

- Brown, J.E. *Heavy Duty Diesel Fine Particulate Matter Emissions: Development and Application of On-Road Measurement Capabilities*; EPA-600/SR-01/079; U.S. Government Printing Office: Washington, DC, 2001.

- Burtscher, H. Diesel Particulate Filter Manufacturers Task Force, Online publications: *Tailpipe Particulate Emission Measurement for Diesel Engines*, Heinz Burtscher, 2001, http://www.akpf.org/pubs.html (accessed January 2004)

- Cardenas-Gonzalez, B.; Ergas, S. J.; Switzenbaum, M.S. Characterization of Compost Biofiltration Media; *J. Air & Waste Manage. Assoc.* **1999**, 49(7), 174-185.

- Chan, S.K.; Ng, K.M. Geometrical Characteristics of the Pore Space in a Random Packing of Equal Spheres; *Powder Tech.* **1998**, 54, 147-155.

- Chandler, R.; Koplik, J.; Lerman, K.; Willemsen, J. Capillary Displacement and Percolation in Porous Media; *J. Fluid Mech.* **1982**, 119, 249-254.

- Chatzis, I.; Dullien, F.A.L. Modeling Pore Structure by 2-D and 3-D Networks with Application to Sandstones; *J. Can. Pet. Tech.* **1977**, 16(1), 97-108.

- Chitwood, D.E.; Devinny, J.S.; Maiburg, E. A Computational Model for Heteregenous Flow through Low Head-loss Biofilter Media; *Environ. Prog* **2002**, 21, 11-19.

- Choi, D.S.; Webster, T.S.; Chang, A.N.; Devinny, J.S. Quantitative Structure-Activity Relationships for Biofiltration of Volatile Organic Compounds. In *Proceedings of the 1996 Conference on Biofiltration, University of Southern California, Los Angeles, CA, October 24-25, 1996;* Reynolds F.E., Ed., The Reynolds Group: Tustin, CA, 1996.

- Chou, M-S.; Shiu, W-Z. Bioconversion of Methylamine in Biofilters; *J. Air & Waste Manage. Assoc.* **1997**, 47(1), 58-65.

- Christen, P.; Domenech, F.; Michelena, G.; Auria, R.; Revah, S. Biofiltration of Volatile Ethanol Using Sugar Cane Bagasse Inoculated with Candida Utilis; *J. Haz. Mat.* **2002**, 89, 253-265.

- Clark, N.N.; Gajendran, P. Effect of Truck Operating Weight on Heavy-Duty Diesel Emissions; *Environ. Sci. Technol.* **2003**, 37, 4309-4317.

- Clement, T.P.; Hooker, B.S.; Skeen, R.S. Macroscopic Models for Predicting Changes in Saturated Porous Media Properties Caused by Microbial Growth; *J. Ground Water.* **1996**, 34, 934-942.

- Cox, H.H. J.; Sexton, T.; Shareefdeen, Z.M.; Deshusses, M.A. Thermophilic Biotrickling Filtration of Ethanol Vapors; *Environ. Sci. Technol.* **2001**, 35(12), 2612-2619.

- Cox, H.H.J.; Deshusses, M.A. The Use of Protozoa to Control Biomass in Biotrickling Filters for Waste Air Treatment. In *Proceedings of A&WMA's 90th Annual Meeting & Exhibition*, Toronto, *Ontario. June 9-13, 1997;* A&WMA: Pittsburgh, PA, 1997; Paper 97- RA71C.05.

- Cox, H.H.J.; Moerman, R E.; Baalen, S.; van Heinningen, W.N.M.; Doddema, H.J.; Harder, W. Performance of a Styrene-Degrading Biofilter Containing the Yeast Exophiala Jeanselmei; *Biotech.Bioeng.* **1997**, 53(3), 259 -266.

- Crueger, W.; Crueger, A. *Biotechnology: A textbook of Industrial Microbiology*, Sinauer Associates: Sunderland, MA, 1990.

- Cunnigham, A.B.; Characklis, W.G.; Abedeen, F.; Crawford, D. Influence of Biofilm Accumulation on Porous Media Hydrodynamics; *Environ. Sci. Technol.* **1991**, 25, 1305-1310.

- D'Ottavio, T.D.; Goren, S.L. Aerosol Capture in Granular Beds in the Impaction Dominated Regime; *Aerosol Sci. Tech.* **1983**, 2, 91-108.

142

- Darlington, A.B.; Dat, J.F.; Dixon, M.A. The Biofiltration of Indoor Air: Air Flux and Temperature Influences the Removal of Toluene, Ethylbenzene, and Xylene; *Environ. Sci. Technol.* **2001**, 35(1), 240-246.

- Datta, S.; Redner,S. Gradient and Percolative Clogging in Depth Filtration; *Int. J. Mod. Phys C.* **1998**, 9(8), 1535-1545.

- Deshusses, M.A.; Cox, H.H.J. Thermophilic Biotricking Filtration of Ethanol Vapors. In *Proceedings of the 2000 Conference on Biofiltration, University of Southern California, Los Angeles, CA, October 19-20,2000;* Reynolds, F.E., Ed., The Reynolds Group, Tustin, CA, 2000.

- Deshusses, M.A.; Harmer, G.; Dunn, I.J. Behavior of Biofilters for Waste Air Biotreatment 1. Dynamic Model Development; *Environ. Sci. Technol.* **1995**, 29(4), 1048-1058.

- Deshusses, M.A.; Johnson, C.T.; Leson, G. Treating High Loads of Ethyl Acetate and Toluene in a Biofilter. In *Proceedings of A&WMA's 90th Annual Meeting & Exhibition*, Toronto, Ontario. *June 9-13, 1997*; A&WMA: Pittsburgh, PA, 1997; Paper 97-WA71A.07.

- Devinny, J.S.; Choi, D.; Webster, T.S. Quantitative Structure-Activity Relationships for Prediction of Treatment Success in Air Phase Biological Reactors. In *Proceedings of AIChE Annual Meeting, Nov. 16-21, 1997, Los Angeles, CA;* AIChE: New York, NY, 1997; Paper 186d.

- Devinny, J.S.; Deshusses, M.A.; Webster, T.S. *Biofiltration for Air Pollution Control*, Lewis: London, 1999.

- Devinny, J.S.; Hodge, D.S. Formation of Acidic and Toxic Intermediates in Overloaded Ethanol Biofilters, *J. Air & Waste Manage. Assoc.* **1995**, 45(2), 125-131.

- Dockery, D. W.; Pope, C. A.; Xu, X.; Spengler, J. D.; Ware, J. H.; Fay, M. E.; Ferris, B. G.; Speizer, F. E. An Association between Air Pollution and Mortality in Six United States Cities; *New Engl. J. Med.* **1993**, 329, 1753-1759.

- Donaldson, K.; MacNee, W. The Mechanism of Lung Injury Caused by PM_{10}. In *Issues in Environmental Science and Technology,* Hester R.E., Harrison, R.M., Eds.; The Royal Society of Chemistry, London, UK, 1998; pp 21-32.

143

- Dullien, F.A.L. *Porous Media: Fluid Transport and Pore Structure*; Academic: New York, 1979.

- Dupin, H.J.; McCarty, P.L. Impact of Colony Morphologies and Disinfection on Biological Clogging in Porous Media; *Environ. Sci. Technol.* **2000**, 34 (8), 1513-1520.

- Ergas, S.J.; Schroeder, E.D.; Chang, D.P.Y.C; and Scow, K.M. Spatial Ditribution of Microbial Populations in Biofilters. In *Proceedings of A&WMA's 87th Annual Meeting & Exhibition, Cincinnati, OH, June 19-24, 1994*; A&WMA: Pittsburgh, PA, 1994; Paper 94-RP115B.01.

- Ferin, J.; Oberdörster, G.; Soderholm, S.C.; Gelein, R. Pulmonary Tissue Access of Ultrafine Particles; *J. Aerosol Med.* **1991**, 4, 57-68.

- Fo, O.B.D.; Marra, W.D.; Kachan, G.C.; Coury, J.R. Filtration of Electrified Solid Particles; *Ind. Eng. Chem. Res.* **2000**, 39, 3884-3895.

- Gal, E.; Tardos, G.; Pfeffer, R. A Study of Inertial Effects in Granular Bed Filtration; *AIChE J*, **1985**, 31, 1093-1104.

- Goldstein, A.H.; Millet, D.B.; Schade, G.W. *Ethanol in the Atmosphere: Elucidating the Balance between Natural and Anthropogenic Sources in a Variety of Environments*; 2002. http://www.cosis.net/abstracts/EAE03/04489/EAE03-A-04489.pdf (accessed March 2004).

- Gostomski, P.A.; Sisson, J.B.; Cherry, R.S. Water Content Dynamics in Biofiltration: the Role of Humidity and Microbial Heat Generation; *J. Air & Waste Manage. Assoc.* **1997**, 47(9), 936-944.

- Govind G.L.; Briggs T.G. Experiences with a Compost Biofilter for VOC Control from Batch Chemical Manufacturing Operations. In *Proceedings of A&WMA's 90th Annual Meeting & Exhibition, Toronto, Ontario. June 9-13, 1997*; A&WMA: Pittsburgh, PA, 1997; 97-RP121C.01.

- Gribbins, M.J.; Loehr, R.C. Effect of Media Nitrogen Concentration on Biofilter Performance; *J. Air & Waste Manage. Assoc.* **1995**, 48 (3), 216 - 220.

- Gupte,S.; Tsamopoulos, J.A. An effective Medium Approach for Modeling Chemical Vapor Infiltration of Porous Ceramic Materials; *J. Electrochem. Soc.* **1990**, 137(5), 1626-1639.

144

- Higuchi, T.; Deshusses, M.A.; Cocker, D.R. The Behavior of Particulate Matter in Bioreactors for Air Pollution Control. In *proceedings of A&WMA's 97th Annual Meeting & Exhibition, Indianapolis, IN, June 22-25, 2004;* A&WMA: Pittsburgh, PA, 2004; Paper 677.

- Hodge, D.; Devinny, J.S. Determination of Transfer Rate Constants and Partition Coefficients for Air Phase Biofilters; *J. Env. Eng.* **1997**, 123(6), 577-586.

- Hodge, D.; Devinny, J.S. Modeling Removal of Air Contaminants by Biofiltration; *J. Env. Eng.* **1995**, 121(1), 21-32.

- Hodge, D.S. Ph.D. Dissertation, University of Southern California, December 1993.

- Hodge, D.S.; Medina, V.F.; Islander, R.L.; Devinny, J.S. Treatment of Hydrocarbon Fuel Vapors in Biofilters; *Environ. Tech.* **1991**, 12, 655-662.

- Holmen, B.A.; Ayala, A. Ultrafine PM Emissions from Natural Gas, Oxidation-Catalyst Diesel, and Particle-Trap Diesel Heavy-Duty Transit Buses; *Environ. Sci. Technol.* **2002**, 36, 5041-5050.

- James, J.T. In *Spacecraft Maximum Allowable Concentrations for Selected Airborne Contaminants;* National Academy Press: Washington, 1996; Vol. 3, p 171- 207.

- Janni, K.A.; Nicolai, R.E. Designing Biofilters for Livestock Facilities. In *Proceedings of the 2000 Conference on Biofiltration, University of Southern California, Los Angeles, CA, October 19-20, 2000;* Reynolds, F.E., Ed., The Reynolds Group, Tustin, CA, 2000.

- Johnson C.T.; Deshusses M.A. Quantitative Structure Activity Relationships for VOC Biodegradation in Biofilters. In *Proceedings of the Fourth International In situ and On site Bioreclamation Symposium, April 28- May 1, 1997;* Vol.5, Batelle Press: Colombus, OH, 1997.

- Kaiser, C. A Directed Percolation Model for Clogging in a Porous Medium with Small Inhomogeneities; *Trans. Porous Med.* **1997**, 26, 133-146.

- Kennes, C.; Cox, H. H. J.; Doddema, H. J.; Harder, W. Design and Performance of Biofilters for the Removal of Alkylbenzene Vapors; *J. Chem. Tech. Biotech.* **1996**, 66(3), 300-304.

145

- Kennes, C.; Veiga, M.C., Eds. *Environmental Pollution, Volume 4: Bioreactors for Waste Gas Treatment*; Kluwer Academic Publishers: Boston. 2001; p 47-91.

- Kim, D.S.; Fogler, H.S. Biomass Evolution in Porous Media and Its Effects on Permeability under Starvation Conditions; *Biotech. Bioeng.* **2000**, 69(1), 47-56.

- Kirkpatrick, S. Percolation and Conduction; *Reviews of Mod. Phys.* **1973**, 45(4), 574-588.

- Klasson, K.T.; Davison, B.H. Effect of Temperature on Biofiltration of Nitric Oxide; *App. Biochem. Biotech.* **2001**, 91, 205-211.

- Lenormand, R.; Bories, S. Description of a Bond Percolation Mechanism Used for the Simulation of Drainage with Trapping in Porous-Media; *C. R. Acad. Sci.* **1980**, 291, 279.

- Leson, G.; Winer, A.M. Biofiltration: An Innovative Air Pollution Control Technology for VOC Emissions; *J. Air & Waste Manage. Assoc.* **1991**, 41(8), 1045-1054.

- Lester, D.; Greenberg, L. A. The inhalation of ethyl alcohol by man; *Q. J. Stud. Alcohol.* **1951**, 12, 167-178

- Li, N.; Kim S.; Wang, M,; Froines, J.; Sioutas, C, Nel, A.E. Use of a Stratified Oxidative Stress Model to Study the Biological Effects of Ambient Concentrated and diesel exhaust particulate matter; *Inhal. Toxicol.* **2002**, 14, 459-486.

- Li, N.; Sioutas, C.; Cho, A.; Schmitz, D.; Misra, C.; Sempf, J.; Wang, M.Y.; Oberley, T.; Froines, J.; Nel, A. Ultrafine Particulate Pollutants Induce Oxidative Stress and Mitochondrial Damage, *Environ. Health Perspect.* **2003**, 111 (4), 455-460.

- Loehle, C.; Johnson, P. A Framework for Modeling Microbial Transport and Dynamics in the Subsurface; *Ecol. Model.* **1994**, 73, 31-49.

- Madigan, M.T.; Martinko, J.M.; Parker, J. *Biology of Microorganisms, 8th Ed.;* Prentice Hall: Upper Saddle River, New Jersey, 1997.

146

- Madl, L.S. Cleaning up Waste Naturally: 'Low-Tech' Approaches to VOCs and Wastewater Treatment have Their Advantages; *Food Proces.* **1998**, 59 (11), 91-95.

- Mann L.A.; Goren, S.L. Capture in Granular Beds in the Sedimentation and Diffusion Dominated Regimes; *Aerosol Sci. Technol.* **1984**, 3, 195-213.

- Marek, J; Paca, J; Halecky, M, Kousky, B., Sobotka, M., Keshavarz, T. Effect of pH and Loading Manner on the Start-Up Period of Peat Biofilter Degrading Xylene and Toluene Mixture; *Folia Microbiol.* **2001**, 46(3), 205-209.

- Medina, V.F.; Webster, T.; Ramaratnam, M.; Devinny, J.S. Treatment of Gasoline Residuals by Granular Activated Carbon Based Biological Filtration; *J. Environ. Sci. Health Part A Environ. Sci. Eng.* **1995**, 30(2), 407-412.

- Melrose, J. C.; Brandner, C. F. Role of Capillary Forces in Determining Microscopic Displacement Efficiency for Oil Recovery by Water Flooding; *Can. J. Petrol. Tech.* **1974**, 13, 54-59.

- Miguel, A.H.; Kirchstetter, T.W.; Harley, R.A; Hering, S.V. On-Road Emissions of Particulate Polycyclic Aromatic Hydrocarbons and Black Carbon from Gasoline and Diesel Vehicles; *Environ. Sci. Technol.* **1998**, 32, 450-455.

- Morales, M; Revah, S; Auria, R. Start-Up and the Effect of Gaseous Ammonia Additions on a Biofilter for the Elimination of Toluene Vapors; *Biotech. Bioeng.* **1998**, 60(4), 483 -491.

- Morgan-Sagastume, F.; Sleep, B.E.; Grant, A.D. Effects of Biomass Growth on Gas Pressure Drop in Biofilters; *J. Env. Eng.* **2001**, 127(5), 388-397.

- Morgan-Sagastume, J.M.; Revah, S.; Noyola, A. Pressure Drop and Gas Distribution in Compost Based Biofilters: Medium mixing and Composition Effects; *Environ. Tech.* **2003**, 24(7), 797-807.

- Morgenroth, E.; Schroeder, E. D.; Chang, D.P.Y.; Scow, K.M. Nutrient Limitation in a Compost Biofilter Degrading Hexane; *J. Air & Waste Manage. Assoc.* **1996**, 46(4), 300 -308.

- Morrow, R.A.; Merrill, J.R. An Introductory Scattering Experiment by Simulation; *American J. Phys.* **1970**, 38, 1104-1110.

- Noble, R. T.; Fuhrman, J.A. (1998). Use of SYBR Green I for rapid epifluorescence counts of marine viruses and bacteria; *Aquatic Microbial Eco.* **1998**, 14(2), 113-118.

- Noguera, D.R.; Pizarro, G.; Stahl, D.A.; Rittmann, B.E. Simulation of MultiSpecies Biofilm Development in Three Dimensions; *Water Sci. Tech.* **1999**, 397, 123-130.

- Nolan, G.T.; Kavanagh, P.E. The Size Distribution of interstices in Random Packings of Spehres; *Powder Tech.* **1994**, 78, 231-238.

- Nukunya, T. Ph.D. Dissertation, University of Southern California, May 2004.

- Nukunya, T.; Devinny, J.S.; Tsotsis, T.T. Application of A Pore Network Model to a Biofilter Treating Ethanol Vapor; *Chem. Eng. Sci.* **2005**, 60, 665-675.

- Nukunya, T.; Tsotsis, T.T.; Devinny, J.S. Application of Pore Network Model to a Lava Rock Biofilter Treating Ethanol. In *Proceedings of the 2002 Conference on Biofiltration, University of Southern California, Newport Beach, CA, October 31-November 1, 2002;* Reynolds, F.E., Ed., The Reynolds Group, Tustin, CA, 2002.

- Oberdörster, G.; Ferin, J.; Gelein, R.; Soderholm, S.C.; Finkelstein, J. Role of Alveolar Macrophage in Lung Injury; Studies with Ultrafine Particles; *Environ. Health Perspect.* **1992**, 102, 173-179.

- Oberdörster, G.; Gelein, R.M.; Ferin, J.; Weiss, B. Association of Particulate Air Pollution and Acute Mortality: Involvement of Ultrafine Pfarticles; *Inhal. Toxicol.* **1995**, 7, 111-124.

- Ortíz, I.; Morales, M.; Gobbée, C.; Guerrero, V.; Auria, R.; Revah, S. Biofiltration of Gasoline VOCs with Different Support Media, In *proceedings of A&WMA's 91st Annual Meeting & Exhibition, San Diego, CA, June14-18, 1998;* A&WMA: Pittsburgh, PA, 1998; Paper WAA.14P.

- Otani, Y.; Kanaoka, C.; Emi, H. Experimental Study of Aerosol filtration by the Granular Bed over a Wide Range of Reynolds Numbers; *Aerosol Sci.Technol.* **1989**, 10, 463-474.

- Ottengraf, S.P.P. In *Biotechnology and Bioengineering;* Rehm, H.J.; Reed, G. Eds.; VCH Verlagsgesellsch: Weinheim, 1986.

- Ottengraf, S.P.P. In *Biotechnology*; Rehm, H.J.; Reed G., Eds.; VCH Verlagsgesellschaft, Weinheim, 1987, vol 8.

- Ottengraf, S.P.P.; Diks, R. In *Biotechniques for Air Pollution Abatement and Odour Control Policies;* Dragt, A.J.; van Ham, J., Eds.; Elsevier: Amsterdam, The Netherlands, 1992; pp17-32.

- Ottengraf, S.P.P.; van den Oever, A.H.C. Kinetic of Organic Compound Removal from Waste Gases with a Biological Filter; *Biotechnol. Bioeng.* **1983**, 25(12), 3089-3102.

- Ozis, F.; Bina, A.; Devinny, J.S. Application of a Percolation-Biofilm Growth Model to Biofilters with a Known Packing Particle Size Distribution, In *Proceedings of the 2004 Conference on Biofiltration, University of Southern California, Redondo Beach, CA. October 19-22, 2004c;* Reynolds, F.E., Ed., The Reynolds Group, Tustin, CA, 2004.

- Ozis, F.; Bina, A.; Devinny, J.S. In *Biotechnology for Odor and Air Pollution Control;* Shareefdeen, Z.; Singh, A. Eds.; Springer: Berlin, 2005.

- Ozis, F.; Bina, A.; Yortsos, Y.; Devinny, J.S. A Percolation-Biofilm-Growth Model Describing Biomass Clogging in Biofilters, In *Proceedings of A&WMA's 96th Annual Meeting & Exhibition, San Diego, CA. June22-26, 2003*; A&WMA: Pittsburgh, PA, 2003; Paper # 81866.

- Ozis, F.; Singh, M.; Devinny, J.S.; Sioutas, C. Removal of Ultrafine and Fine Airborne Particulate Matter by Granular Filter; *J. Air & Waste Manage. Assoc.* **2004**a, 54(8):935-940.

- Ozis, F.; Singh, M.; Devinny, J.S.; Sioutas, C. Removal of Ultrafine and Fine Particles in a Granular Bed Filter with Possible Applications to Biofiltration, In *Proceedings of A&WMA's 97th Annual Meeting & Exhibition, Indianapolis, IN. June22-25, 2004b*; A&WMA: Pittsburgh, PA, 2004; Paper #507.

- Ozis, F.; Yortsos, Y.; Devinny, J.S. Numerical Percolation Model for Describing Biomass Clogging in Biofilters, In *Proceedings of the 2002 Conference on Biofiltration, University of Southern California, Redondo Beach, CA. October 31-November 1, 2002;* Reynolds, F.E., Ed., The Reynolds Group, Tustin, CA, 2002.

- Pekannen, J.; Timonen, K.L.; Ruuskanen, J.; Reponen, A.; Mirme, A. Effects of Ultrafine and Fine Particles in Urban Air on Peak Flow Expiratory Flow among Children with Asthmatic Symptoms; *Environ. Res.* **1997**, 74, 24-33.

- Pérez, W.T., Domenech, F.m Roger, P. and Christen, P.Effect of Mineral Salts Addition on the Behavior of an Ethanol Biofilter; *Environ. Tech.* **2002**, 23, 981-989.

- Peters, A.; Dockery, D.W.; Heinrich, J.; Wichmann, H.E. Short-Term Effects of Particulate Air Pollution on Respiratory Morbidity in Asthmatic Children; *Eur. Respir. J.* **1997b**, 10, 872-879.

- Peters, A.; Wichmann, H.E.; Tuch, T.; Heinrich, J.; Heyder, J. Respiratory Effects are Associated with the Number of Ultrafine Particles; *American J Respir. Crit. Care Med.* **1997a**, 155, 1376-1383.

- Picioreanu, C.; Van Loosdrecht, M.C.M.; Heijnen, J.J. A Theoretical Stidy on the Effct of Surface Roughness on Mass Transport and Transformation in Biofilms; *Biotechnol. Bioeng.* **2000**, 68, 355-369.

- Picioreanu, C.; Van Loosdrecht, M.C.M.; Heijnen, J.J. Mathematical Modelling of Biofilm Structure with a Hybrid Differential-discrete Cellular Automaton Approach; *Biotechnol. Bioeng.* **1998**, 58, 101-116.

- Pizarro, G.; Griffeath, D., Noguera, D.R. Quantitative Cellular Automaton Model for Biofilms; *J. Env. Eng.* **2001**,127, 782-789.

- Plessis, C.A. du; Kinney, K.A.; Schroeder, E.D.; Chang, D.P.Y.; Scpw, K.M. Denitrification and Nitric Oxide Reduction in an Aerobic Toluene Treating Biofilter; *Biotechnol. Bioeng.* **1998**, 58(4), 408 - 416.

- Pomeroy, R.D. De-odorizing of Gas Streams by the Use of Microbial Growths. U.S. patent, 2,793,096, 1957.

- Pope, C. A.; Dockery, D. W.; Schwartz, J. Review of Epidemiological Evidence of Health Effects of Particulate Air Pollution; *Inhal Toxicol.* **1995**, 7, 1-18.

- Prado, J.; Mendoza, A.; Veiga, C., Kennes, C. Optimization of Nutrient Supply in a Downflow Gas-Phase Biofilter Packed with an Inert Carrier; *App. Microb. Biotech.* **2002**, 59(4), 567 - 573.

150

- Raynor, P.C.; Leith, D. The Influence of Accumulated Liquid on Fibrous Filter Performance; *J. Aerosol Sci.* **2000**, 31, 19-34.

- Reyes, P.O.; Ergas, S.J.; Djaferis, T.E. Developing a Moisture Content Feedback Control System for Biofiltration; *Haz. Indust. Wastes: Proceedings of the Mid-Atlantic Indust. Haz. Waste.* **1999**, 31, 14-26.

- Ronault, Y.; Assouline, S. A Probabilistic Approach towards Modeling the Relationships between Particle and Pore Size Distribution: Multi-component Packed Sphere Case; *Powder Tech.* **1998**, 96, 33-41.

- Sahimi, M. *Applications of Percolation Theory;* Taylor and Francis: London, 1994.

- Schwarz, B.C.E.; Devinny, J.S.; Tsotsis, T.T. A Biofilter Network Model-Importance of the Pore Structure and Other Large Scale Heterogeneities, *Chem. Eng. Sci.* **2001**, 56 (2), 475-483.

- Schwarz, B.C.E.; Nukunya, T.; Devinny, J.S.; Tsostis, T.T. A Pore Network Model of Biofilter Clogging, In *Proceedings of the 2000 Conference on Biofiltration, University of Southern California, Los Angeles, CA, October 19-20, 2000;* Reynolds, F.E., Ed., The Reynolds Group, Tustin, CA, 2000.

- Shapiro, M.; Gutfinger, C.; Laufer, G. Electrostatic Mechanisms of Aerosol Collection by Granular Filters: Review; *J. Aerosol Sci.* **1988**, 19, 651-677.

- Shareefdeen, Z.; Baltzis, B.C. Biofiltration of Toluene Vapor under Steady-State and Transient Conditions: Theory and Experimental Results; *Chem. Eng. Sci.* **1994**, 49, 4347-4360.

- Shareefdeen, Z.; Baltzis, B.C.; Oh, Y-S.; Bartha, R. Biofiltration of Methanol Vapor; *Biotechnol. Bioeng.* **1993**, 41, 512-524.

- Shariati, M.; Lu, C.; Devinny, J.S.; Yortsos, Y. Application of Percolation Theory to Biofilm Accumulation and Head Loss in Biofilters, In *Proceedings of the 2000 Conference on Biofiltration, University of Southern California, Los Angeles, CA, October 19-20, 2000;* Reynolds, F.E., Ed., The Reynolds Group, Tustin, CA, 2000.

- Shuler, M.L.; Kargi, F. *Bioprocess Engineering,* Prentice Hall PTR: Upper Saddle River, NJ, 2001; 2nd Ed.

- Son, H.-K.; Striebig, B.A. Critical Biofilter Design Factors as Nutrient, pH, and Loading Rate; *Haz. Indust. Wastes: Proceedings of the Mid-Atlantic Indust. Haz. Waste.* **2000**, 32, 349-358.

- Song, J.; Kinney, K.A. A Model to Predict Long-Term Performance of Vapor-Phase Bioreactors: A Cellular Automaton Approach; *Environ. Sci. Technol,* **2002**, 36(11), 2498-2507.

- Sorial, G. A.; Smith, F. L.; Suidan, M. T.; Biswas, P.; Brenner, R.C. Evaluation of the Performance of Trickle Bed Biofilters - Impact of Periodic Removal of Accumulated Biomass. In *Proceedings of A&WMA's 87th Annual Meeting & Exhibition, Cincinnati, OH, June 19-24, 1994;* A&WMA: Pittsburgh, PA, 1994; Paper 94-RP115B.07.

- Sorial, G.A.; Smith, F.L.; Suidan, M.T.; Pandit, A.; Biswas, P.; Brenner, R.C. Performance of Peat Biofilter: Impact of the Empty Bed Residence Time, Temperature and Toluene Loading; *J. Haz. Mat.* **1997**, 53, 19-33.

- Spencer, R.; Alix, C. Biofilter Design Care and Feeding; *BioCycle.* **2003**, 44(1), 45-50.

- Steele, J.; Ozis, F.; Furhman, J.A.; Devinny, J.S. Structure of Microbial Communities in Ethanol Biofilters, In *Proceedings of the 2004 Conference on Biofiltration, University of Southern California, Redondo Beach, CA. October 19-22, 2004;* Reynolds, F.E., Ed., The Reynolds Group, Tustin, CA, 2004.

- Striebig, B.A.; Son, H-K.; Regan, R.W. Understanding Water Dynamics in the Biofilter; *Biocycle.* **2001**, 42(1), 48-50.

- Suchomel, B.J.; Chen, B.M.; Allen M.B. Network Model of Flow, Transport and Biofilm Effects in Porous Media; *Trans. Porous Med.* **1998**, 30, 1-23.

- Tardos, G. I.; Abuaf, N.; Gutfinger, C. Dust Deposition in Granular Bed Filters: Theories and Experiments; *J. Air Pollut. Control Assoc.* **1978**, 28(4), 354-370.

- Taylor, S.W.; Milly, P.C.D.; Jaffé, P.R. Biofilm Growth and the Related Changes in the Physical Properties of a Porous Medium 1. Experimental Investigations; *Water Resour. Research.* **1990**, 6(9), 2153-2159.

- Thullner, M.; Zeyer, J.; Wolfgang, K. Influence of Microbial Growth on Hydraulic Properties of Pore Networks; *Trans. Porous Med.* **2002**, 9, 99-122.

- Togna, A.P.; Singh, M. A Comparative Study of Biofilter and Biotrickling Filter Performance for Isopentane Removal. In *Proceedings of A&WMA's 87th Annual Meeting & Exhibition, Cincinnati, OH, June 19-24, 1994*; A&WMA: Pittsburgh, PA, 1994; Paper 94-RP115B.04.

- Toledo, P.G.; Davis, H.T.; Scriven, L.E. Transport Properties of Anisotropic Porous Media: Effective Medium Theory; *Chem. Eng. Sci.* **1992**, 47(2), 391-405.

- Torkian, A.; Dehghanzadeh, R.; Koutsky, B. Performance Evaluation of Biofilters in Treating Waste Gas-Streams Contaminated with Aromatic VOCs. In *Proceedings of the 2002 Conference on Biofiltration, University of Southern California, Newport Beach, CA, October 31-November 1, 2002*; Reynolds, F.E., Ed., The Reynolds Group, Tustin, CA, 2002.

- U.S. Environmental Protection Agency. *Alternative Control Technology Document for Bakery Oven Emissions*; EPA-453/R-82-017; U.S. Government Printing Office: Washington, DC, 1992. http://www.epa.gov/ttn/atw/bakery/bakery92.pdf, (accessed March, 2004).

- U.S. Environmental Protection Agency. *EPA, Federal Register, Proposed Rules 40 CFR Parts 80 and 86, Vol 65, No:151*; U.S. Government Printing Office: Washington, DC, 2000. http://www.epa.gov/otaq/regs/toxics/fr-nprm.pdf (accessed January, 2004)

- U.S. Environmental Protection Agency. EPA, Serageldin, M., *Air Bio-Reactor Systems: different Designs and Operational Aspects*; U.S. Government Printing Office: Washington, DC. Paper # 42952 http://www.epa.gov/ttnatw01/bio/serageldin42952.pdf (accessed March, 2004)

- Van Lith C.; Ottengraf, S.P.P.; Diks, R.M.M. The control of Clogging in a Biotrickling Filter. In *Proceedings of the Biological Waste Cleaning International Symposium, March 9-11, 1994;* VDI BERICHTE NR, 1994.

- Vandevivere, P.P.; Baveye, D.; de Lozada, S.; DeLeo P. Microbial Clogging of Saturated Soils and Aquifer Materials: Evaluation of Mathematical Models; *Water Resour. Research.* **1995**, 31(9), 2173-2180.

- Veiga, M.C.; Kennes, C. Parameters Affecting Performance and Modeling of Biofilters Treating Alkybenzene-Polluted Air; *Appl. Microbiol. Biotechnol.* **2001**, 55, 254-258.

- Wani, A.H.; Branion, R.M.R.; Lau, A.K. Effects of Periods of Starvation and Fluctuating Hydrogen Sulfide Concentration on Biofilter Dynamics and Performance; *J. Haz. Materials.* **1998**, 60(3), 287-303.

- Weber F.J.; Hartmans, S. Toluene Degradation in a Trickle Bed Reactor-Prevention of Clogging. In *Proceedings of the Biological Waste Cleaning International Symposium, March 9-11, 1994;* VDI BERICHTE NR, 1994.

- Webster, T.S.; Devinny, J.S.; Torres, E.M.; Basrai, S.S. Biofiltration of Odors, Toxics and Volatile Organic Compounds from Publicly Owned Treatment Works, *Environ. Prog.* **1996**, 15(3), 141-147.

- Webster, T.S.; Devinny, J.S.; Torres, E.M.; Basrai, S.S. Microbial Ecosystem in Compost and Granular Activated Carbon Biofilters; *Biotechnol. Bioeng.* **1997**, 53(3), 296-303.

- Wilkinson, D.; Barsony, M. Monte-Carlo Study of Invasion Percolation Clusters in Two Dimensions and Three Dimensions; *J.Phys. A.* **1984**, 17, 129-135.

- Williamson, K.; McCarty, P.L. A Model of Substrate Utilization by Bacterial Films; *J. Water Pollut. Control Fed.* **1976**, 48, 9-24.

- Wu, G.; Dupuy, A.; Leroux, A.; Leroux, A.; Brzezinski, R.; Heitz, M. Peat-Based Toluene Biofiltration: A New Approach to the Control of Nutrients and pH; *Environ. Tech.* **1999**, 20(4), 367-376.

- Yortsos, Y.; Shankar, K. Asymptotic Analysis of Pore Closure Reactions; *Ind. Eng. Chem. Fundam.* **1984**, 23, 132-137.

- Yortsos, Y.C. Flow of Fluids in Porous Media, Unpublished Notes, 1997.

- Yortsos, Y.C.; Sharma, M. Application of Percolation Theory to Noncatalytic Gas-Solid Reactions; *AIChE J.* **1986**, 32(1), 46-55.

- Yoshida, H.; Tien, C. A New Correlation of the Initial Collection Efficiency of Granular Aerosol Filtration; *AIChE J.* **1985**, 31, 1752-1754.

- Zhi, N.; Shuangxi, L.; Bo, S. *Study on the Characteristics of Diesel Engine Exhaust Particulate*, 2002. http://www.cse.polyu.edu.hk/~activi/BAQ2002/BAQ2002_files/Proceedings/PosterSession/47.pdf (accessed January, 2004).

154

NOTATION

p_c: percolation threshold, %

Z: coordination number, unitless

$f(n)$: pore-size distribution

$A(n)$: the fraction of the total number of pores that is available, %

$p(n)$: the fractionof pores with radius less than or equal to the biofilm thickness, %

$X_a(n)$: the fraction of pores available to contribute to the treatment process, %

$X_f(n)$: the fraction of filled pores that don't contribute to the treatment process, %

n': a sum over other values of n

n: step number

$X_{na}(n)$: the fraction of pores that are neither filled nor available, %

r: pore radius, cm

r_i: biofilm thickness, cm

K: ethanol degradation constant for surface limited case, cm sec^{-1}

K_v: ethanol degradation constant for volume limited case, sec^{-1}

μ : the location parameter of log-normal distribution

σ : the shape parameter of log-normal distribution

X_{act}: active biomass density, gm^{-3}

μ_m : the growth constant, h^{-1}

K_s : the half saturation constant, gm^{-3}

C : concentration of the substrate, ppm

155

k_d : the death rate constant, h^{-1}

D: the diffusion coefficient, $m^2\ hr^{-1}$

Y: biomass yield, mg biomass/mg substrate

R: maximum pore radius, cm

APPENDICES

I: DERIVATIONS OF EQUATIONS FOR THE MODEL

157

Flat Plate Pores, Surface Area Limited Growth

Half of the separation between the plates is r_o, the thickness of the biomass is r_i, and the half the thickness of the air apace is r.

Growth of biomass is assumed to be proportional to surface area of the biomass, which is the same with the surface of the pore in this case.

$$\frac{dV_B}{dt} = \frac{kbC}{\rho_B} A = KA$$

Where:

ρ_B = biomass density, g biomass/cm^3

V_B = volume of biomass on one plate, cm^3

k = reaction constant, cm/s

b = stoichiometric coefficient, g biomass/ g contaminant

C = concentration of contaminant in liquid phase, g/cm^3

A = surface area of one plate, cm^2 and

$$K = \frac{kbC}{\rho_B}$$

Since biomass only grows outwards from the surface, so:

$$LW\frac{d_{ri}}{dt} = KLW$$

where L and W are length and width of the pore.

So,

$$\frac{d_{ri}}{dt} = K$$

and

$$r_i = Kt$$

or

$$t = \frac{r_i}{K}$$

This shows that as the biofilm grows, the available surface area doesn't change.

Flat Plate Pores, Biomass Volume Limited Growth

The basic equation:

$$\frac{dV_B}{dt} = K_V V_B$$

where:

$$K_V = \frac{k_V bC}{\rho_B}$$

and k_V is the reaction rate constant, s^{-1}

But biomass can only grow outwards so:

$$LW \frac{d_{ri}}{dt} = K_V LW r_i$$

or

159

$$\frac{d_{ri}}{dt} = K_V r_i$$

$$\ln r_i = K_V t$$

$r_i = Ce^{K_V t}$ at t= 0, and r_i= r_{io} (initial value of r_i)

$$r_i = r_{io}e^{K_V t}$$

$$t = \frac{1}{K_V}\ln(\frac{r_i}{r_{io}})$$

As growth proceeds, the volume of biomass increases and the rate increases.

Cylindrical Pores, Surface Area Limited Growth

The basic equation is:

$$\frac{dV_B}{dt} = KA_B$$

where A_B = is the surface area of the biofilm(at radius r)

$$\frac{d}{dt}\left(L\pi r_o^2 - L\pi r^2\right) = KL2\pi r$$

Only the inner radius of the biofilm changes, so:

$$-2r\frac{dr}{dt} = 2Kr$$

160

noting,

$$\frac{dr_i}{dt} = -\frac{dr}{dt}$$

$$\frac{dr_i}{dt} = K$$

so, $r_i = Kt$

and $t = \dfrac{r_i}{K}$

As the growth proceeds, the available surface declines, but so does the amount of biomass needed to increase the thickness of the film.

Cylindrical Pores, Biomass Volume Limited Growth

The basic equation is:

$$\frac{dV_B}{dt} = KV_B$$

$$\ln V_B = K_V t$$

$$V_B = Ce^{K_V t}$$

$$V_B = 2\pi L[r^2 - (r - r_i)^2]$$

$$V_B = 2\pi L[2rr_i - r_i^2]$$

$$2\pi L[2rr_i - r_i^2] = Ce^{K_V t}$$

at $t=0$; $r_i = r_{io}$ ➔ $2\pi L[2rr_{io} - r_{io}^2] = C$

161

$$2\pi L[2rr_i - r_i^2] = 2\pi L[2rr_{io} - r_{io}^2]e^{K_V t}$$

$$t = \frac{1}{K_V}\ln\left[\frac{2rr_i - r_i^2}{2rr_{io} - r_{io}^2}\right]$$

The volume of the biofilm is proportional to the difference between the square of the original radius of the pore and the square of the remaining open radius.

Calculation of Available Surface Area:

Parallel plate pores:

For parallel plate pores, it is assumed that each has a total fixed surface area of A_P,(independent of the pore size r_i, which is the half the distance between the plates). The total available surface area is:

$$S_p(n) = A_p A(n)$$

This can be related to the maximum possible surface area in the biofilter, occurring at t=0 (a trivial case, because the area doesn't change with r_i):

$$S_{rp}(n) = \frac{A_p A(n)}{A_p \sum_{n'=0}^{N} f(n')} = A(n)$$

for the special case of uniform pores, all the pores remain open and with the same surface area until the biofilter fills with biomass.

$S_{rp}=1$ for n<N and $S_{rp}=0$ or n $\geq$ N

162

Cylindrical Pores:

For cylindrical pores, the biofilm surface is a cylinder with the same length L as the pore but with radius reduced by the thickness of the biofilm:

pore surface area $= 2\pi L[r(n') - r_i]$

so the total surface area for available pores is:

$$S_c(n) = \frac{A(n)}{[1 - p(n)]} \sum_{n'=n+1}^{N} 2\pi L[r(n') - r_i]f(n')$$

relative to the maximum surface area, which occur at the beginning of the process when the thickness of the biofilm is negligible and all of the pores are available, at t=0,

$$S_{rc}(n) = \frac{\dfrac{A(n)}{[1 - p(n)]} \displaystyle\sum_{n'=n+1}^{N} 2\pi L[r(n') - r_i]f(n')}{\displaystyle\sum_{n'=0}^{N} 2\pi L r(n')f(n')} = \frac{A(n)}{[1 - p(n)]} \frac{\displaystyle\sum_{n'=n+1}^{N}[r(n') - r_i]f(n')}{\displaystyle\sum_{n'=0}^{N} r(n')f(n')}$$

For the special case of uniform pore radius r*,

$$S_{cu} = [2\pi L(r * - r_i)]\sum_{n'=0}^{N} f(n') = [2\pi L(r * - r_i)]$$

for the case of uniform pores, the area relative to the maximum area at t=0 is:

163

$$S_{rcu}(n) = \frac{2\pi L(r*-r_i)\sum_{n'=0}^{N} f(n')}{2\pi r*L\sum_{n'=0}^{N} f(n')} = \frac{(r*-r_i)}{r*}$$

Calculation of Available Biomass:

Parallel plate pores

For parallel plate pores, the volume of the available biomass is equal to the available surface area multiplied by the thickness of the biofilm:

$$B_p(n) = A(n)A_p r_i$$

relative to the amount of biomass that would be present if all the pores were completely filled:

$$B_{rp}(n) = \frac{A(n)A_p r_i}{\sum_{n'=0}^{N} A_p r(n') f(n')} = \frac{A(n)r_i}{\sum_{n'=0}^{N} r(n') f(n')}$$

for the special case of parallel plate uniform pores of separation 2r*, all pores are available

$$B_{pu}(n) = \sum_{n'=0}^{N} f(n')A_p r_i = A_p r_i$$

Relative to initial total porosity of the biofilter:

$$B_{rpu}(n) = \frac{A_p r_i}{\sum_{n'=0}^{N} A_p r* f(n')} = \frac{r_i}{r*}$$

164

Cylindrical Pores

For cylindrical pores, the biomass occupies annular layer on the inside of the pores

between the radius r(n') of the pore and r(n')-r_i

$$B_c = \frac{A(n)}{[1-p(n)]} \sum_{n'=n+1}^{N} \{\pi[r(n')]^2 L - \pi[r(n')-r_i]^2 L\} f(n')$$

$$= \frac{A(n)}{[1-p(n)]} \pi L \sum_{n'=n+1}^{N} \{2r(n')r_i - r_i^2\} f(n')$$

Relative to the initial total porosity of the biofilter:

$$B_{rc} = \frac{\pi L \frac{A(n)}{[1-p(n)]} \sum_{n'=n+1}^{N} [2r(n')r_i - r_i^2] f(n')}{\pi L \sum_{n'=0}^{N} [r(n')]^2 f(n')} = \frac{\frac{A(n)}{[1-p(n)]} \sum_{n'=n+1}^{N} \{2r(n')r_i - r_i^2\} f(n')}{\sum_{n'=0}^{N} [r(n')]^2 f(n')}$$

in the special case of uniform pores of radius r*, all the pores are available:

$$B_{cu} = \pi L \sum_{n'=0}^{N} [2r * r_i - r_i^2] f(n') = \pi L[2r * r_i - r_i^2]$$

relative to the initial total porosity of the biofilter:

$$B_{rcu} = \frac{[2r * r_i - r_i^2]}{\sum_{n'=0}^{N} (r*)^2 f(n')} = \frac{[2r * r_i - r_i^2]}{(r*)^2}$$

165

Effective Conductance, Permeability and Head loss Calculation

Effective permeability is given as $k \sim \beta r_m^2$ by Yortsos (1997).

Headloss is calculated using the effective medium approximation. In this approach, a value of pore conductance is chosen such that local variations on conductance average to zero. Kirkpatrick (1973) has shown that this condition reduces to

$$\int G(g) \left[\frac{g_m - g}{g + (z/2 - 1)g_m} \right] dg$$

Where g is the conductance of a single pore, z is the connectivity of the pores, and G (g) is the frequency distribution of pores of conductivity g. For each pore, the headloss $\Delta P = gQ$, where Q is the airflow through the pore, g_m is the equivalent conductance, proportional; to the overall conductance of the medium. Thi sis equivalent to:

$$\sum_{n'=0}^{N} G(n') \left[\frac{g_m - g(n')}{g(n') + (z/2 - 1)g_m} \right] = 0$$

the sum may be divided into a portions for which g(n') is zero (pores filled or inaccessible) and portion for which g(n') is nonzero (accessible pores).

$$[1 - A(n)] \left[\frac{[g_m - 0]}{[0 + (z/2 - 1)g_m]} \right] + \frac{A(n)}{[1 - p(n)]} \sum_{n'=n+1}^{N} G(n') \left[\frac{g_m - g(n')}{g(n') + (z/2 - 1)g_m} \right] = 0$$

$$\frac{[1 - A(n)]}{(z/2 - 1)} + \frac{A(n)}{[1 - p(n)]} \sum_{n'=n+1}^{N} G(n') \left[\frac{g_m - g(n')}{g(n') + (z/2 - 1)g_m} \right] = 0$$

but G(n')dn = f(n')dn, so

166

$$\frac{[1-A(n)]}{(z/2-1)}+\frac{A(n)}{[1-p(n)]}\sum_{n'=n+1}^{N}f(n')\left[\frac{g_m-g(n')}{g(n')+(z/2-1)g_m}\right]=0$$

an alternate formulation is possible in terms of the frequency distribution of available

pores, $f_a(n')$:

$$f_a(n')=\frac{f(n'+n)}{[1-p(n)]}$$

$[1-p(n)]f_a(n')=f(n'+n)$

or $\quad [1-p(n)]f_a(n'-n)=f(n')$

$$\frac{[1-A(n)]}{(z/2-1)}+\frac{A(n)}{[1-p(n)]}\sum_{n'=n+1}^{N-n}[1-p(n)]f_a(n'-n)\left[\frac{g_m-g(n'-n)}{g(n'-n)+(z/2-1)g_m}\right]=0$$

$$\frac{[1-A(n)]}{(z/2-1)}+A(n)\sum_{n'=n+1}^{N-n}f_a(n'-n)\left[\frac{g_m-g(n'-n)}{g(n'-n)+(z/2-1)g_m}\right]=0$$

using the presumption that conductance is proportional; to the cube of pore radius:

$$g=kr^3$$

$$\frac{[1-A(n)]}{(z/2-1)}+\frac{A(n)}{[1-p(n)]}\sum_{n'=n+1}^{N}f_a(n')\left[\frac{kr_m^3-k[r(n')]^3}{k[r(n')]^3+(z/2-1)kr_m^3}\right]=0$$

this equation canbe solved numerically to determine the root r_m

$$\frac{[1-A(n)]}{(z/2-1)}+\frac{A(n)}{[1-p(n)]}\sum_{n'=n+1}^{N}f(n')\left[\frac{r_m^3-[r(n')]^3}{[r(n')]^3+(z/2-1)r_m^3}\right]=0$$

167

Permeability

Darcy's law

$$q = \frac{k_o \Delta P}{\mu L}$$

where: q is fluid flow velocity, k_o is the initial permeability and ΔP is the pressure difference between two positions separated by L, and μ is the fluid dynamic viscosity.

From Yortsos (1997)

$$k \sim \beta \, r_m^2$$

Initially if one can measure the headloss, the experimental permeability can be determined, that is proportional to effective radius (r_m):

$$k_o = \frac{\mu q}{(\Delta P / L)} = \beta r_m^2$$

Therefore: $\beta = \dfrac{k_o(\exp)}{r_m^2(th)}$

Further permeability values can be calculated by

$$k = \beta r_m^2 = \frac{k_o(\exp)}{r_m^2(th)} r_m^2$$

Headloss

By using above equation head loss could be back calculated by using Darcy's equation, therefore head loss:

168

$$\Delta P = \frac{q \mu L}{k}$$

where μ is the fluid dynamic viscosity (Pa.s), L is the height of the biofilter media, ΔP is the head loss (Pa), q is the flow velocity (m/s).

Calculation of Pore Size Distribution for Accessible Pores:

The pore size distribution for the accessible pores is a distribution with the same shape as f_x, but normalized so that the sum is equal to 1.

$$f_a(r) = f_x(r + r_i) \frac{\displaystyle\sum_{0}^{R} f(r)}{\displaystyle\sum_{r_i}^{R} f_x(r)}$$

This can be multiplied by a factor equal o 1:

$$f_a(r) = f_x(r + r_i) \frac{\displaystyle\sum_{0}^{R} f(r)}{\displaystyle\sum_{r_i}^{R} f_x(r)} \frac{\displaystyle\sum_{r_r}^{R} f(r)}{\displaystyle\sum_{r_i}^{R} f(r)} = f_x(r + r_i) \frac{\displaystyle\sum_{0}^{R} f(r) \sum_{r_r}^{R} f(r)}{\displaystyle\sum_{r_i}^{R} f(r) \sum_{r_i}^{R} f_x(r)} = \frac{f_x(r + r_i)}{(1-p)A(n)}$$

further

$$f_x(r + r_i) = A(n) f(r + r_i)$$

so

$$f_a(r) = \frac{f(r + r_i)}{(1-p)}$$

II: MATLAB PROGRAM FOR THE MODEL FOR SAND

BIOFILTER

170

PERCOLATION MODEL:

```
clear all;
close all;

global sub
sub = zeros(100,1);
global time
time = zeros(100,1);
global STARTVALUE
global changeTime


Cg = 100;
H = 29.5;


STARTVALUE(1) = Cg/H;

for part=1:5

    part

    sandfitting_oxygen   % call for CELLULAR AUTOMATON PART

    R = 0.135/2;   % cm, maximum pore radius comes from Horiba analysis
    N = 100;
    rc = R/N;
    r = rc : rc : R;               % pore radius, cm
    ri = rc : rc : R;
    inp= 0.39; % initial porosity, measured
    pc = 0.75;
    K = 9.72*10^-9;   % cm/sec
    Kv = 8.33*10^-7;   % 1/sec
    z=6;

    % create arrays
    p=linspace(0,0,100);Xb=linspace(0,0,100);Xa=linspace(1,1,100);
    Xnab=linspace(0,0,100); Xna=linspace(0,0,100);An=linspace(1,1,100);
    fr= linspace (0,0,100);Src=linspace (0,0,100);Brc= linspace (0,0,100);
    rm = linspace(0,0,100);tcs = linspace (0,0,100);DeltaP=linspace(0,0,100);
```

171

```
% normalize the fr

    for n=1:100
    if ( n < 36 )
       fr(n) = 0;
    elseif (n >= 36)&(n < 66)
       fr(n) = (-119080*r(n)^3 + 9028.8*r(n)^2 - 191.52*r(n) + 1.1339);
    elseif (n >= 67)
       fr(n)=0;
    end

end

loopfr=0;
for i=1:100
   loopfr = (loopfr + fr(i));
end

c=1/loopfr;

fr(1)= 0;
p(1)= fr(1);
An(1)= 1- p(1);


for n = 2: 100
   if ( n < 36 )
      fr(n) = 0;
   elseif (n >= 36)&(n < 66)
      fr(n) = c*(-119080*r(n)^3 + 9028.8*r(n)^2 - 191.52*r(n) + 1.1339);
   elseif (n >= 67)
      fr(n)=0;
   end

   p(n) = p(n-1)+ fr(n);

   %An= accessibility function

   if ( p(n) > pc )
      An(n) = 0;
   elseif (p(n) > 0.6) & (p(n) <= pc)
```

172

```
     An(n)= ( (-201.5478*p(n)^3) + (394.3989*p(n)^2)-
(258.3581*p(n))+56.9690);
     elseif (p(n)<= 0.6)
         An(n) = 1- p(n);
     end
  end




%INITIAL VALUES WHEN n=1

Xb(1)= (An(1)/(1-p(1)))*fr(1);

Xa(1)= An(1);

Xnab(1)= ((1- An(1))* fr(1));

Xna (1) = 1- Xa(1)- Xb(1);


loopcc=0;
for i =1:100,
    loopcc = loopcc+ (fr(i)*r(i)*r(i));
end


%cc= uniform pores' surface area /distributed pores' surface area
cc= R^2/(loopcc);


% for first Src
loopSrc1 = 0;
for i = 2: 100
    loopSrc1 = loopSrc1 + ((r(i)- ri(1))*fr(i));
end

loopSrc2 = 0;
for i = 1:100
    loopSrc2 = (loopSrc2 + (r(i)*fr(i)));
end
```

173

```
Src (1) = cc*(An(1)/(1-p(1)) *(loopSrc1/loopSrc2));

tcs(1)=ri(1)/K;

% for first Brc
loopBrc1=0;
for i= 2 : 100
    loopBrc1 = loopBrc1 + ( 2 * r(i)* ri(1) - ri(1)^2 )* fr (i);
end

loopBrc2=0;
for i= 1 : 100
    loopBrc2 = loopBrc2 + r(i)^2*fr(i);
end

Brc(1)= An(1)/(1-p(1))*(loopBrc1/loopBrc2);


% for first rm
Ax=An(1);
px=p(1);
n=1;
rmroot = integral_sandfitting(r,n,c,R,N,Ax,px);
rm(1) = rmroot;




% FOR FIRST HEAD LOSS
length = 0.15/5; % depth of the filter, meter
vis=  0.0000185;    % dynamic viscosity of air , Ns/m^2
Vs= 0.0065; % superficial Velocity, m/s
ko= (vis*Vs)/((19.61/5)/length); %initial-experimental permeability
permeability_beta= ko/(rm(1)/100)^2;
k(1)=permeability_beta* (rm(1)/100)^2; %permeability
DeltaP(1)= (length*vis*Vs/k(1))*(1/9.80665); % mm of water
porosity(1)= inp;
```

174

```
% BIG LOOP !
for n = 2:100,

    Xb(n)= Xb(n-1) + (An(n)/(1-p(n)))*fr(n);

    Xa(n)=An(n);

    Xnab(n)= p(n)- Xb(n);

    Xna(n)= 1- Xa(n)- Xb(n);

    % Surface Area for CYLINDERS
    loop1 = 0;
    for i = n+1 : 100,
        loop1 = loop1 + (r(i)- ri(n))*fr(i);
    end

    Src(n) = cc * (An(n)/(1-p(n))*(loop1/loopSrc2));

    % Biomass for CYLINDERS
        loop3=0;
    for i= n+1 : 100,

        loop3 = loop3 + ( 2 * r(i)* ri (n)- ri(n)^2)* fr (i);
    end
        Brc(n)= (An(n)/(1-p(n)))*(loop3/loopBrc2);

% call integral part for rm calculation

    Ax=An(n);
    px=p(n);
    rmroot = integral_sandfitting(r,n,c,R,N,Ax,px);
    rm(n) = rmroot;

    tcs(n)=ri(n)/K;

    % HEAD LOSS
    k(n)=permeability_beta* (rm(n)/100)^2;
    DeltaP(n)= (length*vis*Vs/k(n))*(1/9.80665);
```

175

```
% calculate porosity of the bed
loopalfa2=0;
for i = n+1 :100,
    loopalfa2= loopalfa2 + (r(i)-ri(n))^2*fr(i);
end
alfa(n) =  An(n)/(1-p(n))*(loopalfa2/loopBrc2);
% alfa is available pore volume/total Pore volume
porosity(n)= alfa(n)*inp; % porosity = initial porosity*alfa

end %end of big loop

    uni=100*inp*2/R; % surface area/volume ratio

for i=1:100
    EC(i) = sub(i)*Src(i)*uni;
end

for i = 1:100
    if (part == 1)
        initial = Cg/H;
    else
        initial = STARTVALUE(i);
    end

    STARTVALUE(i) = initial - (((sub(i)*Src(i)*uni)/1000)*0.0011);
end
changeTime(1:100) = time(1:100);


for i=1:100
    if (part==1)
        firstEC(i)= EC(i);
        firstHL(i)= DeltaP(i);
        firsttime(i)= time(i);

    elseif (part==2)
        secondEC(i)= EC(i);
        secondHL(i)= DeltaP(i);
        secondtime(i)= time(i);

    elseif (part==3)
        thirdEC(i)= EC(i);
```

176

```
% calculate porosity of the bed
loopalfa2=0;
for i = n+1 :100,
    loopalfa2= loopalfa2 + (r(i)-ri(n))^2*fr(i);
end
alfa(n) =  An(n)/(1-p(n))*(loopalfa2/loopBrc2);
% alfa is available pore volume/total Pore volume
porosity(n)= alfa(n)*inp; % porosity = initial porosity*alfa

end %end of big loop

    uni=100*inp*2/R; % surface area/volume ratio

for i=1:100
    EC(i) = sub(i)*Src(i)*uni;
end

for i = 1:100
    if (part == 1)
        initial = Cg/H;
    else
        initial = STARTVALUE(i);
    end

    STARTVALUE(i) = initial - (((sub(i)*Src(i)*uni)/1000)*0.0011);
end
changeTime(1:100) = time(1:100);


for i=1:100
    if (part==1)
        firstEC(i)= EC(i);
        firstHL(i)= DeltaP(i);
        firsttime(i)= time(i);

    elseif (part==2)
        secondEC(i)= EC(i);
        secondHL(i)= DeltaP(i);
        secondtime(i)= time(i);

    elseif (part==3)
        thirdEC(i)= EC(i);
```

176

```
            thirdHL(i)= DeltaP(i);
            thirdtime(i)= time(i);

        elseif (part==4)
            fourthEC(i)= EC(i);
            fourthHL(i)= DeltaP(i);
            fourthtime(i)= time(i);


    elseif (part==5)
            fifthEC(i)= EC(i);
            fifthHL(i)= DeltaP(i);
            fifthtime(i)= time(i);
        end
    end

end % end for part 1 to 5 loop

for i=1:100
    totalHL(i)= firstHL(i)+secondHL(i)+thirdHL(i)+fourthHL(i)+fifthHL(i);
    totalEC(i)= firstEC(i)+secondEC(i)+thirdEC(i)+fourthEC(i) + fifthEC(i);
end

% data from experimental biofilter

    X = [    5.88   6.88    7.75    8.08    8.83   9.00   9.75    9.96   10.71
        11.75  12.71   13.71   14.67  15.67  16.63  16.96  17.67  18.67  19.63
        20.58  22.54   23.54   23.63  24.54   25.54  26.50  27.50  28.42  28.96
        29.42  30.42   32.33   33.33  34.29  35.29  36.29   37.29  39.25  40.25
        41.21  42.25   43.21   44.17  46.17  47.13  48.13  49.13  50.13  51.13
        53.13  54.21   55.08   56.08  57.08  58.08  60.08  61.08  62.08  64.17
        65.13  66.46   67.08   68.08  69.29  70.08  71.13  74.04  75.04  76.13
        77.08  78.04   79.08    81.08  82.08  83.08  84.04  85.04  88.08  89.08
        90.08  91.04   92.04   93.04  95.04  96.04  97.04  98.00  99.00  100.00
        101.96 102.96 103.96 104.96 105.96 108.96 109.96 110.96 111.96 113.04
        115.88 116.83 117.88 118.88 119.88 120.83 122.83 123.92 124.92 125.83
        126.88 129.88 130.88 131.92 136.88 137.88 142.79 143.88 144.92 145.88
        149.88 150.92 151.92 152.88 156.96 157.96 158.96 160.00 163.96 164.92
        165.92 170.92 171.88 172.88 173.92 174.96 177.88 178.88 180.13 180.88
        181.83 185.00 185.83 186.88 187.83 188.92 191.75 194.13 194.88 195.67
        198.75 199.63 204.67 206.58 207.58 208.63];
```

177

EC_Y = [3.17 5.73   24.72 21.51 25.60 22.37 24.47 26.65 19.78 18.80
        11.59 26.22 26.96 24.72 20.74 19.64 14.23 19.15 22.30 2.34
        23.90 20.22 26.28 25.70 25.40 25.59 25.92 17.12 25.42 26.25
        26.38 25.79 26.09 23.91 24.77 25.09 21.79 25.66 21.45 23.00
        23.31 20.90 25.88 25.09 26.08 19.69 24.71 24.96 25.37 23.74
        24.19 26.42 24.05 26.43 23.05 26.13 23.42 26.52 26.31 26.75
        25.67 26.78 22.62 24.80 25.80 25.62 22.42 24.07 24.36 24.67
        25.91 26.44 25.62 26.70 24.42 24.03 26.17 25.58 26.72 27.94
        27.92 27.95 24.87 26.90 23.48 26.92 20.56 24.85 25.05 22.86
        26.83 24.44 24.80 25.87 26.52 23.77 26.97 26.99 26.80 28.36
        23.62 26.63 19.12 8.11   25.67 23.33 25.39 23.89 24.51 25.43
        20.55 24.95 21.89 23.27 25.08 20.77 24.30 21.63 23.49 23.17
        7.68   23.49 26.28 24.20 23.17 23.17 23.37 22.45 24.26 21.58
        24.61 19.83 23.32 19.66 23.77 23.70 19.30 16.87 19.93 19.34
        24.97 22.96 25.64 23.63 15.25 21.72 18.15 24.06 14.97 20.16
        21.63 23.30 21.74 9.12   8.36];

RE_Y= [0.11   0.20   0.84   0.73   0.87   0.76   0.83   0.91   0.67   0.64
        0.40   0.89   0.92   0.84   0.71   0.67   0.49   0.65   0.76   0.08
        0.82   0.69   0.90   0.88   0.87   0.87   0.88   0.58   0.87   0.90
        0.90   0.88   0.89   0.82   0.85   0.86   0.74   0.88   0.73   0.78
        0.80   0.71   0.88   0.86   0.89   0.67   0.84   0.85   0.87   0.81
        0.83   0.90   0.82   0.90   0.79   0.89   0.80   0.90   0.90   0.91
        0.88   0.91   0.77   0.85   0.88   0.87   0.76   0.82   0.83   0.84
        0.88   0.90   0.87   0.91   0.83   0.82   0.89   0.87   0.91   0.95
        0.95   0.95   0.85   0.92   0.80   0.92   0.70   0.85   0.85   0.78
        0.92   0.83   0.85   0.88   0.90   0.81   0.92   0.92   0.91   0.97
        0.81   0.91   0.65   0.28   0.88   0.80   0.87   0.82   0.84   0.87
        0.70   0.85   0.75   0.79   0.86   0.71   0.83   0.74   0.80   0.79
        0.26   0.80   0.90   0.83   0.79   0.79   0.80   0.77   0.83   0.74
        0.84   0.68   0.80   0.67   0.81   0.81   0.66   0.58   0.68   0.66
        0.85   0.78   0.87   0.81   0.52   0.74   0.62   0.82   0.51   0.69
        0.74   0.79   0.74   0.31   0.29];

HL_Y= [2   2   2   2   2   2   2   2   2   2   2
        2   2   2   2   2   2   2   2   2   2   2
        2   2   4   4   4   4   4   4   4   4   4
        4   4   5   5   5   5   5   5   5   5   5
        7   7   7   7   7   7   7   7   7   7   7
        7   8   8   8   9   9   9   9   10 10 10
        13 13 13 13 13 13 13 13 13 13 13
        13 13 13 13 13 13 13 13 13 13 15

178

15	15	15	15	15	16	16	16	16	16	16
16	16	17	17	17	17	17	17	17	17	17
20	20	20	20	20	22	24	26	30	30	30
30	30	30	30	31	33	36	36	42	47	47
48	48	48	50	50	50	50	54	60	68	68
70	70	80	80	80	80	80	80	84	94	
103	110];									

% plot the figures

figure(1)
plot(firsttime(1:end)*0.01667*0.0001/24,
firstHL,'g',secondtime(1:end)*0.01667*0.0001/24, secondHL,'m'...
    ,thirdtime(1:end)*0.01667*0.0001/24, thirdHL,
'k',fourthtime(1:end)*0.01667*0.0001/24, fourthHL,'y'...
    ,fifthtime(1:end)*0.01667*0.0001/24, fifthHL,'b',
fifthtime(1:end)*0.01667*0.0001/24, totalHL,'r')
xlabel('time,days')
ylabel('HL, mm of water')

figure(3)
plot(time(1:end)*0.01667*0.00001/24, porosity, 'b')
xlabel('time, days')
ylabel('porosity')

figure(4)
plot(firsttime(1:end)*0.01667*0.0001/24, firstEC/1000*0.479, 'b:',
secondtime(1:end)*0.01667*0.0001/24, secondEC/1000*0.479,'m--',
thirdtime(1:end)*0.01667*0.0001/24,thirdEC/1000*0.479,'k-.',
fourthtime(1:end)*0.01667*0.0001/24,
fourthEC/1000*0.479,'yd',fifthtime(1:end)*0.01667*0.0001/24,fifthEC/1000*0.479,'
g-o', fifthtime(1:end)*0.01667*0.0001/24, totalEC/5000*0.479,'r-')
xlabel('time, days')
ylabel('total EC, g/m^3.hr')
legend('first part','second part','third part','fourth part','fifth part','overall')

figure(5)
plot(fifthtime(1:end)*0.01667*0.00001/24, totalEC/5000/29.31*0.479)
xlabel('time, days')
ylabel('Overall Removal Efficiency')

179

```
figure(6)
plot(fifthtime(1:end)*0.01667*0.0001/24, totalEC/5000*0.479, 'k-', X, EC_Y, 'ko')
xlabel('time, days')
ylabel('EC, g/m^3/hr')
legend('model','experimental')

figure(7)
plot(fifthtime(1:end)*0.01667*0.0001/24, totalHL,'k-',X,HL_Y,'ko')
xlabel('time, days')
ylabel('Head Loss, mm of water')
legend('model','experimental')


figure(8)
plot(fifthtime(1:end)*0.01667*0.0001/24, (totalEC/5000*0.479)/29.31,'b-',X,
RE_Y,'bo') % 590 works fine for 200 days
xlabel('time, days')
ylabel('Removal Efficiency')
legend('model','experimental')
```

EFFECTIVE PORE RADIUS CALCULATION PART:

```
function [rmroot] = integral_sandfitting(r,n,c,R,N,Ax,px)
rm=0;
z=6;

% routine starts here
int=0;
intx=0;
igraph=0;
intsub=0;
for i=1:10
    rm=i*R/10;

    for j=n+1:N
        if r(j)<(0.02214)
            fx=0;
            intx=intx+ fx*(rm^3-r(j)^3)/(r(j)^3+(z/2-1)*rm^3);
        elseif r(j)>=(0.02214) & r(j) <=(0.04059)
            fx= c*(-119080*r(j)^3 + 9028.8*r(j)^2-191.52*r(j) + 1.1339);
```

180

```
            intx=intx+ fx*(rm^3-r(j)^3)/(r(j)^3+(z/2-1)*rm^3);
         elseif r(j) > (0.04059)
            fx=0;
            intx=intx+ fx*(rm^3-r(j)^3)/(r(j)^3+(z/2-1)*rm^3);
         end
      end
      int= (1-Ax)/ (z/2 -1)+ Ax*intx/(1-px);
      igraph=igraph+1;
      rg(igraph)=rm;
      intg(igraph)=int;
      intx=0;
end

start=0;
for i=1:10
   if (intg(i)<0)
      start=rg(i);
   end
end

for i=1:10
   rm=start+(i-1)*R/100;

   for j=n+1:N
      if r(j)<(0.02214)
         fx=0;
         intx=intx+ fx*(rm^3-r(j)^3)/(r(j)^3+(z/2-1)*rm^3);
      elseif r(j)>=(0.02214) & r(j) <= (0.04059)
         fx= c*(-119080*r(j)^3 + 9028.8*r(j)^2-191.52*r(j) + 1.1339);
         intx=intx+ fx*(rm^3-r(j)^3)/(r(j)^3+(z/2-1)*rm^3);
      elseif r(j) > (0.04059)
         fx=0;
         intx=intx+ fx*(rm^3-r(j)^3)/(r(j)^3+(z/2-1)*rm^3);
      end
   end

   int=(1-Ax)/(z/2 -1)+Ax*intx/(1-px);
   igraph=igraph+1;
   rg(igraph)=rm;
   intg(igraph)=int;
   intx=0;
end
```

```
start2=0;
for i=11:20
   if intg(i)<0
      start2= rg(i);
   end
end


for i=1:10
   rm= start2+(i-1)*R/1000;
   for j= n+1:N
      if r(j)<(0.02214)
         fx=0;
         intx=intx+ fx*(rm^3-r(j)^3)/(r(j)^3+(z/2-1)*rm^3);
      elseif r(j)>=(0.02214) & r(j) <=(0.04059)
         fx= c*(-119080*r(j)^3 + 9028.8*r(j)^2-191.52*r(j) + 1.1339);
         intx=intx+ fx*(rm^3-r(j)^3)/(r(j)^3+(z/2-1)*rm^3);
      elseif r(j) > (0.04059)
         fx=0;
         intx=intx+ fx*(rm^3-r(j)^3)/(r(j)^3+(z/2-1)*rm^3);
      end
   end
   int= (1-Ax)/ (z/2 -1)+ Ax*intx/(1-px);
   igraph=igraph+1;
   rg(igraph)=rm;
   intg(igraph)=int;
   intx=0;
end

index=1;
for i=21:30
   if intg(i)<0
      index=i;
   end
end

rmroot = rg(index);
```

CELLULAR AUTOMATON PART:

```
if (part > 1)
    clear Cl cut a Xinact Xactpast Xset ind t ri changeIndex S tt indValue L epsilon
exceeded cutoff Xtotal Xexcess Xactpresent;
    clear ind1 ind2 t1 t2 ri1 ri2 tFinal steps rm k permeability_beta DeltaP;
end

sub = zeros(100,1);
time = zeros(100,1);


N = 100;
R = 0.135/200; %m
rc = R/N;
W = rc;
deltaX = W;
cut = 0;

a = 0.0001;
deltaT = 0.01667*a;  %hour

m = 0.02; % per hour
Ks = 0.26;     %gm-3
kd = 0.016;    %1/h
beta = 0.17;   %mg/mg
Df = 2.41e-9*3600;    % m2/hr,
Yact = 0.1;   %yield coefficient on oxygen mg biomass/ mg of oxygen consumed
Xinact(1) = 0;
Xactpast(1) = 25000; % mg biomass/L
Xset = 30000; % mg biomass/L

ind = 1;
t = [ ];
ri = [ ];
ri(1) = W;

changeIndex = 1;
S(1) = 0;
tt(1) = 0;
indValue = 0;
```

183

```matlab
Cl = [STARTVALUE(1) STARTVALUE(1) ;STARTVALUE(1)
STARTVALUE(1) ; STARTVALUE(1) STARTVALUE(1)];
L = 1;

while (L < N+2 )

    epsilon = 0;
    exceeded = 0;
    cutoff = 0;
    a=1;

    while (exceeded == 0 & cutoff == 0)

        for layerInd = 1:L

            epsilon = 0;

            layer1 = layerInd;
            layer2 = layerInd +1;
            layer3 = layerInd +2;

            Cl(layer2, 1)= Cl(layer2, 2) + (deltaT * Df * (Cl(layer3, 2) - 2*Cl(layer2, 2)
            + Cl(layer1, 2)) / deltaX^2) - (deltaT * m *  Cl(layer2, 2) *
            Xactpast(layerInd) / ((Ks + Cl(layer2, 2)) * Yact));


            epsilon = epsilon + (Cl(layer2, 1) - Cl(layer2, 2))^2;

            Xactpresent(layerInd) = Xactpast(layerInd) * (1 + ((m*Cl(layer2, 2))/(Ks +
Cl(layer2, 2)))*deltaT*a - kd*deltaT*a);
        end % for

        Xinact(1:L) = Xinact(1:L) + deltaT*beta*kd*Xactpast(1:L)*a;
        Xtotal(1:L) = Xactpresent(1:L) + Xinact(1:L);


        epsilon = sqrt(epsilon/(L));

        if (epsilon < 1e-3)
            a = 10000;
        else
            a = 1;
```

184

```
end

for i = 1:L-1

    if (Xtotal(i) > Xset)

        Xexcess = Xtotal(i) - Xset;
        Xactpresent(i) = Xactpresent(i) - (Xexcess*(Xactpresent(i)/Xtotal(i)));
        Xinact(i) = Xinact(i) - (Xexcess*(Xinact(i)/Xtotal(i)));

        Xactpresent(i+1) = Xactpresent(i+1) +
(Xexcess*(Xactpresent(i)/Xtotal(i)));
        Xinact(i+1) = Xinact(i+1) + (Xexcess*(Xinact(i)/Xtotal(i)));

        Xtotal(i:i+1) = Xactpresent(i:i+1) + Xinact(i:i+1);

    end

end

if (Xtotal(L) > Xset)
    exceeded = 1;

    Xexcess = Xtotal(L) - Xset;
    Xactpresent(L) = Xactpresent(L) - (Xexcess*(Xactpresent(L)/Xtotal(L)));
    Xinact(L) = Xinact(L) - (Xexcess*(Xinact(L)/Xtotal(L)));

    if (L < 1)
        Xactpast(L+1) = Xset;
        Xinact(L+1) = 0;
        Xactpresent(L+1) = Xset;
    else

        Xactpresent(L+1) = Xexcess*(Xactpresent(L)/Xtotal(L));
        Xinact(L+1) = Xexcess*(Xinact(L)/Xtotal(L));
        Xtotal(L:L+1) = Xactpresent(L:L+1) + Xinact(L:L+1);
    end
end


t(ind) = indValue;
ri(ind) = L*W;
```

185

```
    ind = ind + 1;
    indValue = indValue + 1 + a;

    Xactpast = Xactpresent;
    Cl(:,2) = Cl(:,1);
    Cl(1,:) = Cl(2,:);

    if (L == N+1)
        break
    end

end   %while loop

deltaS(1,2) = 0;


for i = 1:L-1
    deltaS(i,1) = m*Cl(i, 2)/(Ks + Cl(i, 2))*(Xactpresent(i)/Yact)*deltaX*1000;
    deltaS(i+1,2) = deltaS(i,2) + m*Cl(i, 2)/(Ks + Cl(i,
2))*(Xactpresent(i)/Yact)*deltaX*1000; % mg/m^2/hr
end

if (L>1)
    S(L) = deltaS(L,2);
    tt(L) = t(ind-1);
end

if (part >1)
    while(tt(L) > changeTime(changeIndex) & (changeIndex < 99))
        changeIndex = changeIndex + 1;
    end
end

Cl = [Cl; STARTVALUE(changeIndex) STARTVALUE(changeIndex)];
value = Cl(L+2,1:2);

Cl(L+2,1:2) = STARTVALUE(changeIndex);

L = L + 1;
if (L > 5 & (abs(S(end) - S(end-1)) < 0.5 & S(end) > 10))
    cut = cut + 1;
end
```

186

```
if (cut == 1)
    ind1 = size(S,2);
    ri1 = ri(end);
    t1 = t(end);
end

if (cut > 5)
    ind2 = size(S,2);
    ri2 = ri(end);
    t2 = t(end);
    break;
end

end  % big while loop

Cl(L+1,1:2) = value;
L = L -2;
Xtotal(L+1) = Xactpresent(L+1) + Xinact(L+1);


tInc = tt(end) - tt(end - 1);
slope = (ri2 - ri1)/(t2 - t1);
tFinal = (R -ri1 + slope*t1)/slope;
steps = fix(tFinal/tInc);


for i = ind2+1:100
    S(i) = S(end);
    tt(i) = tt(i-1) + tInc;
end

time(1)=0;
sub(1)=0;

for i = 2:100
    time(i) = tt(i);
    sub(i) = S(i);
end
```

III: ETHANOL BENCH SCALE BIOFILTER RESULTS

188

LAVA ROCK BIOFILTER TEST RESULTS:

Date	Days	Inlet (ppm)	Outlet (ppm)	RE (%)	HL (mm)	pH
6/8/2004	S	T	A	R	T	
6/9/2004	0.9	74.036	49.403	33%	2	7
6/9/2004	1.2	64.586	64.892	0%	2	
6/10/2004	1.9	120.030	62.192	48%	2	
6/10/2004	2.2	114.658	77.793	32%	2	
6/11/2004	2.9	112..181	66.534	41%	2	
6/11/2004	3.1	75.051	129.438	-72%	2	
6/12/2004	3.8	92.447	68.817	26%	2	
6/13/2004	4.8	133.780	98.153	27%	2	
6/14/2004	5.9	74.105	96.080	-30%	2	
6/15/2004	6.9	121.714	77.292	36%	2	
6/16/2004	7.8	212.980	54.663	74%	2	
6/16/2004	8.1	103.177	33.204	68%	2	
6/17/2004	8.8	85.433	21.723	75%	2	
6/17/2004	9.0	64.183	10.868	83%	2	
6/18/2004	9.8	77.877	10.534	86%	2	
6/18/2004	10.0	91.905	10.450	89%	2	
6/19/2004	10.7	79.922	15.836	80%	2	
6/20/2004	11.8	107.519	15.794	85%	2	
6/21/2004	12.7	91.696	10.367	89%	2	
6/22/2004	13.7	104.054	9.323	91%	2	
6/23/2004	14.7	107.394	8.905	92%	2	
6/24/2004	15.7	75.539	9.365	88%	2	
6/25/2004	16.6	138.331	9.239	93%	2	
6/25/2004	17.0	126.015	9.573	92%	2	
6/26/2004	17.7	109.523	11.035	90%	2	
6/27/2004	18.7	263.540	10.951	96%	2	
6/28/2004	19.6	159.749	9.281	94%	2	
6/29/2004	20.6	118.332	9.866	92%	2	
7/1/2004	22.5	88.982	9.323	90%	3	
7/2/2004	23.5	45.645	11.202	75%	3	
7/2/2004	23.6	66.187	9.072	86%	3	
7/3/2004	24.5	74.286	9.072	88%	3	
7/4/2004	25.5	54.622	9.198	83%	3	
7/5/2004	26.5	87.771	8.864	90%	3	
7/6/2004	27.5	75.539	11.703	85%	3	
7/7/2004	28.4	73.284	29.655	60%	3	
7/8/2004	29.0	101.424	9.072	91%	3	
7/9/2004	29.4	97.165	9.198	91%	4	
7/10/2004	30.4	84.348	18.557	78%	4	
7/12/2004	32.3	75.079	9.010	88%	4	

Date	Days	Inlet (ppm)	Outlet (ppm)	RE (%)	HL (mm)	pH
7/13/2004	33.3	99.127	15.860	84%	4	
7/14/2004	34.3	61.385	8.989	85%	4	7
7/15/2004	35.3	85.809	9.323	89%	4	
7/16/2004	36.3	66.855	9.156	86%	5	
7/17/2004	37.3	40.134	10.951	73%	5	
7/19/2004	39.3	74.495	16.086	78%	5	7.5
7/20/2004	40.3	62.471	15.878	75%	5	
7/21/2004	41.2	31.868	16.212	49%	5	
7/22/2004	42.3	29.488	9.740	67%	5	
7/23/2004	43.2	20.512	8.905	57%	5	7.5
7/24/2004	44.2	39.425	10.492	73%	5	
7/26/2004	46.2	38.089	9.072	76%	5	
7/27/2004	47.1	81.718	9.114	89%	7	
7/28/2004	48.1	25.104	9.239	63%	7	
7/29/2004	49.1	39.216	9.031	77%	8	
7/30/2004	50.1	47.065	9.991	79%	8	
7/31/2004	51.1	65.393	10.659	84%	8	
8/2/2004	53.1	42.973	10.283	76%	8	
8/3/2004	54.2	62.346	9.031	86%	8	
8/4/2004	55.1	61.177	9.615	84%	8	
8/5/2004	56.1	38.172	9.406	75%	8	
8/6/2004	57.1	93.491	9.031	90%	8	
8/7/2004	58.1	66.228	13.707	79%	8	
8/9/2004	60.1	51.532	8.947	83%	8	
8/10/2004	61.1	85.976	19.134	78%	9	
8/11/2004	62.1	70.236	11.870	83%	9	
8/13/2004	64.2	58.672	17.464	70%	9	
8/14/2004	65.1	63.389	13.957	78%	9	
8/15/2004	66.5	39.717	11.202	72%	10	
8/16/2004	67.1	89.107	16.379	82%	10	
8/17/2004	68.1	90.736	8.738	90%	10	
8/18/2004	69.3	35.625	8.530	76%	10	
8/19/2004	70.1	62.638	9.156	85%	10	
8/20/2004	71.1	62.471	9.323	85%	10	
8/23/2004	74.0	49.194	8.905	82%	10	
8/24/2004	75.0	47.775	8.655	82%	11	
8/25/2004	76.1	35.291	8.947	75%	11	
8/26/2004	77.1	55.498	9.907	82%	11	
8/27/2004	78.0	55.081	9.114	83%	11	
8/28/2004	79.1	59.214	9.072	85%	11	
8/30/2004	81.1	28.319	8.738	69%	11	
8/31/2004	82.1	60.843	8.655	86%	11	
9/1/2004	83.1	49.319	9.740	80%	11	
9/2/2004	84.0	43.892	15.210	65%	12	7

190

Date	Days	Inlet (ppm)	Outlet (ppm)	RE (%)	HL (mm)	pH
9/3/2004	85.0	81.175	15.293	81%	12	
9/6/2004	88.1	91.070	9.198	90%	12	
9/7/2004	89.1	93.032	8.822	91%	12	
9/8/2004	90.1	174.403	10.742	94%	12	
9/9/2004	91.0	78.879	8.780	89%	12	
9/10/2004	92.0	176.741	18.717	89%	12	
9/11/2004	93.0	70.696	13.748	81%	12	
9/13/2004	95.0	88.356	10.116	89%	12	
9/14/2004	96.0	61.928	17.255	72%	12	
9/15/2004	97.0	116.913	21.764	81%	12	
9/16/2004	98.0	70.362	11.369	84%	12	
9/17/2004	99.0	79.338	21.430	73%	12	
9/18/2004	100.0	32.703	9.239	72%	12	
9/20/2004	102.0	30.490	9.824	68%	12	
9/21/2004	103.0	35.792	8.989	75%	12	
9/22/2004	104.0	76.040	9.281	88%	12	
9/23/2004	105.0	109.982	11.202	90%	12	
9/24/2004	106.0	74.328	11.202	85%	12	
9/27/2004	109.0	137.621	15.001	89%	12	
9/28/2004	110.0	34.874	14.208	59%	13	
9/29/2004	111.0	98.835	8.822	91%	13	
9/30/2004	112.0	92.280	10.742	88%	13	
10/1/2004	113.0	294.435	15.043	95%	13	
10/4/2004	115.9	418.224	16.546	96%	13	
10/5/2004	116.8	40.719	9.198	77%	13	7.6
10/6/2004	117.9	39.341	9.281	76%	13	
10/7/2004	118.9	851.507	9.239	99%	13	7.5
10/8/2004	119.9	10.951	9.114	17%	13	
10/9/2004	120.8	65.059	9.824	85%	13	7.5
10/11/2004	122.8	55.373	9.323	83%	13	
10/12/2004	123.9	60.843	13.623	78%	13	
10/13/2004	124.9	39.842	8.905	78%	13	
10/14/2004	125.8	59.006	11.118	81%	13	
10/15/2004	126.9	86.310	15.418	82%	13	
10/18/2004	129.9	72.825	9.657	87%	13	
10/19/2004	130.9	110.734	8.989	92%	13	7
10/20/2004	131.9	43.182	10.575	76%	15	7
10/25/2004	136.9	55.457	14.291	74%	15	
10/26/2004	137.9	37.379	10.241	73%	15	
11/1/2004	142.8	68.191	16.295	76%	15	
11/2/2004	143.9	49.987	14.750	70%	15	
11/3/2004	144.9	39.091	13.790	65%	17	
11/4/2004	145.9	38.089	18.550	51%	17	
11/8/2004	149.9	61.093	11.410	81%	17	7

191

Date	Days	Inlet (ppm)	Outlet (ppm)	RE (%)	HL (mm)	pH
11/9/2004	150.9	31.534	12.120	62%	17	
11/10/2004	151.9	23.852	8.738	63%	17	
11/11/2004	152.9	32.619	5.469	83%	17	
11/15/2004	157.0	26.482	9.198	65%	17	7
11/16/2004	158.0	22.766	9.156	60%	17	
11/17/2004	159.0	36.544	9.156	75%	20	
11/18/2004	160.0	26.106	9.448	64%	20	
11/22/2004	164.0	58.045	9.866	83%	20	
11/23/2004	164.9	60.592	11.202	82%	20	
11//24/2004	165.9	40.552	10.659	74%	20	
11/29/2004	170.9	52.492	15.585	70%	23	
11/30/2004	171.9	33.955	17.464	49%	23	
12/1/2004	172.9	32.745	9.281	72%	25	
12/2/2004	173.9	50.280	12.454	75%	25	
12/3/2004	175.0	36.210	8.738	76%	25	
12/6/2004	177.9	55.999	12.037	79%	25	
12/7/2004	178.9	33.204	9.365	72%	25	7
12/8/2004	180.1	40.761	9.198	77%	27	
12/9/2004	180.9	59.590	10.534	82%	27	
12/10/2004	181.8	35.041	11.202	68%	27	
12/13/2004	185.0	21.556	9.198	57%	27	
12/14/2004	185.8	42.765	9.031	79%	27	
12/15/2004	186.9	50.154	9.699	81%	30	
12/16/2004	187.8	28.361	9.532	66%	30	
12/17/2004	188.9	21.389	9.323	56%	30	
12/20/2004	191.8	62.805	8.780	86%	32	
12/22/2004	194.1	13.373	9.031	32%	32	
12/23/2004	194.9	27.776	11.494	59%	32	
12/24/2004	195.7	21.263	10.450	51%	32	
12/27/2004	198.8	42.264	9.156	78%	32	
12/28/2004	199.6	16.838	9.448	44%	32	
1/1/2005	204.7	26.524	10.033	62%	32	
1/3/2005	206.6	22.432	9.573	57%	34	
1/4/2005	207.6	22.224	9.490	57%	34	
1/6/2005	209.6	31.033	10.033	68%	36	
1/7/2005	210.6	21.597	10.033	54%	36	
1/8/2005	211.6	18.842	10.784	43%	38	
1/10/2005	213.6	11.661	9.281	20%	38	
1/11/2005	214.6	46.313	15.084	67%	40	
1/12/2005	215.6	34.081	14.166	58%	40	
1/13/2005	216.6	25.104	8.947	64%		
1/14/2005	217.6	17.923	9.198	49%		
1/17/2005	220.5	24.269	10.909	55%		
1/18/2005	221.6	48.651	15.210	69%		

Date	Days	Inlet (ppm)	Outlet (ppm)	RE (%)	HL (mm)	pH
1/19/2005	222.6	46.522	26.607	43%		
1/20/2005	223.6	56.041	21.681	61%		
1/21/2005	224.6	67.105	16.754	75%		
1/24/2005	227.6	40.427	11.160	72%		
1/26/2005	229.6	49.737	10.534	79%		
1/27/2005	230.7	50.655	9.573	81%		
1/28/2005	231.6	21.848	9.406	57%		
1/31/2005	234.6	52.993	8.822	83%		
2/2/2005	235.6	42.723	9.323	78%		
2/3/2005	236.6	103.135	11.703	89%		
2/4/2005	237.6	20.721	10.116	51%		7
2/7/2005	240.6	90.276	10.116	89%		
2/8/2005	241.6	58.421	9.281	84%		
2/10/2005	242.7	32.661	9.532	71%		
2/11/2005	243.7	32.411	9.072	72%		
2/14/2005	246.6	34.248	10.492	69%		
2/15/2005	247.6	42.305	10.158	76%		
2/16/2005	248.6	27.275	9.198	66%		
2/18/2005	250.6	28.319	9.198	68%		
2/21/2005	253.6	43.683	10.408	76%		
2/23/2005	255.6	45.896	15.043	67%		
2/24/2005	256.6	37.880	11.786	69%		
2/25/2005	257.5	90.402	11.243	88%		
2/28/2005	260.6	64.224	9.072	86%		
3/1/2005	261.7	47.190	9.031	81%		
3/2/2005	262.6	36.293	9.949	73%		
3/4/2005	264.6	48.860	20.595	58%		
3/7/2005	267.6	49.528	12.538	75%		7
3/8/2005	268.7	37.003	17.589	52%		
3/9/2005	269.7	44.852	16.128	64%		
3/10/2005	270.6	37.755	16.462	56%		
3/14/2005	274.7	54.705	20.094	63%		
3/17/2005	277.7	54.121	19.218	64%		
3/21/2005	281.6	37.003	17.589	52%		7
3/23/2005	283.7	52.284	16.629	68%		
3/25/2005	285.7	39.926	23.393	41%		
3/28/2005	288.7	39.717	17.422	56%		7
3/30/2005	290.7	33.830	12.997	62%		
4/1/2005	292.8	15.502	9.991	36%		
4/4/2005	295.7	19.176	12.579	34%		7
4/5/2005	296.7	24.102	18.842	22%		
4/6/2005	297.7	24.228	19.134	21%		
4/7/2005	298.7	29.154	23.184	20%		
4/11/2005	302.8	34.707	29.488	15%		7

SAND BIOFILTER TEST RESULTS:

Date	Days	Inlet (ppm)	Outlet (ppm)	RE (%)	HL (mm)	pH
6/8/2004	S	T	A	R	T	
6/9/2004	0.9	85.31	71.57	16%	2	7.5
6/9/2004	1.2	149.98	72.53	52%	2	
6/10/2004	1.9	104.78	119.46	-14%	2	
6/10/2004	2.2	97.50	79.39	19%	2	
6/11/2004	2.9	105.61	93.31	12%	2	
6/11/2004	3.1	71.04	87.69	-23%	2	
6/12/2004	3.8	93.03	70.32	24%	2	
6/13/2004	4.8	79.21	91.07	-15%	2	
6/14/2004	5.9	84.51	75.39	11%	2	
6/15/2004	6.9	74.16	59.67	20%	2	
6/16/2004	7.8	84.31	13.21	84%	2	
6/16/2004	8.1	37.67	10.03	73%	2	
6/17/2004	8.8	75.37	9.53	87%	2	
6/17/2004	9.0	39.38	9.32	76%	2	
6/18/2004	9.8	100.38	16.59	83%	2	
6/18/2004	10.0	122.34	11.12	91%	2	
6/19/2004	10.7	82.34	26.77	67%	2	
6/20/2004	11.8	105.39	37.80	64%	2	
6/21/2004	12.7	76.12	46.02	40%	2	
6/22/2004	13.7	89.36	9.41	89%	2	
6/23/2004	14.7	111.57	8.95	92%	2	
6/24/2004	15.7	119.71	18.76	84%	2	
6/25/2004	16.6	123.84	36.21	71%	2	
6/25/2004	17.0	157.45	51.96	67%	2	
6/26/2004	17.7	67.23	34.58	49%	2	
6/27/2004	18.7	371.26	128.64	65%	2	
6/28/2004	19.6	184.84	44.18	76%	2	
6/29/2004	20.6	118.21	108.75	8%	2	
7/1/2004	22.5	91.70	16.92	82%	2	
7/2/2004	23.5	124.80	38.69	69%	2	
7/2/2004	23.6	87.31	9.03	90%	2	
7/3/2004	24.5	75.96	9.36	88%	2	
7/4/2004	25.5	69.53	9.28	87%	4	
7/5/2004	26.5	91.82	11.66	87%	4	
7/6/2004	27.5	78.75	9.11	88%	4	7.5
7/7/2004	28.4	52.62	21.89	58%	4	
7/8/2004	29.0	81.17	10.78	87%	4	
7/9/2004	29.4	94.20	9.82	90%	4	
7/10/2004	30.4	93.87	9.39	90%	4	
7/12/2004	32.3	74.08	8.89	88%	4	

Date	Days	Inlet (ppm)	Outlet (ppm)	RE (%)	HL (mm)	pH
7/13/2004	33.3	92.36	10.16	89%	4	
7/14/2004	34.3	48.32	8.91	82%	4	7.5
7/15/2004	35.3	73.62	11.41	85%	4	
7/16/2004	36.3	61.22	8.82	86%	5	
7/17/2004	37.3	50.20	12.87	74%	5	
7/19/2004	39.3	81.84	10.20	88%	5	7.5
7/20/2004	40.3	60.76	16.30	73%	5	
7/21/2004	41.2	40.97	8.82	78%	5	
7/22/2004	42.3	49.61	10.16	80%	5	
7/23/2004	43.2	40.51	11.62	71%	5	7.5
7/24/2004	44.2	76.04	8.91	88%	5	
7/26/2004	46.2	76.08	10.95	86%	5	
7/27/2004	47.1	99.34	10.95	89%	7	
7/28/2004	48.1	34.12	11.20	67%	7	
7/29/2004	49.1	78.21	12.29	84%	7	
7/30/2004	50.1	68.98	10.24	85%	7	
7/31/2004	51.1	67.81	9.11	87%	7	
8/2/2004	53.1	58.55	11.12	81%	7	
8/3/2004	54.2	85.43	14.92	83%	7	
8/4/2004	55.1	93.16	9.20	90%	7	
8/5/2004	56.1	57.59	10.32	82%	7	
8/6/2004	57.1	94.91	9.32	90%	7	
8/7/2004	58.1	56.79	12.12	79%	7	
8/9/2004	60.1	83.30	9.03	89%	7	
8/10/2004	61.1	83.30	16.75	80%	8	
8/11/2004	62.1	97.58	9.28	90%	8	
8/13/2004	64.2	100.17	10.24	90%	8	
8/14/2004	65.1	112.36	9.82	91%	9	
8/15/2004	66.5	77.50	9.62	88%	9	
8/16/2004	67.1	139.00	11.99	91%	9	
8/17/2004	68.1	61.55	14.04	77%	9	
8/18/2004	69.3	74.62	11.49	85%	10	
8/19/2004	70.1	110.53	13.25	88%	10	
8/20/2004	71.1	76.12	9.57	87%	10	
8/23/2004	74.0	71.11	16.71	76%	13	
8/24/2004	75.0	97.00	17.34	82%	13	
8/25/2004	76.1	68.82	11.62	83%	13	
8/26/2004	77.1	89.69	14.21	84%	13	
8/27/2004	78.0	85.14	9.87	88%	13	
8/28/2004	79.1	114.12	11.16	90%	13	
8/30/2004	81.1	78.38	9.87	87%	13	
8/31/2004	82.1	112.15	9.99	91%	13	
9/1/2004	83.1	67.65	11.29	83%	13	
9/2/2004	84.0	74.70	13.46	82%	13	6.5

Date	Days	Inlet (ppm)	Outlet (ppm)	RE (%)	HL (mm)	pH
9/3/2004	85.0	101.84	10.91	89%	13	
9/6/2004	88.1	74.95	9.53	87%	13	
9/7/2004	89.1	145.80	12.87	91%	13	
9/8/2004	90.1	215.90	10.07	95%	13	
9/9/2004	91.0	210.93	10.03	95%	13	
9/10/2004	92.0	216.24	10.03	95%	13	
9/11/2004	93.0	100.59	15.25	85%	13	
9/13/2004	95.0	166.97	13.71	92%	13	
9/14/2004	96.0	85.93	17.09	80%	13	
9/15/2004	97.0	153.53	12.54	92%	13	
9/16/2004	98.0	72.87	21.76	70%	13	
9/17/2004	99.0	81.59	12.41	85%	15	
9/18/2004	100.0	67.23	9.78	85%	15	
9/20/2004	102.0	46.15	10.16	78%	15	
9/21/2004	103.0	112.24	9.49	92%	15	
9/22/2004	104.0	69.69	11.58	83%	15	
9/23/2004	105.0	73.37	11.29	85%	15	
9/24/2004	106.0	135.66	15.92	88%	16	
9/27/2004	109.0	188.81	17.97	90%	16	
9/28/2004	110.0	75.83	14.33	81%	16	
9/29/2004	111.0	215.86	17.21	92%	16	
9/30/2004	112.0	174.40	13.83	92%	16	
10/1/2004	113.0	289.09	24.73	91%	16	
10/4/2004	115.9	455.05	14.71	97%	16	
10/5/2004	116.8	132.86	25.81	81%	16	3
10/6/2004	117.9	112.61	10.28	91%	17	4
10/7/2004	118.9	656.83	228.39	65%	17	5
10/8/2004	119.9	12.08	8.74	28%	17	
10/9/2004	120.8	70.65	8.78	88%	17	5.5
10/11/2004	122.8	81.51	16.63	80%	17	4.5
10/12/2004	123.9	68.23	9.11	87%	17	4.5
10/13/2004	124.9	48.40	8.95	82%	17	6.5
10/14/2004	125.8	67.44	11.03	84%	17	7
10/15/2004	126.9	95.33	12.62	87%	17	4
10/18/2004	129.9	69.86	20.89	70%	20	4
10/19/2004	130.9	69.61	10.37	85%	20	5.5
10/20/2004	131.9	47.02	11.91	75%	20	7
10/25/2004	136.9	74.04	15.25	79%	20	7
10/26/2004	137.9	64.02	9.24	86%	20	6
11/1/2004	142.8	71.95	20.97	71%	22	6.5
11/2/2004	143.9	72.20	12.33	83%	24	6
11/3/2004	144.9	47.23	12.37	74%	26	6.5
11/4/2004	145.9	72.41	14.37	80%	30	7
11/8/2004	149.9	100.71	21.10	79%	30	7

196

Date	Days	Inlet (ppm)	Outlet (ppm)	RE (%)	HL (mm)	pH
11/9/2004	150.9	12.58	9.28	26%	30	
11/10/2004	151.9	53.66	10.66	80%	30	
11/11/2004	152.9	87.73	9.07	90%	30	
11/15/2004	157.0	69.23	12.08	83%	30	
11/16/2004	158.0	100.71	21.10	79%	30	
11/17/2004	159.0	100.71	21.10	79%	31	
11/18/2004	160.0	53.41	10.83	80%	33	
11/22/2004	164.0	77.25	18.09	77%	36	
11/23/2004	164.9	73.28	12.62	83%	36	
11//24/2004	165.9	61.80	16.30	74%	42	
11/29/2004	170.9	107.06	17.17	84%	47	
11/30/2004	171.9	70.90	22.93	68%	47	
12/1/2004	172.9	86.23	17.63	80%	48	
12/2/2004	173.9	53.91	17.76	67%	48	
12/3/2004	175.0	55.33	10.45	81%	48	
12/6/2004	177.9	74.91	14.33	81%	50	
12/7/2004	178.9	61.64	21.05	66%	50	
12/8/2004	180.1	77.83	33.04	58%	50	
12/9/2004	180.9	118.79	38.01	68%	50	
12/10/2004	181.8	31.33	10.66	66%	54	
12/13/2004	185.0	59.05	8.74	85%	60	
12/14/2004	185.8	72.12	15.63	78%	68	
12/15/2004	186.9	90.15	11.29	87%	68	
12/16/2004	187.8	55.83	10.83	81%	70	
12/17/2004	188.9	35.54	17.05	52%	70	
12/20/2004	191.8	108.02	27.99	74%	80	
12/22/2004	194.1	32.49	12.37	62%	80	
12/23/2004	194.9	61.18	10.95	82%	80	
12/24/2004	195.7	52.24	25.56	51%	80	
12/27/2004	198.8	76.29	23.81	69%	80	
12/28/2004	199.6	49.78	13.04	74%	80	
1/1/2005	204.7	66.85	13.71	79%	84	
1/3/2005	206.6	53.54	13.83	74%	94	
1/4/2005	207.6	27.36	18.84	31%	103	7
1/5/2004	208.6	28.82	20.60	29%	110	

IV: HORIBA INSTRUMENTS CAM SIZER TEST RESULTS FOR

LAVA ROCK AND SAND

198

HORIBA

November 19, 2003

Dr. Fethiye Ozis
UNIVERSITY OF SOUTHERN CALIFORNIA
Environmental Engineering
3620 S. Vermont Ave., Kap. 210
Los Angeles, CA 90089

REF: QUARTZ SAND & LAVA ROCK SAMPLES
MODEL: CAMSIZER

Dear Dr. Ozis:

Please find enclosed the results of our analyses from the samples that you recently submitted. We ran them on the HORIBA Camsizer.

The samples ran very easily. During the measurement, we used the minXc measurement model, which shows a distribution that will closely correlate to sieving. Shape calculations for sphericity and aspect ratio have been reported for each size class. All data and sample images have been enclosed for your review.

When reviewing the data sheets, it is helpful to know some of the terms and abbreviations used by the Camsizer software. The software uses ISO terminology: 0 = number, 1 = length, 2 = area, 3 = volume. For example, Q3 is the cumulative distribution (percent passing), based on volume. P3 is the proportion of particles in the fraction (percent retained), based on volume. SPHT3 is sphericity based on volume. L/b3 is aspect ratio based on volume. PD0 is particle detections based on number, etc. A definitions list with relevant ISO terminology has been attached to this report.

This proved to be an excellent application for the Camsizer. The experimental method employed is described on the following page. In addition, I have included an overlay of three (3) runs for each sample to display repeatability.

After reviewing the data, should you have any questions, please feel free to call.

Sincerely,

Amy Q. Hou
Laboratory Supervisor

Enclosures

cc: Dr. Michael C. Pohl/HORIBA
        Andy Gunewardena/HORIBA
        Bruce Heninger/HORIBA
        Tom Costa/Para Ventures
        File No. 5761-BWS

HORIBA

November 19, 2003

Dr. Fethiye Ozis
UNIVERSITY OF SOUTHERN CALIFORNIA
Environmental Engineering
3620 S. Vermont Ave., Kap. 210
Los Angeles, CA 90089

REF: QUARTZ SAND & LAVA ROCK SAMPLES
MODEL: CAMSIZER

The samples were prepared and tested on the Camsizer by the following method:

1. Power-up the Camsizer and start the software.

2. Input all measurement parameters; use the basic camera only with the 60mm stainless steel feed chute. Use a coverage area of 1.0%.

3. Press the measure icon to begin the measurement. Measure the entire sample. Once finished, review the data and repeat the measurement as necessary.

SUMMARY OF DRY DATA
Median Size (microns)

SAMPLE ID	RUN #1	RUN #2	RUN #3	AVERAGE
Quartz Sand	2227	2226	2227	2227
Lava Rock	4802	4771	4785	4786

File 5761-BWS
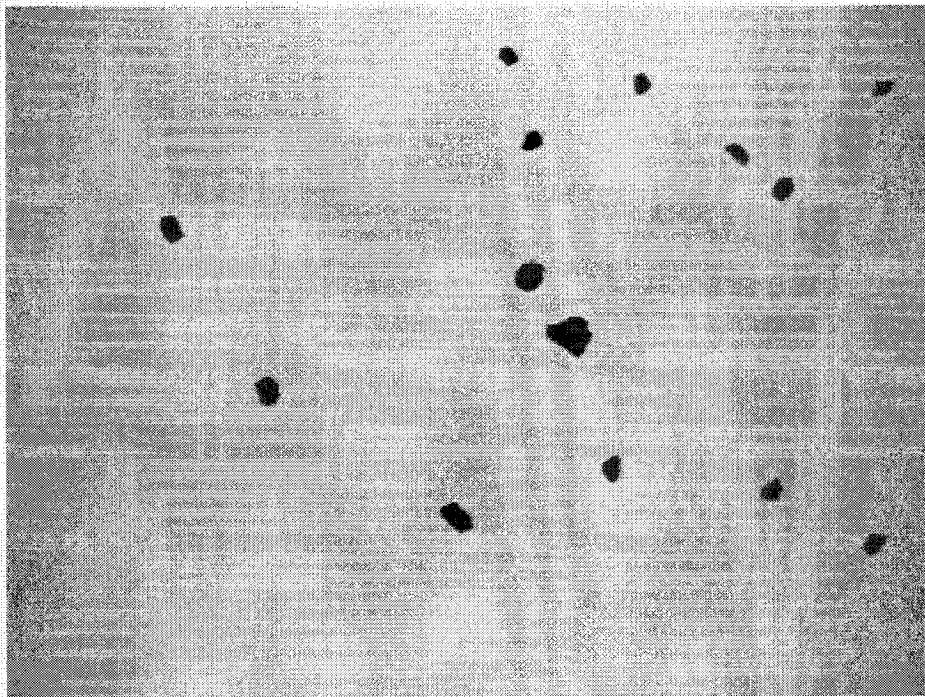
CCD - Basic , C:\Program Files\CAMSIZER\CAMDAT\USC\Quartz Sand_004a.bmp

201
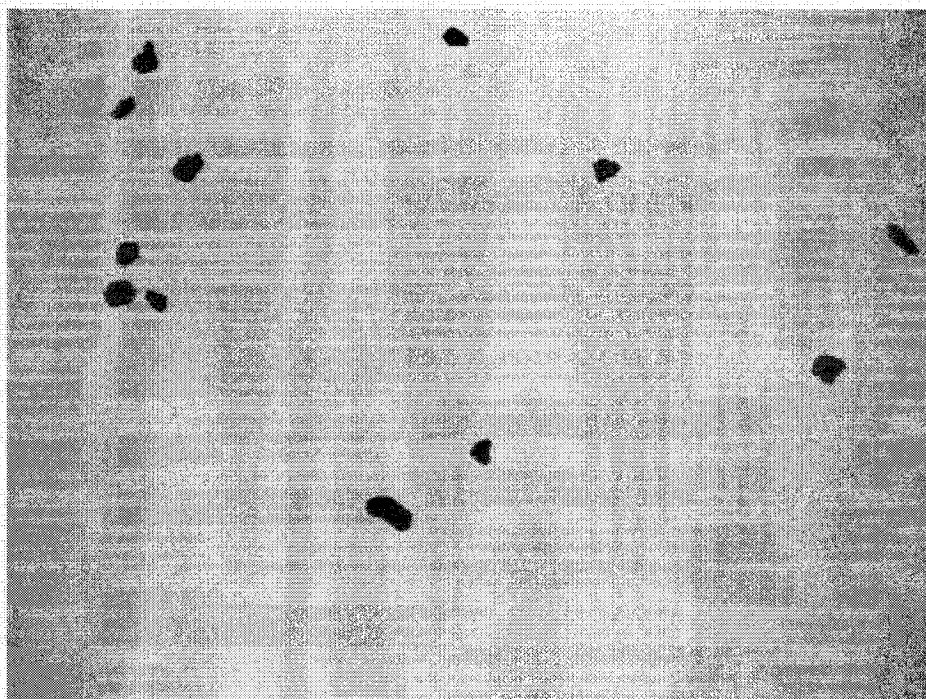
CCD - Basic , C:\Program Files\CAMSIZER\CAMDAT\USC\Quartz Sand_004b.bmp

Graph of measurement results:
C:\Program Files\CAMSIZER\CAMDAT\USC\Quartz Sand_004.rdf
Task file: USC_QUARTZ_.afg

HORIBA CAMSIZER® Retsch® TECHNOLOGY
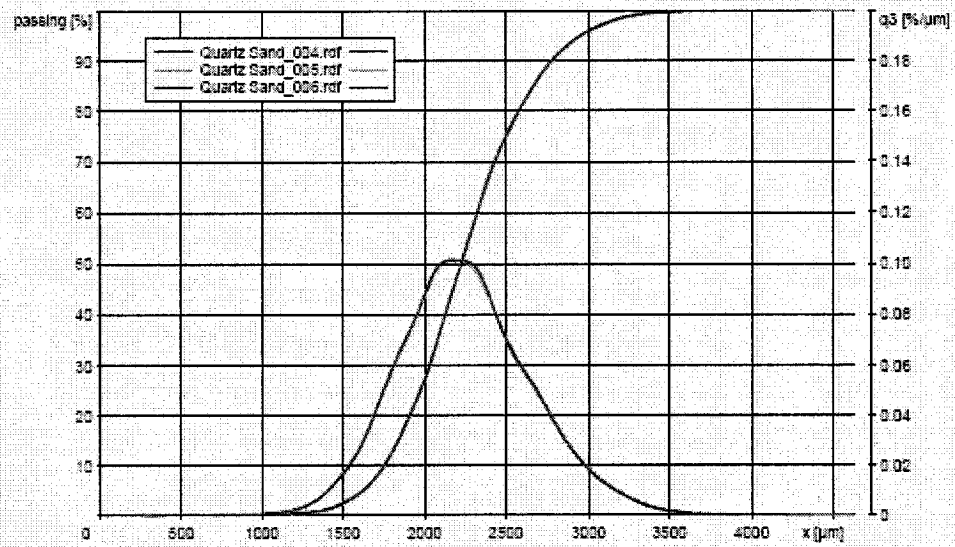
USC QUALITY REPORT

Company:	Horiba
User:	bws
Result file:	C:\Program Files\CAMSIZER\CAMDAT\USC\Quartz Sand_004.rdf
Task file:	C:\Program Files\CAMSIZER\CAMSYS\USC_QUARTZ_.afg
Time:	19.11.2003 , 9:35 , duration 8 min 55 s at 1.0 % covered area, image rate 1:1 and 50 mm feeder

Particle model:	min(xc)
No. of particles:	CCD-S = 181573 , CCD-Z not active
Fitting:	no

Material:

Size class	[µm]	retained [%]	passing [%]	SPHT3	b/l3	PD0
> 4000		0.0	100.0	0.689	1.319	2
3350 -	4000	0.6	100.0	0.845	1.310	196
2800 -	3350	5.5	99.4	0.877	1.296	4807
2360 -	2800	27.3	90.6	0.881	1.329	22339
2000 -	2360	36.5	63.5	0.880	1.382	44501
1700 -	2000	19.4	27.0	0.856	1.498	37514
1400 -	1700	6.5	7.6	0.842	1.634	17029
1180 -	1400	0.6	1.1	0.809	1.825	3690
1000 -	1180	0.2	0.3	0.783	1.886	835
0 -	1000	0.1	0.1	0.862	1.565	50560

Characteristics

Q3 [%]	x [µm]
10.0	1751
50.0	2227
90.0	2776

SPAN3 = 0.461
U3 = 1.328
MW3(x) = 2246 µm
Sigma3(x) = 405 µm

Q0 [%]	x [µm]
10.0	191
50.0	1673
90.0	2461

SPAN0 = 1.223
U0 = 10.557
MW0(x) = 1576 µm
Sigma0(x) = 875 µm

Sv = 2.904 / mm

User

204

HORIBA CAMSIZER® Retsch TECHNOLOGY

USC QUALITY REPORT

Company:	Horiba
User:	bws
Result file:	C:\Program Files\CAMSIZER\CAMDAT\USC\Quartz Sand_005.rdf
Task file:	C:\Program Files\CAMSIZER\CAMSYS\USC_QUARTZ_.afg
Time:	19.11.2003 , 10:09 , duration: 7 min 55 s at 1.0 % covered area, image rate 1:1 and 60 mm feeder

Particle model:	min(xc)
No. of particles:	CCD-B = 191117 , CCD-Z not active
Fitting:	no

Material:

Size class	[µm]	retained [%]	passing [%]	SPHT3	b3	PDO
> 4000		0.0	100.0	0.678	1.339	4
3350 -	4000	0.5	100.0	0.837	1.285	188
2800 -	3350	8.7	99.4	0.676	1.296	4809
2360 -	2800	27.1	90.7	0.660	1.333	22294
2000 -	2360	36.6	63.6	0.879	1.383	44649
1700 -	2000	19.2	27.0	0.856	1.498	37499
1400 -	1700	5.6	7.8	0.842	1.638	17150
1180 -	1400	0.9	1.2	0.807	1.832	3726
1000 -	1180	0.1	0.3	0.795	1.830	929
0 -	1000	0.2	0.2	0.879	1.676	59869
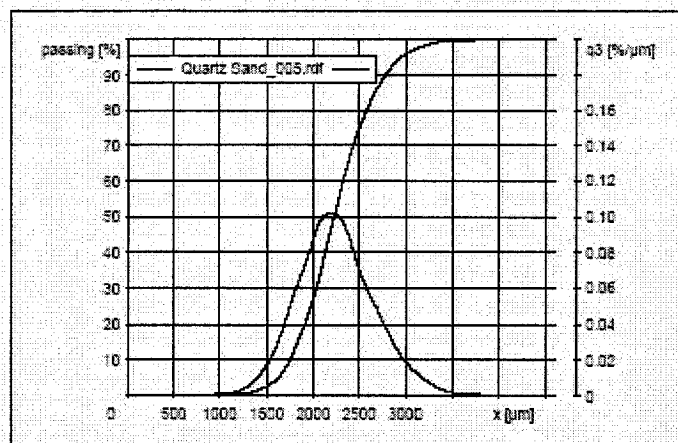
Characteristics

Q3 [%]	x [µm]
10.0	1746
50.0	2226
90.0	2760

SPAN3 =	0.453
U3 =	1.329
MW3(x) =	2246 µm
Sigma3(x) =	457 µm

Q0 [%]	x [µm]
10.0	160
50.0	1635
90.0	2454

SPAN0 =	1.244
U0 =	11.060
MW0(x) =	1515 µm
Sigma0(x) =	900 µm
Sv =	2.909 / mm

User

205

HORIBA CAMSIZER® Retsch TECHNOLOGY

USC QUALITY REPORT

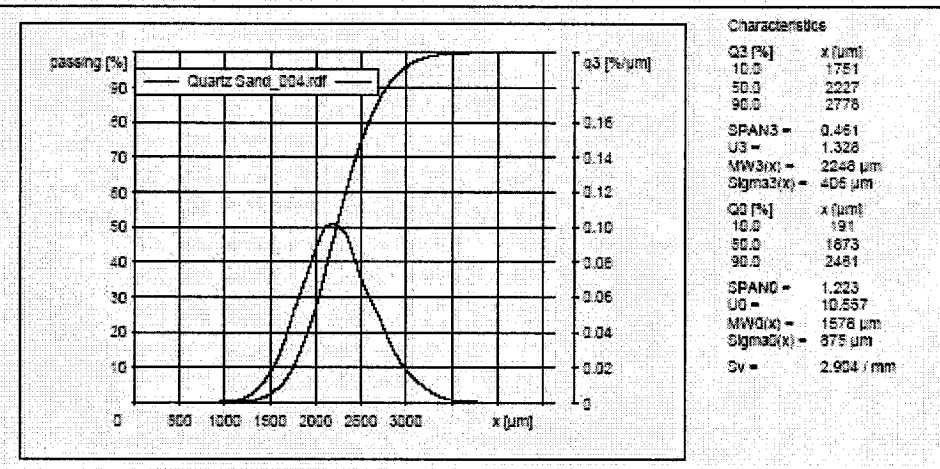|	
Company:	Horiba
User:	bws
Result file:	C:\Program Files\CAMSIZER\CAMDAT\USC\Quartz Sand_006.rdf
Task file:	C:\Program Files\CAMSIZER\CAMSYS\USC_QUARTZ_.afg
Time:	19.11.2003 , 10:24 , duration 7 min 56 s at 1.0 % covered area. image rate 1:1 and 60 mm feeder

Particle model:	mth(xc)
No. of particles:	CCD-B = 200646 , CCD-Z not active
Fitting:	no

Material:

Size class	[µm]	retained [%]	passing [%]	SPHT3	b3	PD0
> 4000		0.0	100.0			0
3350 -	4000	0.6	100.0	0.850	1.290	186
2800 -	3350	8.5	99.4	0.876	1.299	4782
2350 -	2800	27.2	90.9	0.880	1.331	22392
2000 -	2350	36.5	63.7	0.879	1.383	44694
1700 -	2000	19.4	27.2	0.865	1.499	37711
1400 -	1700	6.6	7.8	0.841	1.638	17189
1180 -	1400	0.9	1.2	0.809	1.815	3871
1000 -	1180	0.1	0.3	0.797	1.831	1011
0 -	1000	0.2	0.2	0.884	1.560	58612

Characteristics

Q3 [%]	x [µm]
10.0	1750
50.0	2227
90.0	2776

SPAN3 =	0.451
U3 =	1.328
MW3(x) =	2245 µm
Sigma3(x) =	405 µm

Q0 [%]	x [µm]
10.0	175
50.0	1604
90.0	2453

SPAN0 =	1.252
U0 =	11.185
MW0(x) =	1454 µm
Sigma0(x) =	915 µm
Sv =	2.913 / mm

User

206
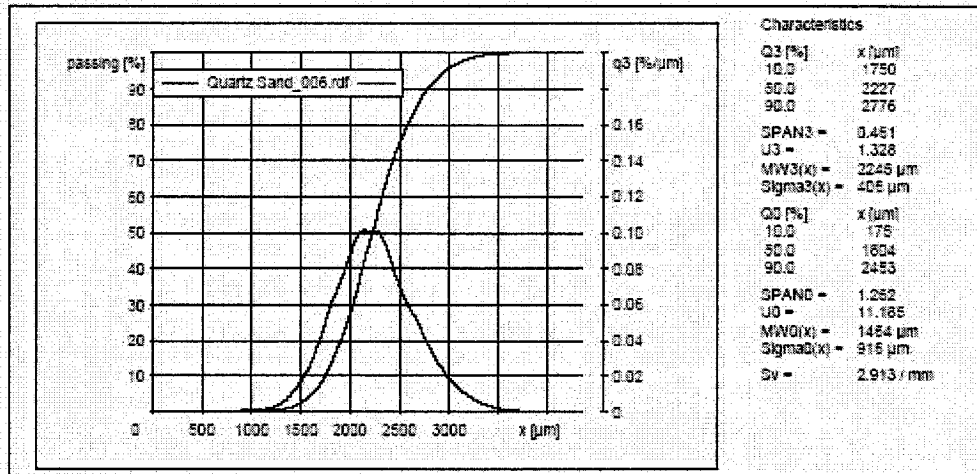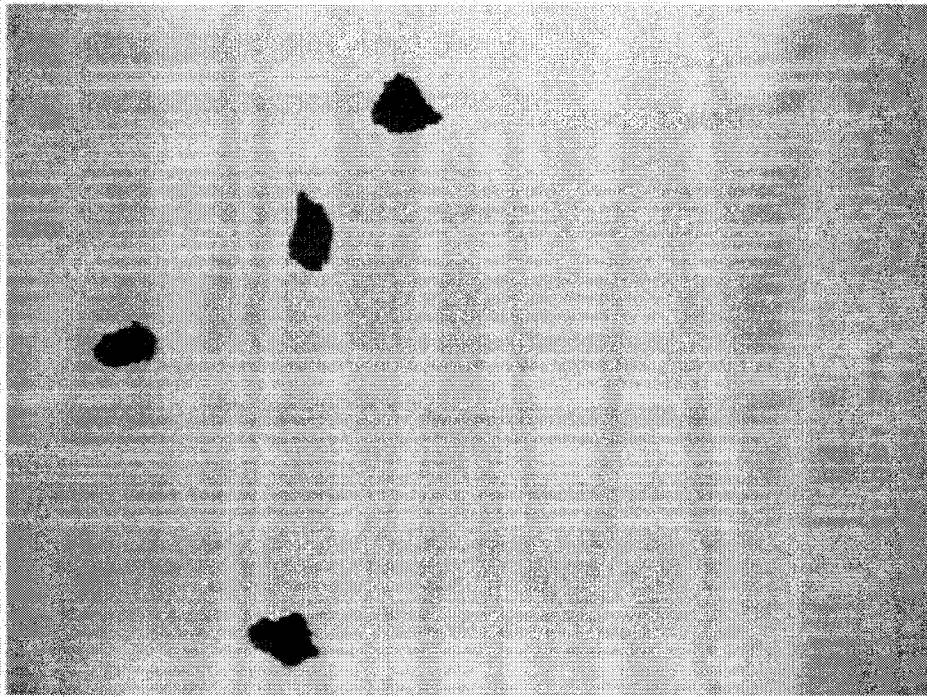
CCD - Basic , C:\Program Files\CAMSIZER\CAMDAT\USC\Lava Rock_004a.bmp

207
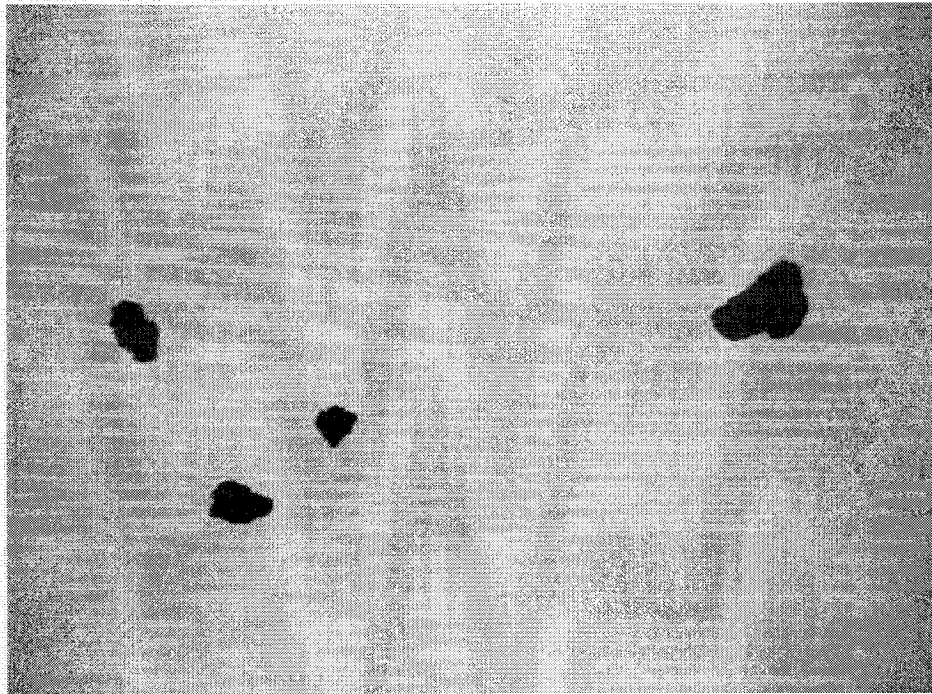
CCD - Basic , C:\Program Files\CAMSIZER\CAMDAT\USC\Lava Rock_004b.bmp

208

Graph of measurement results:
C:\Program Files\CAMSIZER\CAMDAT\USC\Lava Rock_004.rdf
Task file: USC_LAVA_.afg

209

HORIBA CAMSIZER® Retsch® TECHNOLOGY

USC QUALITY REPORT

Company:	Horiba
User:	bws
Result file:	C:\Program Files\CAMSIZER\CAMDAT\USC\Lava Rock _004.rdf
Task file:	C:\Program Files\CAMSIZER\CAMSYS\USC_LAVA_.afg
Time:	19.11.2003 , 10:42 , duration 4 min 1 s at 1.2 % covered area, image rate 1:1 and 60 mm feeder

Particle model:	min(xc)
No. of particles:	CCD-B = 69316 , CCD-Z not active
Fitting:	no

Material:

Size class	[µm]	retained [%]	passing [%]	SPHT3	b/c3	PD0
> 6700		1.2	100.0	0.781	1.379	40
6300 -	6700	3.6	98.8	0.752	1.354	174
5600 -	6300	16.9	95.2	0.761	1.383	1008
4750 -	5600	30.3	78.3	0.764	1.450	2546
4000 -	4750	23.9	48.0	0.759	1.496	3190
3350 -	4000	15.8	24.1	0.756	1.531	3505
2800 -	3350	6.7	8.3	0.750	1.643	2264
2360 -	2800	1.3	1.6	0.711	1.927	637
2000 -	2360	0.2	0.3	0.667	2.254	131
1700 -	2000	0.0	0.1	0.646	2.535	28
1400 -	1700	0.0	0.1	0.605	2.940	9
1180 -	1400	0.0	0.1	0.792	1.550	15
1000 -	1180	0.0	0.1	0.607	1.629	16
0 -	1000	0.1	0.1	0.926	1.517	55755
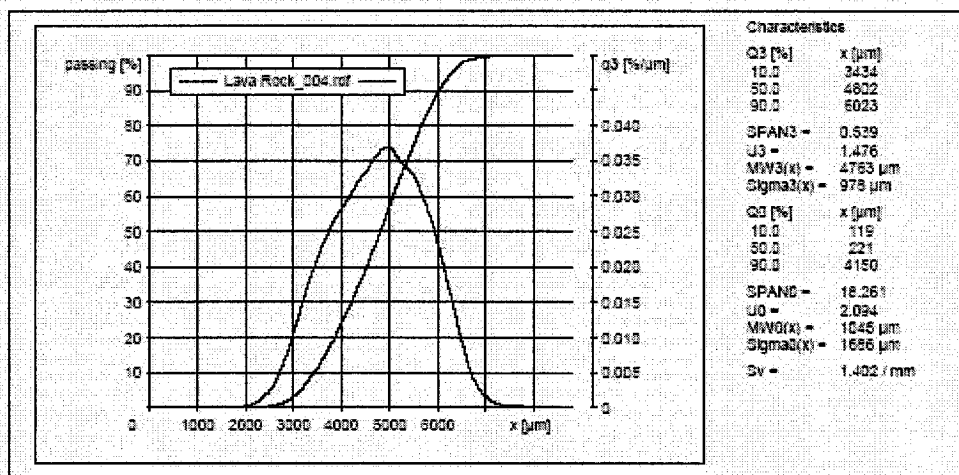
Characteristics

Q3 [%]	x [µm]
10.0	3434
50.0	4602
90.0	6023

SPAN3 = 0.529
U3 = 1.476
MW3(x) = 4763 µm
Sigma3(x) = 978 µm

Q0 [%]	x [µm]
10.0	119
50.0	221
90.0	4150

SPAN0 = 18.261
U0 = 2.094
MW0(x) = 1045 µm
Sigma0(x) = 1656 µm

Sv = 1.402 / mm

User

HORIBA CAMSIZER Retsch TECHNOLOGY

USC QUALITY REPORT

Company:	Horiba
User:	bws
Result file:	C:\Program Files\CAMSIZER\CAMDAT\USC\Lava Rock_006.rdf
Task file:	C:\Program Files\CAMSIZER\CAMSYS\USC_LAVA_.afg
Time:	19.11.2003 , 10:53 , duration 4 min 11 s at 1.0 % covered area, image rate 1:1 and 60 mm feeder

Particle model:	min(xc)
No. of particles:	CCD-5 = 90368 , CCD-Z not active
Fitting:	no

Material:

Size class	[µm]	retained [%]	passing [%]	SPHT3	b3	PD0
> 6700		1.3	100.0	0.737	1.324	51
6300 -	6700	3.5	98.7	0.756	1.328	169
5600 -	6300	16.4	95.2	0.757	1.378	981
4750 -	5600	30.1	78.8	0.763	1.443	2544
4000 -	4750	24.8	48.7	0.756	1.499	3300
3350 -	4000	15.6	23.9	0.757	1.521	3483
2800 -	3350	6.6	8.3	0.748	1.646	2224
2360 -	2800	1.4	1.7	0.711	1.904	695
2000 -	2360	0.2	0.3	0.670	2.231	134
1700 -	2000	0.0	0.1	0.609	2.636	35
1400 -	1700	0.0	0.1	0.611	2.711	16
1180 -	1400	0.0	0.1	0.805	1.515	13
1000 -	1180	0.0	0.1	0.776	1.621	29
0 -	1000	0.1	0.1	0.926	1.510	76595
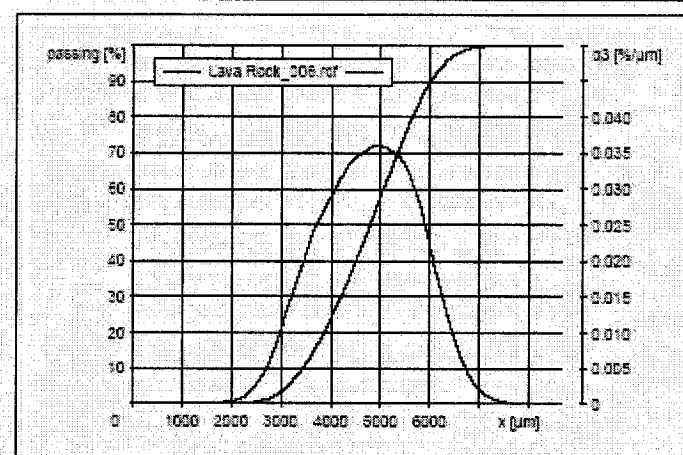
Characteristics

Q3 [%]	x [µm]
10.0	3443
50.0	4785
90.0	5997

SPAN3 = 0.534
U3 = 1.469
MW3(x) = 4752 µm
Sigma3(x) = 976 µm

Q0 [%]	x [µm]
10.0	119
50.0	216
90.0	2778

SPAN0 = 16.905
U0 = 2.037
MW0(x) = 355 µm
Sigma0(x) = 1524 µm

Sv = 1.410 / mm

User

HORIBA CAMSIZER® Retsch TECHNOLOGY

USC QUALITY REPORT

Company:	Horiba
User:	bws
Result file:	C:\Program Files\CAMSIZER\CAMDAT\USC\Lava Rock_005.rdf
Task file:	C:\Program Files\CAMSIZER\CAMSYS\USC_LAVA_.afg
Time:	19.11.2003 , 10:46 , duration 4 min 17 s at 1.0 % covered area, image rate 1:1 and 60 mm feeder

Particle model:	min(xc)
No. of particles:	CCD-6 = 79858 , CCD-Z not active
Fitting:	no

Material:

Size class	[µm]	retained [%]	passing [%]	SPHT3	b/l3	P03
> 6700		1.5	100.0	0.750	1.327	57
6300 -	6700	3.6	98.5	0.756	1.321	175
5600 -	6300	15.4	94.9	0.755	1.372	934
4750 -	5600	30.3	79.5	0.755	1.445	2642
4000 -	4750	25.0	49.2	0.757	1.600	3340
3350 -	4000	15.9	24.2	0.756	1.624	3564
2800 -	3350	6.6	8.3	0.746	1.655	2197
2360 -	2800	1.4	1.7	0.716	1.939	686
2000 -	2360	0.2	0.3	0.664	2.246	132
1700 -	2000	0.0	0.1	0.615	2.528	23
1400 -	1700	0.0	0.1	0.676	2.315	7
1180 -	1400	0.0	0.1	0.831	1.438	19
1000 -	1180	0.0	0.1	0.846	1.528	21
0 -	1000	0.1	0.1	0.927	1.509	66162
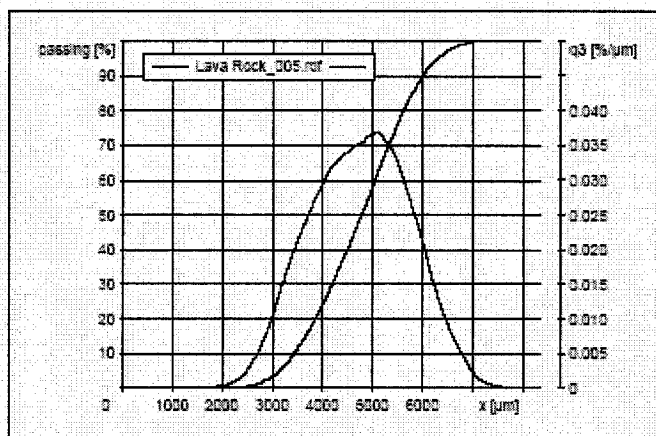
Characteristics

Q3 [%]	x [µm]
10.0	3433
50.0	4771
90.0	6004

SPAN3 =	0.539
U3 =	1.470
MW3(x) =	4744 µm
Sigma3(x) =	976 µm

Q0 [%]	x [µm]
10.0	120
50.0	220
90.0	3963

SPAN0 =	17.431
U0 =	2.062
MW0(x) =	942 µm
Sigma0(x) =	1596 µm
Sv =	1.409 / mm

User

212

CAMSIZER CHARACTERISTICS:

Particle size distribution:

x_{area} x by area	Particle diameter calculated by the area of particle $x = \sqrt{\dfrac{4A}{\pi}}$
$x_{c\,min}$	**Breadth**, particle diameter which is the shortest chord of the measured set of max. chords of a particle (for results close to screening)
$x_{Fe\,max}$	**Length**, particle diameter which is the longest Feret diameter of the measured set of Feret diameter (for results close to microscopy)
$x_{Fe\,min}$	**Length**, particle diameter which is the shortest Feret diameter of the measured set of Feret diameter
$Q_3(x)$	**Cumulative distribution**, based on volume: volume proportion of particles smaller than x in proportion to the total volume
$1-Q_3(x)$	Cumulative distribution of residue $1-Q_3(x)$, based on volume
$p_3(x_1, x_2)$	Fractions $p_3\,(x_1, x_2)$ – volume proportion of particles in the range (x_1, x_2): $p_3(x_1, x_2) = Q_3(x_2) - Q_3(x_1)$
$q_3(x)$	**Density distribution** $q_3(x)$ based on volume, first derivative of $Q_3(x)$ $q_3(x) = \dfrac{dQ_3(x)}{dx}$
$Q_0(x)$	Cumulative distribution $Q_0(x)$, based on number of particles: number of particles smaller than x in proportion to the total number of particles
$1-Q_0(x)$	Cumulative distribution of residue $1-Q_0(x)$, based on number of particles
$P_0(x_1, x_2)$	Fractions $p_0(x_1, x_2)$ - number of particles in the range (x_1, x_2): $p_0(x_1, x_2) = Q_0(x_2) - Q_0(x_1)$
$q_0(x)$	Density distribution $q_0(x)$, based on number of particles, first derivative of $Q_0(x)$ $q_0(x) = \dfrac{dQ_0(x)}{dx}$

Characteristics:

$Q_3(x)$	Q_3 value, whereat a given particle diameter x is reached, based on volume
$x(Q_3)$	x, whereat which a given Q_3 value is reached, based on volume
$SPAN_3$	Span value, based on volume: $$Span_3 = \frac{x(Q_{3,3}) - x(Q_{3,1})}{x(Q_{3,2})}$$ Here the first index indicates that the values are based on volume. In the program the first index has been left off, since for $SPAN_3$ and $SPAN_0$ the same Q(x) values are used.
U_3	nonuniformity, based on volume $$U_3 = \frac{x_{60}}{x_{10}}$$ x_{10}: x value for $Q_3 = 10\%$; x_{60}: x value for $Q_3 = 60\%$

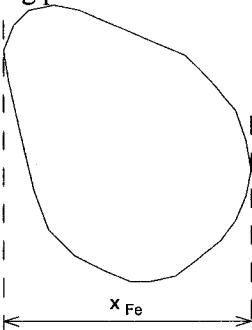| $Q_0(x)$	Q_0 value, whereat a given particle diameter x is reached, based on number
$X(Q_0)$	x, whereat a given Q_0 value is reached, based on number
$SPAN_0$	Span value, based on number of particles $$Span_0 = \frac{x(Q_{0,3}) - x(Q_{0,1})}{x(Q_{0,2})}$$ Here the first index indicates that values are based on the number of particles. In the program the first index was left off as for $SPAN_3$ and $SPAN_0$ the same Q values are used.
U_0	Nonuniformity, based on number of particles $$U_0 = \frac{x_{60}}{x_{10}}$$ x_{10}: x value for $Q_0 = 10\%$ x_{60}: x value for $Q_0 = 60\%$
MA CV SGN UI	Mean aperture $x_{50} = d_{50} = D_{50}$ Mean diameter Coefficient of Variation Size guide number $x_{50} = d_{50} = D_{50}$ Mean diameter from sieve analysis Uniformity index

214

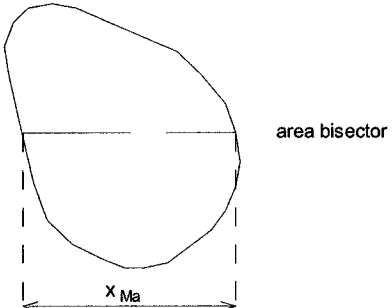## Indirect determination of the specific surfaces S_v and S_m:

S_V	$S_v = \dfrac{\text{surface of all particles}}{\text{volume of all particles}}$	
S_m	$S_m = \dfrac{\text{surface of all particles}}{\text{mass of all particles}}$ density	for a given specific
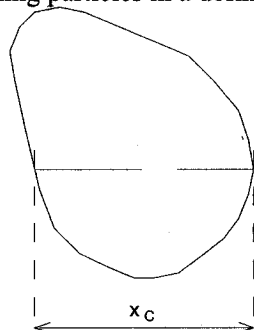
RRSB - characteristics:

N	Slope of the RRSB line
D'	x value, whereat the line reaches a value of 0.632
correlation	Correlation between the RRSB line and Q(x) in the range between Q_1 and Q_2

Shape characteristics:

x_{Fe}	Feret diameter x_{Fe} Distance between two tangents placed perpendicular to the measuring direction. For a convex particle the mean Feret diameter (mean value of all directions) is equal to the diameter of a circle with the same circumference. (Set of diameter by scanning particles in a defined number of directions.)
max (x_{Fe})	The longest Feret diameter out of the measured set of Feret diameters.
min (x_{Fe})	The shortest Feret diameter out of the measured set of Feret diameters.

X_{Ma}	Martin diameter x_{Ma} Length of the area bisector in the measuring direction ![area bisector diagram] area bisector x_{Ma}

x_c	max. chord x_c in measuring direction (Set of diameter by scanning particles in a defined number of directions.) ![chord diagram] x_c
min (x_c)	The shortest chord out of the measured set of max. chords x_c. A breath/width which is very close to sieving.

SPHT	Sphericity $\quad SPHT = \dfrac{4\pi A}{U^2}$ U – measured circumference of a particle A – measured area covered by a particle **For an ideal sphere SPHT is expected to be as 1.** **Otherwise it is smaller than 1.**
Symm $_{0,3}$	$Symm_{0,3} = \dfrac{1}{2}\left(1 + min\left(\dfrac{r_1}{r_2}\right)\right)$ r_1 und r_2 are distances from the centre of area to the borders in the measuring direction. For unsymmetrical particles Symm is < 1. If the centre of area is outside the particle i.e. $\dfrac{r_1}{r_2} < 0$

216

	Symm is < 0.5 $x_{Ma} = r_1 + r_2$ Symm is minimum value of measured set of symmetry values.
$b/l_{0,3}$	$$b/l_{0,3} = \frac{\min(x_c)}{\max(x_{Fe})}$$ min (x_c) and max (x_{Fe}) out of the measured set of x_c and x_{Fe} values
$(b/l)_{rec\,0,3}$	$$(b/l)_{rec0,3} = \min\left(\frac{x_c}{x_{Fe}}\right)$$ min quotient of perpendicular x_c and x_{Fe} out of the measured set of x_c and x_{Fe} values.
$B/L_{0,3}$	$$B/L_{0,3} = \frac{\min(x_{Fe})}{\max(x_{Fe})}$$ min (x_{Fe}) and max (x_{Fe}) out of the measured set of x_{Fe} values
$(B/L)_{rec\,0,3}$	$$(B/L)_{rec0,3} = \min\left(\frac{x_{Fe1}}{x_{Fe2}}\right)$$ min quotient of perpendicular x_{Fe1} and x_{Fe2} out of the measured set of x_{Fe} values.
$x_p = x_{mean}$	The Feret diameter, the Martin diameter, the max. chord and the sphericity for the various size classes are determined by calculating a mean value, based on the number of particles within a size class: $$\overline{x} = \frac{1}{n}\sum_{i=1}^{n} x_i$$ As the objects within a class can be distributed unevenly, the mean equivalent diameter of circles equal in area, xp, should be used as reference value for class-related information.
PD_0, PD_3	Number of **particle detections**, measure of the statistical reliability of the shape characteristics. The larger PD the more reliable is the value of x_{Fe}, x_{Ma}, x_c and SPHT.
$Sigma(v)_0$	Standard deviation of the ratio $$Sigma(v) = \sqrt{\frac{1}{n}\sum_{i=1}^{n}(1 - v_i)^2}$$

217

	with the ratio $v_i = \dfrac{\max(x_{Fe}, x_c)}{\min(x_{Fe}, x_c)}$ of the particle no. i, in which the measuring directions of the Feret diameter and the maximal chord are perpendicular to each other.
$Q_0(SPHT) = NSP_0$ $Q_3(SPHT) = NSP_3$	Proportion of **non-s**pherical **p**articles, whose sphericity is smaller than a given threshold; based on number of particles or on volume
$Q_{0/3}$; Symm; b/l, $(b/l)_{(rec)}$ B/L, $(B/L)_{(rec)}$	Proportion of particles or volume, whose symmetry, or various b/l-ratios is smaller than a given threshold
$MW_{0/2/3}(x)$	**Mean value** of a chosen characteristic, weighted; $x_{1,r} = \sum x\ q_r(x)\ \Delta x$
Sigma(x)	**Standard deviation** of a chosen x
Konv$_0$ Konv$_3$	**Convexity** = (square root) ratio of real particle area and convex area of particle (as if a band was put around the particle)
rD	**relative Density**, mass of sample divided by the volume of the sample measured with the CAMSIZER®
SGN	**SIZE GUIDE NUMBER,** Calculated diameter of the "average particle", expressed in millimeters and multiplied with 100 (for example: d50 = 0.123 mm => SGN = 12.3)
UI	**UNIFORMITY INDEX,** ratio of the size of "SMALL PARTICLES" to "LARGE PARTICLES" in the sample, expressed in percentage; UI is the ratio, times 100, of the two extreme sizes in the range of particles at the 95% level and the 10% level. UI =100 means that the particles have the same size, perfectly uniform; UI = 50 means that the small particles are half the size of the large particles in the sample
CV	**COEFFICIENT OF VARIATION (of SGN or UI)** the coefficient of variation is the standard deviation (SD) of SGN or UI devided by the average; it is dimensionless
MA	D_{50} value

218

V: GRANULAR BED EXPERIMENTS FOR PARTICULATE

MATTER REMOVAL

219

LAVA ROCK BED EXPERIMENTS:

Dry-Lava rock

9 cm bed dp[1]	RE q[2]=1.2	RE q=2.4	RE q=3.6
0.05	80%	58%	44%
0.1	75%	46%	39%
0.15	56%	42%	33%
0.2	54%	40%	31%
0.25	56%	39%	34%
0.5	55%	34%	38%
0.7	52%	27%	31%
1	50%	30%	27%
1.8	52%	37%	46%
2.5	71%	35%	50%

Wet-Lava rock

27 cm bed dp	RE q=1.2	RE q=2.4	RE q=3.6
0.05	66%	59%	55%
0.1	66%	51%	54%
0.15	73%	59%	49%
0.2	81%	66%	63%
0.25	89%	75%	68%
0.7	79%	74%	70%
1	79%	75%	73%
1.8	87%	86%	83%
2.5	97%	91%	87%

18 cm bed dp	RE q=1.2	RE q=2.4	RE q=3.6
0.05	83%	68%	66%
0.1	78%	57%	52%
0.15	76%	49%	45%
0.2	70%	45%	43%
0.25	68%	41%	40%
0.5	68%	43%	48%
0.7	64%	46%	40%
1	66%	45%	44%
1.8	71%	48%	48%
2.5	83%	55%	59%

27 cm bed dp	RE q=1.2	RE q=2.4	RE q=3.6
0.05	85%	84%	83%
0.1	81%	81%	81%
0.15	77%	78%	75%
0.2	78%	78%	76%
0.25	74%	77%	75%
0.5	76%	53%	45%
0.7	78%	59%	49%
0.83	83%	61%	53%
1	86%	60%	47%
1.8	90%	59%	52%
2.5	94%	57%	58%

1- Particle diameter (μm)
2- Flow rate (liters per minute)

220

SAND BED EXPERIMENTS:

Dry sand 27 cm bed

dp	1.2 LPM RE	2.4 LPM RE	3.6 LPM RE
0.05	99%	98%	95%
0.1	97%	86%	78%
0.15	94%	87%	76%
0.2	92%	84%	71%
0.25	89%	81%	68%
0.3	87%	80%	67%
0.35	87%	77%	65%
0.4	85%	78%	65%
0.5	83%	72%	67%
0.7	87%	68%	64%
0.83	90%	76%	65%
1	92%	68%	66%
1.8	93%	74%	71%
2.5	97%	77%	75%

Wet sand 27 cm bed

dp	1.2 LPM RE	2.4 LPM RE	3.6 LPM RE
0.05	63%	64%	70%
0.1	68%	68%	65%
0.15	74%	68%	70%
0.2	77%	71%	68%
0.25	78%	75%	73%
0.3	80%	78%	76%
0.4	86%	82%	79%
0.5	66%	69%	67%
0.7	69%	66%	65%
0.83	82%	73%	71%
1	72%	66%	68%
1.8	85%	77%	72%
2.5	98%	81%	79%

221